UNIVERSITÀ DEGLI STUDI DI TORINO

SCUOLA DI DOTTORATO

DOTTORATO IN
SCIENZE AGRARIE, FORESTALI E ALIMENTARI

CICLO: XXXIII

STRIGOLACTONES INVOLVEMENT IN TOMATO PLANTS RESPONSE TO LOW P LEVELS

Veronica Santoro

Docente guida:
Prof.ssa Luisella Celi

Coordinatore del Ciclo:
Prof.ssa Eleonora Bonifacio

ANNI
2018; 2019; 2020

CONTENTS

CHAPTER 1

Introduction

Phosphorus (P) is one of the **essential elements** that plants require to develop and function. It is a **structural component of key biomolecules** and takes part in **primary cellular metabolic processes**, as photosynthesis, nucleic acid synthesis, respiration and glycolysis (Péret *et al*., 2011; Vance *et al*., 2003).

Despite its importance as macronutrient, P reserves are finite, and much of the P supply in agricultural soils is not bioavailable after application due to reactions as soil **adsorption, immobilization, precipitation and coprecipitation,** which make P one of the most **immobile, inaccessible, and unavailable among all nutrient elements** (Holford, 1997; Niu *et al*., 2013; Richardson *et al*., 2009).

Phosphorus is absorbed and assimilated by plants as **inorganic phosphate (Pi).** Such a P form, because of the abovementioned retention processes, occurs at fairly low concentrations in the soil solution, typically in the **1–10 µM range** (Bieleski, 1973). In addition, **20 to 80% of the total soil P is present as organic P**, in the form of inositol phosphates, orthophosphate diesters, monoesters, and organic polyphosphates, which require mineralization to Pi prior to acquisition (Jarosch *et al*., 2015; Turner *et al*., 2002). These organic forms of P can undergo the same interactions with soil colloids as Pi (Celi *et al*., 2004), leading to the **retention of a potentially important source of P for the nutrition of plants** (Hayes *et al*., 2000).

The concentrations of available P in soil can thus range from null to values that remain anyway well below the critical level needed for optimal plant growth, which corresponds to **up to tens of µM for the most demanding species, as tomato** (Hinsinger, 2001)**.**

Plants have evolved many **strategies to cope with P deficiency**, as a more efficient use of internal P and P recycle, modification of root architecture, physiological adjustments and symbiotic interactions with mycorrhizal fungi to increase P acquisition in the soil (Dixon *et al*., 2020). Recent studies have indicated a major role for **strigolactones** (SLs), a group of carotenoid-derived

compounds, as **signalling molecules able to trigger morphological, physiological and biochemical responses associated with plant acclimation to P deficiency conditions** (Czarnecki *et al*., 2013). **SL biosynthesis and exudation are increased under P starvation** (Niu *et al*., 2013). Also, SLs affect lateral root formation, primary root growth, number and density of root hair and suppress tiller bud outgrowth (Mayzlish-Gati *et al*., 2012; Niu *et al*., 2013; Ruyter-Spira *et al*., 2011). The involvement of SLs in the regulation of plant responses to P deficiency likely occurs through their crosstalk with other phytohormones, such as cytokinins, auxin and ethylene, thus highlighting a complex network of hormonal signals (Kapulnik *et al*., 2011a; Koltai, 2011; Ruyter-Spira *et al*., 2011).

Despite the roles of SLs in modulating plant acclimation to P stress have been investigated in different **model plant species** thanks to the generation of many SL-biosynthesis and -sensitivity mutants (Kohlen *et al*., 2012; Vogel *et al*., 2010), **whether SLs affect the morphological and physiological adjustments in tomato in response to P shortage has not been thoroughly investigated yet**. A better comprehension of these putative SLs' roles in such a high-value crop could help improving agronomical practices and the selection of **genotypes with enhanced P-use efficiency** able to better adapt to low P environments by mobilizing the nutrient that would be otherwise unavailable, improving plant growth, development and yield.

1.1 Phosphorus

Phosphorus is one of the essential macronutrients required by plants for their growth and development (Vance *et al*., 2003). It constitutes about 0.2% of the plant's dry matter, takes part in primary cellular metabolic processes and is a structural component of key biomolecules, including sugar phosphates, nucleotides and nucleic acids, phospholipids, and energy-rich compounds like adenosine triphosphate (ATP) (Abel *et al*., 2002; Czarnecki *et al*., 2013; Marschner, 1995; Schactman *et al*., 1998; Vance *et al*., 2003). In contrast to carbon (C) that can be fixed from the atmosphere, P derives from minerals in soil, and is typically supplied to plants through fertilizers application (Schlesinger and

Bernhard, 2013). Primary P minerals including apatites, strengite, and variscite are very stable, and the release of available P from these minerals by weathering is generally too slow to meet crop demand, even though direct application of phosphate rocks has proved to be relatively efficient to sustain crop growth in acidic soils (Shen *et al*., 2011). Nevertheless, rock phosphate constitutes the primary material used to manufacture P fertilizers (Dixon *et al*., 2020). Secondary P minerals including calcium (Ca), iron (Fe), and aluminium (Al) phosphates vary in their dissolution rates, depending on the size of mineral particles and soil pH, and constitute an alternative source of P for plants (Shen *et al*., 2011).

Apart from the soluble inorganic P form (Pi) deriving from primary and secondary P minerals, which accounts for 35 to 70% of total P in soil (Harrison, 1987), soil P exists in various organic forms, whose accumulation in soil depends on vegetation and climate, and leads to range from 20 to 80% of the total soil P (Jarosch *et al*., 2015). Soil organic P mainly occurs in stabilized forms as phosphonates and inositol phosphates, a group of mono- to poly-phosphorylated inositols widely found in natural environments, and active forms as orthophosphate diesters, labile orthophosphate monoesters, and organic polyphosphates (Condron *et al*., 2005; Turner *et al*., 2002). All these organic P forms, along with Pi, exist in complex equilibria with each other (Fig. 1.1), forming a blend of very stable (sparingly-available) and plant-available P pools such as labile P and soluble P, the latter constituting < 0.1 % of total soil P, regardless of the use of mineral fertilizers (Khan *et al*., 2009).

Due to the growing demand for agricultural production and the progressive exhaustion of P mines for the production of P fertilizers, P is attaining increasingly attention as a non-renewable resource, and poses the necessity of increasing the P-use efficiency by crops (Cordell *et al*., 2009; Gilbert, 2009). In fact, despite P has great importance for plant development, P deficiency represents one of the major constraints in agricultural production, with whole-plant growth substantially reduced or inhibited by P limitation (Shen *et al*., 2011). Although soils generally contain a large amount of total P, only a small proportion is immediately available for plant uptake under most soil conditions (Dixon *et al*., 2020).

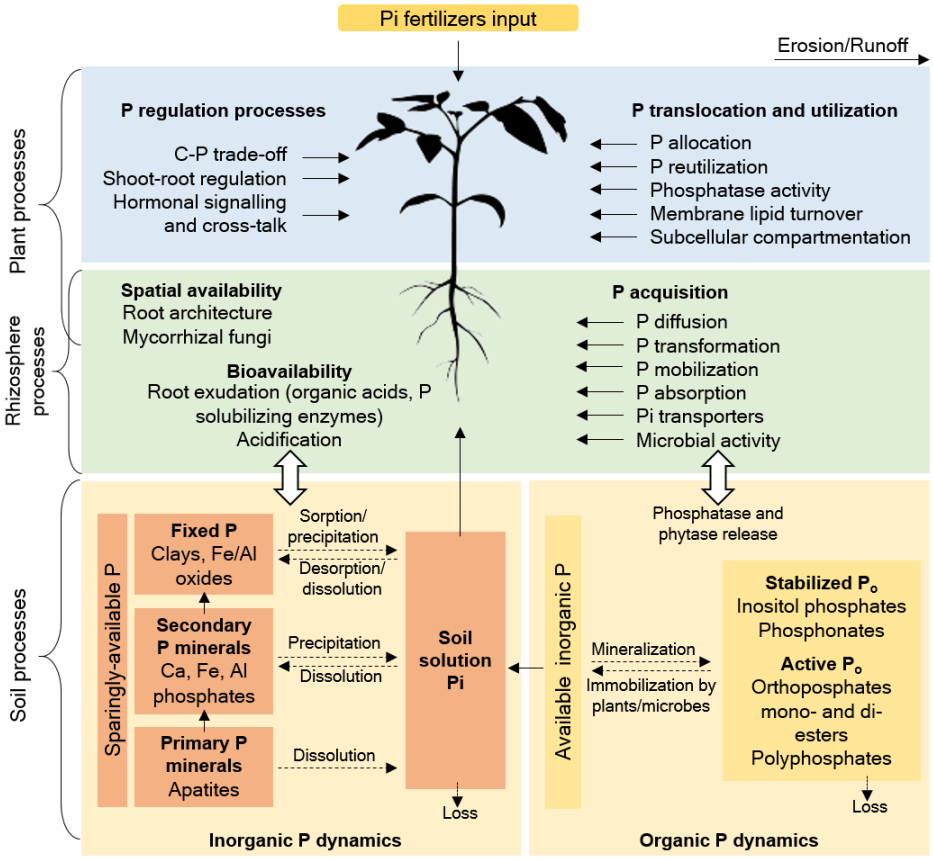

Figure 1.1: Phosphorus dynamics in the soil/rhizosphere-plant continuum (based on Shen *et al*., 2011).

1.1.1 *Phosphorus retention in soil*

Many abiotic processes may contribute to stabilize P in soils and sediments, leading to the accumulation of certain organic P compounds and hampering their biodegradation and therefore availability to plants. Fixation reactions are affected by soil properties as the presence of Fe and Al oxides, clay minerals, soil organic matter, pH, and other factors, like temperature and flooding events, while P immobilization to organic P and mineralization to Pi are driven by soil microorganisms (Dixon *et al*., 2020 and references therein; Turner, 2006). It is well-known that P exhibits a high affinity for Fe and Al oxides, which are present in soil as positively charged nano- to micro-particles in a large range of pH (3–9),

which can hence behave as adsorbing surfaces onto which Pi and organic P molecules can be retained. The extent of P adsorption strongly depends on environmental conditions (pH, ionic strength, P concentration), as well as on the chemico-physical characteristics of the sorbent phase (e.g., functional groups, stability, particle size, specific surface area) (Li *et al*., 2016). In acidic soils, both inorganic and organic P can be dominantly adsorbed on the surface of Al and Fe oxides and hydroxides, such as gibbsite, ferrihydrite, hematite, and goethite, by forming various surface complexes (Celi *et al*., 1999; Parfitt, 1989), while in neutral-to-calcareous soils, P can also be adsorbed on the surface of Ca carbonate and clay minerals (Celi *et al*., 2000; Shen *et al*., 2011). In the case of Pi, the non-protonated and protonated bidentate complexes on the surface of ferrihydrite may coexist at pH from 4 to 9, while the protonated bidentate inner-sphere complex was shown to be predominant under acidic soil conditions (Arai and Sparks, 2001). With aging, P may be also occluded in nanopores that frequently occur in Al and Fe oxides, and thereby become unavailable to plants (Arai and Sparks, 2007).

Apart from adsorption, P retention is also dominated by precipitation reactions, with the formation of Fe and Al phosphates at pH <6 and of Ca phosphates at pH >7, resulting in P greatest availability at pH 6–7 (Dixon *et al*., 2020). In addition to adsorption and precipitation, P retention through coprecipitation with Fe due to changes in pH, redox potential or ionic strength is a common process occurring in water and sediment environments. The oxidation of Fe(II), released into solution during mineral weathering and/or reductive dissolution under anoxic conditions, and precipitation of Fe (hydr)oxides is indeed known to contribute significantly to the retention of many inorganic and organic anions, including phosphate (Gorra *et al*., 2012; Mikutta *et al*., 2014; Senn *et al*., 2015; Voegelin *et al.*, 2010; 2013). However, so far only few works investigated the mechanisms governing inorganic phosphate retention when coprecipitated with Fe, and little is known about the extent and mechanisms of organic P retention during coprecipitation.

All these processes that contribute to P retention in soil and strongly reduce its

bioavailability, compel the adoption by plants of specific and non-specific hormone-mediated responses to increase P uptake and optimize internal P usage (Table 1.1).

Table 1.1: Plant adaptive mechanisms to cope with P deficiency in soil (based on Aziz *et al*., 2014).

Trait	Efficient genotypes	Inefficient genotypes
P contents in harvested portion	Low	High
Internal critical P concentration	Low	High
Number of adventitious roots	More	Less
Root diameter	Fine	Course
Root volume	High	Low
Rooting density	High	Low
Root architecture and root growth angle	More shallower roots exploring surface soil	Less shallower roots
Root hairs	More and long	Less and short
Root exudates Organic acid anions Phosphatases	Higher amounts	Lower amounts
Internal P utilization	High	Lower
P remobilization	Yes	No or minimum
Specialized root structures	Cluster roots (proteoid or dauciform roots)	No or very little cluster roots
Symbioses with fungi	Yes	No

1.1.2 *Morphological, physiological, and biochemical responses of plants to P deficiency*

Phosphorus concentration in crop plants ranges from 0.15 to 0.5% dry weight (Epstein, 1994), but since typical Pi concentrations in soils are in the range of 1-10 µM (Frossard *et al*., 2000; Schachtman *et al*., 1998), P availability in both terrestrial and aquatic ecosystems is limited. Phosphorus is absorbed and assimilated by plants as orthophosphate anion (predominantly in the form of $H_2PO_4^-$ and HPO_4^{2-}) that, after uptake, either remains as Pi or is assimilated by forming an ester with a hydroxyl group of a carbon chain (e.g., sugar phosphates) or attaches to another Pi by forming an energy-rich pyrophosphate bond (e.g., in

ATP) (Marschner, 2012). Typical symptoms of P starvation in plants include stunted growth, dark green leaf colour caused by accumulation of anthocyanins and leaf necrosis (Czarnecki *et al*., 2013). Phosphorus shortage usually correlates with decreased levels of ATP, photosynthetic activity, and stomatal conductance, all resulting in reduced biomass production (Czarnecki *et al*., 2013). The complex regulatory mechanisms adopted by plants under P-deficiency conditions are collectively known as P starvation responses (PSRs) and aim at optimizing the external and internal use of this nutrient (de Souza Campos *et al*., 2019). These responses can improve the overall P-use efficiency (PUE), and include changes at genetic, physiological, and morphological levels. They can be divided into modifications that could enhance P-acquisition and those affecting P-utilization efficiency (PAE and PUtE, respectively) (Dixon *et al*., 2020; Vance *et al*., 2003). Acquisition efficiency is referred to the capacity of a plant to absorb nutrients, given a certain external nutrient concentration, while utilization efficiency is the capacity of plants to produce a large amount of biomass per unit of nutrient absorbed (Aziz *et al*., 2014). Phosphorus starvation responses aimed at reducing P use and increase P-use efficiency include decreased growth rate, remobilization of internal P, modifications in C metabolism, utilization of alternative respiratory pathways, and modifications in the biosynthesis of membranes requiring less P (Aziz *et al*., 2014). Root exudation of Pi-solubilizing enzymes and low molecular weight organic acids, rhizosphere acidification, modification of plant architecture, enhanced expression and activity of high-affinity Pi transporters (PHTs) and symbiotic interactions with mycorrhizae are instead responsible for enhanced P uptake (Aziz *et al*., 2014; de Souza Campos *et al*., 2019).

So far, the majority of *in vitro* and field experiments reported in the literature addressed these mechanisms in response to a fixed low P concentration (Wissuwa *et al*., 2005). Less attention has been devoted to plant's adaptation strategies following evolving P availability or to different levels of P limitations, that more realistically resemble P conditions in soil. In addition, as observed by de Groot and coworkers (2003), the normally used P-deficiency concentrations

generally exceed the optimal P amount for plant growth, resulting in plants acclimation to high P concentrations that could mask or delay the onset of the typical P starvation responses. Therefore, it is necessary to adopt the appropriate P conditions to simultaneously sustain an optimal plant growth and prevent an excessive P accumulation that plants could use as a reserve in case of P shortage. Furthermore, plant response could depend not only on the P level in the external medium, but also on its variability throughout the duration of the experiment and/or the establishment of an acclimation period before P depletion. The amount of P available in the soil solution in fact does not only depend on the intrinsic scarcity of this nutrient or on its low bioavailability, but can fluctuate following seasonality and fertilizations, forcing plants to adapt to slight or sudden decrease of P availability. All these aspects should be taken into consideration while studying the strategies adopted by plants to respond to P deficiency, so as to observe the mechanisms that are more likely to occur under normal soil conditions.

1.1.2.1 *Internal P remobilization*

Phosphorus deficiency is typically accompanied by within-plant remobilization of P from senescent to developing tissue (Dixon *et al*., 2020). The primary cellular compartment for P storage is the vacuole, in which 85 to 95% of P reserves are typically stored. In particular, excess P gets stored in organic compounds, such as phytate, in the vacuoles of leaf cells (Haran *et al*., 2000). Internal P is fairly mobile and P recycling is an effective way to temporarily ensure maximum use of P reserves under P shortage. This strategy may result in reduced growth rates, decreased vacuolar P content, reuse of P from membrane lipids and reduced P nucleic acid pools (Rausch and Bucher, 2002). A phosphate transporter (*OsPht1;8*) was found to be involved in P redistribution from old to young leaves in rice (Li *et al*., 2015), while Besford (1979) observed that P deficiency induced a mobilization and rapid export of P from tomato leaves when plants were transferred from a P-rich (20 mM Pi) into P-free medium. Intracellular acid phosphatases may also help to recycle P from expendable intracellular organophosphate pools. A study with tomato suspension cells revealed that low

P induced expression of a phosphatase catalyzing internal P remobilization, which allowed tomato seedlings using stores of phytic acid and preventing the onset of the typical morphological and biochemical symptoms of P deficiency during the first 10 days of growth (Bozzo *et al*., 2005).

1.1.2.2 *Root architecture modifications*

In order to implement a prompt reaction to P shortage, plants need first to sense the P status both locally and systemically so as to orchestrate the appropriate responses, with a large set of genes (>1000) being regulated (de Souza Campos *et al*., 2019). Svistoonoff and coworkers (2007) provided evidence for an important role of the tip of the primary root in sensing P deficiency and/or responding to it in *Arabidopsis*, highlighting how the external P supply rather than internal P status triggers the local root growth response to P availability (Abel, 2011).

Modifications of root growth and architecture following P sensing at the root tip are the most obvious and best-documented responses of plants to P starvation (Czarnecki *et al*., 2013; Lynch, 2007). Root system architecture (RSA), defined as the spatial configuration of plant roots, is highly plastic in response to low P conditions, and is characterized by a modular structure which enables exceptional flexibility, thus allowing root deployment in nutrient-rich zones (Hodge, 2004).

A common RSA response to P deficiency is the increased root-to-shoot (R/S) ratio, due to a preferred biomass partitioning towards the roots at the expense of shoot growth (Hodge, 2004; Péret *et al*., 2014; Ramaekers *et al*., 2010).

Low soil P availability also changes the distribution of growth among various root types. In the model plant *Arabidopsis thaliana*, a highly branched root system with reduced primary root and increased number and length of lateral roots was observed when seedlings were grown under low P availability (López-Bucio *et al*., 2003; Williamson *et al*., 2001). The reduction of primary root elongation is a complex process that involves the reduction of cell elongation and progressive reduction in the length of the meristem (Sánchez-Calderón *et al*., 2005). However, in other crop plants, the elongation of the main root axis was

maintained under low P, allowing roots to grow until they encountered localized patches of higher P availability (Niu *et al*., 2013; Ramaekers *et al*., 2010). Also, the response of lateral rooting under P stress shows genetic variation even for different genotypes of the same species, underlying how the adaptive mechanisms are variegate and may differ among and within plant species (Aziz *et al*., 2014; Niu *et al*., 2013). Many species, as maize and *Arabidopsis,* have been reported to adopt the strategy of lateral root modification (Dixon *et al*., 2020), while this response has not been reported in tomato, where high P levels (2 mM Pi) were shown to increase lateral root number (Jiang *et al*., 2015). On the other hand, tomato plants can respond to P-deficiency by increasing root surface area, and decreasing total root weight and average root diameter, the latter being a root architecture modification widely occurring under P stress (Garcia and Asencio, 1992).

Another common adaptation to low P is the stimulation of root hair formation (Niu *et al*., 2013). Root hairs can occupy up to 90% of the root surface, facilitating water and nutrient uptake and allowing soil exploration at reduced metabolic costs (Czarnecki *et al*., 2013; Hodge, 2004; Lynch, 2007; Ramaekers *et al*., 2010). Root hair elongation may be driven by a shoot-originating signal, possibly auxin-derived, translocated to the roots upon sensing low P (Lambers *et al*., 2006). Tomato root hair length was shown to increase from 0.1 to 0.2–0.7 mm when Pi concentration decreased from 100 to 2 µM (Foehse and Jungk, 1983). By enhancing both root hair length and density, the soil volume explored by roots for P absorption significantly increases, which may further increase P availability, as root hairs may assist in the exudation of P-mobilizing compounds such as organic acid anions, protons and phosphatases (Ramaekers *et al*., 2010).

The importance of strategic root trait adjustments to compensate for low P availability is further underlined by root growth directed towards P-rich pockets within the soil (Czarnecki *et al*., 2013). As the topsoil is the layer with greatest bioavailability of P in most natural soils, root systems that enhance the so-called “topsoil foraging” were demonstrated to enable better P acquisition. This resulted

in shallower growth of basal roots, increased adventitious rooting and greater dispersion of lateral branching from the basal root (Lynch, 2007).

Finally, a very impressing root-related response to P starvation is the formation of highly branched root systems named cluster roots (Czarnecki *et al*., 2013). The best-known root clusters are the proteoid roots formed in Proteaceae and *Lupinus albus*, but also dauciform roots clusters, characterized by short, carrot-shaped, lateral roots with remarkably dense and long root hairs, are an important specialized root structure developed in monocotyledonous sedges to acquire P from nutrient-poor, P-fixing soils (Purnell, 1960; Shane *et al*., 2006). These types of roots are specialized in the synthesis and exudation of organic acid anions (Czarnecki *et al*., 2013).

1.1.2.3 *Root exudation*

Plant roots exude a variety of C compounds and inorganic ions into the rhizosphere, significantly influencing its chemistry, soil microflora and fauna, and plant growth (Hinsinger, 2001; Marschner, 1995; Vance *et al*., 2003). Root exudates are crucial as they can favour nutrient acquisition, especially under nutrient stress, representing a major source of energy for microbial growth in soils and play key roles in plant-microbe and plant-plant communication (Wang *et al.*, 2020 and references therein).

The nature of root exudates varies significantly in response to P deficiency, which might involve proton release to acidify the rhizosphere, organic acid anion exudation to mobilize sparingly-available P and release of phosphatases or phytases to mobilize organic P by enzyme-catalyzed hydrolysis (Aziz *et al*., 2014; Neumann and Römheld, 2002).

H^+-ATPase is the driving force behind rhizosphere acidification. This enzyme couples ATP hydrolysis with proton transport, establishing electrochemical gradients across the plasma membrane (Duby and Boutry, 2009). Root-induced acidification can decrease rhizosphere pH by 2 to 3 units relative to the bulk soil, which may result in substantial dissolution of sparingly-available soil P (Marschner, 1995). The pH change in the rhizosphere is mainly affected by cation/anion uptake ratios and N assimilation, and is also related to the soil-

buffering capacity, microbial activity, and plant genotype (Dixon *et al*., 2020). Proton exudation as a coping mechanism for a P deficiency has been observed in numerous species such as bean, tomato, white lupin, and tea (Dixon *et al*., 2020). In particular, tomato plants were shown to exude approximately 30 nM H^+ h^{-1} g^{-1} FW at high P levels (200 µM Pi) and approximately 80 nM H^+ h^{-1} g^{-1} FW at low P concentration (10 µM Pi) (Zhang *et al*., 2018).

Besides proton release, increased C exudation is a common strategy to enhance P acquisition. Among the diverse C compounds, organic acid anions and sugars are important for the mineral nutrition of plants, as well as for microbial growth in the rhizosphere (Jones and Darrah, 1995). Under P-deficient conditions, exudation of acetate, aconitate, citrate, malate, fumarate, lactate, oxalate, and succinate increase in many plant species (Aziz *et al*., 2014; Lambers *et al*., 2006). These compounds help to improve P uptake by plants by increasing the availability of both inorganic and organic P. In particular, they can complex and chelate cations bound to P, as Fe, Al, and Ca (Gerke, 2015; Hinsinger, 2001; Römheld and Marschner, 1990), compete with Pi for sorption sites, so that the dissolution of sparingly-soluble P minerals is increased (Gerke, 2005). The cations excreted with the organic acid anions to maintain a charge balance may in fact be protons, thereby leading to rhizosphere acidification (Hinsinger, 2001). However, other cations (especially K^+), are at least similarly important, explaining why organic anion exudation is not invariably associated with rhizosphere acidification (Lambers *et al*., 2006).

Enhanced organic anion exudation has consistently been reported in many plant species, such as white lupin (Johnson *et al*., 1996; Neumann *et al.,* 2000; Neumann and Römheld, 1999), alfalfa (Lipton *et al.,* 1987), rice (Kihara *et al.*, 2003) and oilseed rape (Hoffland *et al*., 1992). The dominant organic anions released by exudation are species-specific and can vary between genotypes. Citrate has been reported to be dominantly exuded by tomato, followed by succinate and fumarate (Dixon *et al*., 2020).

Exudation of phenolics and mucilage may also be enhanced under P deficiency (Lambers *et al*., 2006). These compounds can act reducing Fe(III) to Fe(II)

leading to oxide dissolution and release of possibly bound P, but tend to be less effective than organic acid anions (Neumann and Römheld, 2002).

Finally, the activity of phytase and acid phosphatase can increase in roots and root exudates of various species grown under low P supply (Vance *et al*., 2003). Soil organic P compounds, after being mobilized by organic anions, must be first hydrolyzed to release Pi for plant uptake (Lambers *et al*., 2006). Acid phosphatases can hydrolyse a wide range of organic P compounds (Tarafdar and Claassen, 2001), while phytases specifically hydrolyze phytates (*myo*-inositol penta- and hexa-phosphate), which accounts for 50% of the total organic P in soil (Anderson, 1980) and is fairly resistant to other phosphatases (Hayes *et al*., 2000). As for other P starvation responses, P-deficiency-tolerant genotypes of different crops can display a greater activity of extracellular phosphatases in the rhizosphere than genotypes sensitive to P deficiency (Asmar *et al.*, 1995). However, the efficacy of these phosphohydrolases can be greatly altered by the substrate availability, interactions with soil microorganisms, and soil pH, depending on soil physical and chemical properties (Giaveno *et al*., 2010). Similarly, exuded organic acid anions may have strong interactions with soil components, resulting in underperforming P mobilization. Therefore, root-induced bioavailability and acquisition of P in association with root exudation should be systemically evaluated for communication in the soil-rhizosphere-plant continuum.

1.1.2.4 *Mycorrhizal associations*

The association of arbuscular mycorrhizal (AM) fungi with plant roots is one of the most important symbiotic relationship between plants and microorganism (Redecker and Raab, 2006). This symbiosis is formed by the roots of more than 80% of land plants with fungi from the phylum Glomeromycota (Smith and Read, 2008). Arbuscular mycorrhizal fungi are obligate biotrophs and depend entirely on the plant to complete their life cycle. They colonize the root cortex of the host plant and form specialized tree-like subcellular structures called arbuscules, which are involved in the nutrient exchange between the two partners (Rausch and Bucher, 2002). In exchange for photosynthetically fixed C, root colonizing

AM fungi translocate water and nutrients, primarily P and N, to the host plants, and effectively increase the surface area of plant roots, enabling greater soil exploitation and uptake of soil P (Smith and Read, 2008). Specifically, the hyphae of AM fungi may exploit either the soil Pi pool by mining for distant pools of available P, or the soil organic P pool by producing phosphatase enzymes (Nasto *et al*., 2014). For this reason, this symbiosis is maximised under P deficiency, and it has been observed that root exudates produced by plants grown under P-limited conditions are more stimulatory to AM fungi than exudates produced under adequate P nutrition (Nagahashi and Douds, 2004). Moreover, increased soil P levels resulted in a decreased AM fungi colonization of the roots.

1.1.2.5 *Phosphorus uptake by plants*

Phosphorus slowly moves toward plant roots by diffusion due to its strong reaction with soil constituents (Hinsinger, 2001). The concentration of P in root cells can be up to 1000-fold higher than in the soil solution, therefore the uptake of soluble or mobilized soil P needs to occur against a high concentration gradient (Czarnecki *et al*., 2013). Molecular research has revealed that plants possess both a low- and high-affinity P uptake system (Furihata *et al*., 1992). The low-affinity system appears to be constitutive in plants and operate at the mM range (Raghothama, 1999), while high-affinity systems are induced at low P conditions (µM range), increasing the potential for enhanced P uptake from low P soils (Chen *et al*., 2014a). Inorganic phosphate is likely absorbed in its most abundant forms $H_2PO_4^-$ or HPO_4^{2-} by high-affinity Pi/H^+ symporters that belong to the PHOSPHATE TRANSPORTER1 (PHT1) gene family, in a process that requires a H^+-ATPase driven proton gradient across the plasma membrane (Liu *et al*., 1998). A total of eight putative PHT1 genes (*LePT1* to *8*) have been identified in tomato genome (Chen *et al*., 2014a). *LePT1* and *LePT7* are ubiquitously expressed in roots, stems, young leaves, flowers and fruits, and their transcripts are abundantly induced in response to P starvation (Chen *et al*., 2014a). *LePT2* and *LePT6* are predominantly expressed in P-deficient roots, while *LePT3*, *LePT4* and *LePT5* are strongly activated in roots colonized by AM fungi under low, but not high, P conditions (Chen *et al*., 2014a). Liu and coworkers (1998)

showed that the root transcript levels of both *LePT1* and *LePT2* significantly increased within 1 day after plant transfer to a P-deficient medium (below 100 µM Pi), and reached a maximum after about 5 days of starvation. Resupplying P (250 µM Pi) to P-starved tomato plants repressed *LePT1* and *LePT2* transcripts back to their uninduced levels within 2 days (Liu *et al*., 1998). In addition, following results from a split-root experiment, the authors hypothesized that signals for the P-starvation response may arise internally because of the changes in cellular concentration of P (Liu *et al.*, 1998). Earlier reports have in fact shown that the supply of P to a part of the root system may partly or fully systemically compensate for the deficiency in other parts of the root system by greater rates of nutrient uptake, depressing the expression of phosphate transporters genes (Drew *et al.*, 1984).

1.1.2.6 *Metabolomic changes*

Besides the morphological and physiological adaptations described so far, P starvation also causes striking metabolomic changes in plants (Czarnecki *et al*., 2013). In general, metabolic redundancies allow activation of enzymes that do not require ATP or Pi as substrates and replacement of phospholipids with non-phosphorus galactolipids in extraplastidic membranes (Plaxton and Tran, 2011). P deficiency-caused reduction in ATP and ADP levels inhibits glycolytic enzymes, and P-independent enzymes that bypass classical glycolysis are up-regulated (Czarnecki *et al*., 2013). De Groot and coworkers (2001) applied a wide range of increasing P supply rates to young tomato plants (*Lycopersicon esculentum* L.) and observed a decreased rate of photosynthesis and a reduced production of assimilates at severe P limitation. Interestingly, in the same study, extra P under P limitation was used by tomato plants for improving growth rather than increasing the plant P concentration, and the authors observed that the relative importance of the morphological or physiological modifications changed with the severity of P limitation (de Groot *et al*., 2001). In particular, mild P limitation mainly altered the morphological traits of plant, while severe P limitation affected their physiological responses. This highlights, as previously observed, that even slight differences in P provision can bring about modifications at different levels of plant

responses. It is therefore important to carefully choose the level of P-deficiency when setting up P stress experiments, as different responses can be activated in plants.

1.1.2.7 *Complex signalling network underlying plant response to P deficiency*

Although a complete picture of how plants sense external and internal P concentrations and transduce this information into the described morphological, physiological, and biochemical responses is far from being completely achieved, significant progresses towards the understanding of the complex signalling pathways underlying plant responses to P deficiency were brought about in the last decade (Czarnecki *et al*., 2013). The P-deficiency signalling network can be subdivided into local and systemic (or long distance) signalling. Phosphorus homeostasis is regulated at the systemic level, whereas the root developmental changes are locally regulated by P availability in the external medium (Péret *et al*., 2011). In fact, the sensing of external P concentrations likely takes part at the root tip and induces changes in root architecture, as described in section 1.1.2.2. There is evidence to support that Pi itself acts as a signalling molecule (Ticconi *et al*., 2004). Although a detailed model depicting the local signalling pathway from sensing external P concentrations to transcriptional responses in root tips is still lacking, it has been shown that this process is dependent on the auxin receptor TRANSPORT INHIBITOR RESPONSE1 (TIR1) (Mayzlish-Gati *et al*., 2012) and MORE AXILLARY GROWTH 2 (MAX2), a key signalling component in the SL pathway (see section 1.2) (Al-Babili and Bouwmeester, 2015; Wang and Smith, 2016).

Several systemic signalling pathways have been proposed to be involved in P-deficiency signalling. One of the best-understood P-dependent systemic signalling pathways involves the micro-RNA miR399. PHOSPHATE 2 (*PHO2*) is a ubiquitin-conjugating enzyme likely involved in targeting the PHT Pi transporters for proteolytic degradation. Micro-RNA miR399 not only directs the cleavage and degradation of *PHO2* mRNA, but also acts as a systemic signal moving from shoots to roots via the phloem. Under P-deficient conditions, the expression of miR399 is strongly induced, resulting in down-regulation of *PHO2*

mRNA, decreased proteolytic degradation of PHT proteins and enhanced P uptake (Aung *et al*., 2006; Bari *et al*., 2006; Chiou *et al*., 2006; Lin *et al*., 2008; Pant *et al.*, 2008).

It is likely that the many systemic signalling pathways involved in P-deficiency signalling act in an interconnected manner (Chiou and Lin, 2011; Rouached *et al*., 2010). In fact, it is well known that phytohormones such as auxins, cytokinins, abscisic acid, ethylene, and in particular strigolactones play complementary roles in the regulation of P homeostasis when plants are subjected to P stress, through modulation of the P signalling- and homeostasis-associated pathways (Waters *et al*., 2017; Chien *et al*., 2018). SLs are the latest class of phytohormones described and are reported to function as regulators of plant development and architecture and as signalling molecules in the rhizosphere to recruit AM fungi under P limitation (López-Ráez *et al*., 2017; Waters *et al*., 2017). Indeed, their biosynthesis is highly promoted under P stress condition (Yoneyama *et al*., 2007, 2012; López-Ráez *et al*., 2008), and their effects have been shown to be associated with differential activation of the auxin and ethylene signalling pathways, highlighting their pivotal and interconnected regulatory role in the adaptive response to low P (Koltai, 2013).

1.2 Strigolactones

Strigolactones are carotenoid-derived plant terpenes that have endogenous roles in plant and exogenous roles in the rhizosphere once released by roots. In the rhizosphere, SLs promote the association with beneficial microorganisms as AM fungi, but also affect plant interactions with harmful organisms as root parasitic plants. In plant, SLs are a group of plant hormones regulating many aspects of both shoot and root growth and development. Strigolactones also act as modulators of plant responses to biotic and abiotic stress, especially P deficiency.

1.2.1 *History of SL discovery*

The collective name “strigolactones" was coined by Butler to designate a small group of compounds that are exuded from roots of different plant species and induce seed germination in root parasitic plants of the genus *Striga*, commonly

known as witchweeds (Butler, 1995). Since the discovery of strigol in cotton root exudates as a germination stimulant of *Striga lutea* (Cook *et al*., 1966), other SLs have been identified in exudates of different plant species (Fig. 1.2) and have been shown to stimulate seed germination in root parasitic plants of the genera *Striga*, *Orobanche, Phelipanche* and *Alectra,* that cause significant losses to agricultural production all over the world (Xie *et al*., 2010). Among plant secondary metabolites known to induce seed germination of root parasites, SLs are the most active, inducing germination at 10^{-7}–10^{-15} M (Xie *et al*., 2010). In addition to stimulating parasitic plants, SLs are also able to induce seed germination of non-parasitic plants such as shepherd's purse, lettuce and wild oats (Bradow *et al*., 1990).

Development of the synthetic SL analog GR24 (Fig. 1.3d) accelerated SL research (Johnson *et al*., 1981). However, it took many years to clarify why host plants have evolved to produce SLs despite the risk of parasitism by root parasitic plants (Umehara, 2011). In fact, SLs had been known for over 40 years as germination stimulants and had therefore been considered as wastes or harmful metabolites until their function as host-recognition signal for AM fungi was uncovered by Akiyama and coworkers (2005) (Fig. 1.2). Approximately 80% of land plants engages in symbiosis with these soilborne microorganisms, in which photosynthesized C from the plant is exchanged for minerals absorbed by the fungus through an extensive network of hyphae (Gutjahr and Parniske, 2013; Schmitz and Harrison, 2014). This is particularly important for nutrients with low mobility in soil, such as P in the form of Pi. However, non-mycotrophic plant species such as *Arabidopsis*, white lupin and spinach were also found to produce SLs (Yoneyama *et al*., 2008), indicating that these molecules have biological functions inside SL-producing plants, perhaps for normal growth and development.

In 2008, Gomez-Roldan and coworkers and Umehara and coworkers independently identified SLs, or their downstream metabolites, as a novel class of phytohormones, acting as long-distance branching factors that regulate shoot branching by suppressing the growth of preformed axillary shoot buds (Fig. 1.2).

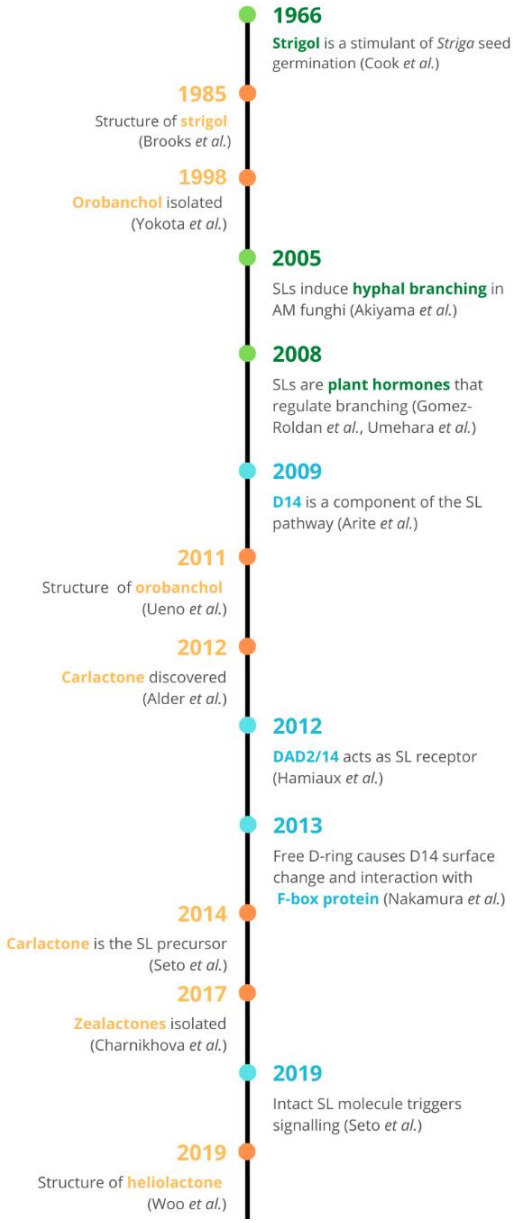

Figure 1.2: History of the discoveries in the strigolactone field. Green points indicate key discoveries of the biological functions of SLs. Blue points indicate discoveries concerning the signalling mechanism. Orange points indicate discoveries of SL molecules. Based on Bürger and Chory, 2020. Abbreviations: SL, strigolactones; AM, arbuscular mycorrhiza.

In both studies, SL application in the form of synthetic analogue *rac*GR24 (i.e., the mixture of the two enantiomers) to shoot branching mutants of pea (Gomez-Roldan *et al.*, 2008) and rice (Umehara *et al.*, 2008) restored the wild-type branching phenotype.

Besides their endogenous role in the control of shoot branching, SLs play pivotal roles in modulating the coordinated development of roots and shoots (Akiyama *et al*., 2005; Gomez-Roldan *et al*., 2008; Kapulnik *et al*., 2011) and have been shown to be involved in the regulation of leaf senescence, secondary growth, reproduction (including flower and seed setting), protection against pathogens and root-knot nematodes (Decker *et al*., 2017; Xu *et al*., 2019) and responses to abiotic stresses (Brewer *et al*., 2013; Cardinale *et al*., 2018). Many studies proved that part of the molecular and morphological responses needed for acclimatization to a nutritionally poor environment are indeed mediated by SLs (Marzec *et al*., 2013), and that they may be one of the endogenous molecules involved in acclimatization responses to water deprivation (Cardinale *et al*., 2018). Furthermore, the ubiquitous presence of SLs in the rhizosphere implies that the whole array of organisms in the rhizosphere is exposed to SLs, and thus, it is likely that they have other hidden roles in the interactions between SLs producing plants and rhizosphere organisms yet to be discovered (Yoneyama *et al*., 2013).

1.2.2 *Chemistry of SLs*

All natural SLs identified to date are carotenoid-derived compounds consisting of a butenolide ring (D-ring) linked by an enol ether bridge to a less conserved second moiety (Fig. 1.3). Based on the second moiety, the SL family is divided into (a) the ‘canonical’ strigol-type and orobanchol-type compounds, containing the tricyclic lactone (ABC ring, Fig. 1.3a,b), and (b) SLs lacking the tricyclic lactone, such as the SL precursor carlactone and zealactone (Charnikhova *et al*., 2017) and heliolactone (Ueno *et al*., 2014), produced by maize and sunflower, respectively, and collectively called ‘non-canonical’ SLs (Fig. 1.3c) (Al-Babili and Bouwmeester, 2015; Xie *et al*., 2010; Yoneyama *et al*., 2009; 2010). Finally, SLs with a 2’S configuration between the C and D-ring are called ‘non-natural’ SLs

and, to the best of our knowledge, they do not exist in nature but are product of racemic chemical synthesis (Flematti *et al*., 2016; Zwanenburg and Pospisil, 2013).

So far, 23 canonical SLs have been characterized from plant root exudates (Yoneyama *et al*., 2018), with a tricyclic lactone (ABC ring) and 2'R configured butenolide ring (D ring), being these two structural features required for biological activity (Flematti *et al*., 2016; Scaffidi *et al*., 2014). Strigol- and orobanchol-like SLs differ for the stereochemistry of the B-C-ring junction: the C ring of the strigol-like SLs is in the β orientation (up, 8bS configuration, Fig. 1.3a), whereas that of orobanchol-like SLs is in the α orientation (down, 8bR configuration, Fig. 1.3b) (Al-Babili and Bouwmeester, 2015). The AB part in both families can be modified through methylation, hydroxylation, epoxidation or ketolation, giving rise to the diversity of SLs (Fig. 1.3). Strigol and orobanchol, named after their germination-stimulating activity in seeds of *Striga* and *Orobanche* spp., respectively, are frequently used as references to designate other SLs distinguished by a substitution (e.g., 7-hydroxyorobanchol) or by a different stereochemistry at the C-2' atom or the B-C junction.

Recent advancements in chromatography and spectroscopy have fuelled isolation and identification of novel SLs. In particular, the development of qualitative and quantitative analytical methods for SLs by liquid chromatography connected to tandem mass spectrometry (LC-MS/MS) allow a rapid search for novel SLs in root exudates of various plant species (Sato *et al*., 2003; 2005). Usually, SLs are analyzed by LC-MS/MS using the multiple reaction monitoring (MRM) method. For MRM, transitions of $[M + H]^+$ or $[M + Na]^+$ to $[M + H – D\ ring]^+$ or $[M + Na – D\ ring]^+$, respectively, are monitored to detect SLs as all known SLs contain the same D ring moiety (Xie *et al*., 2010).

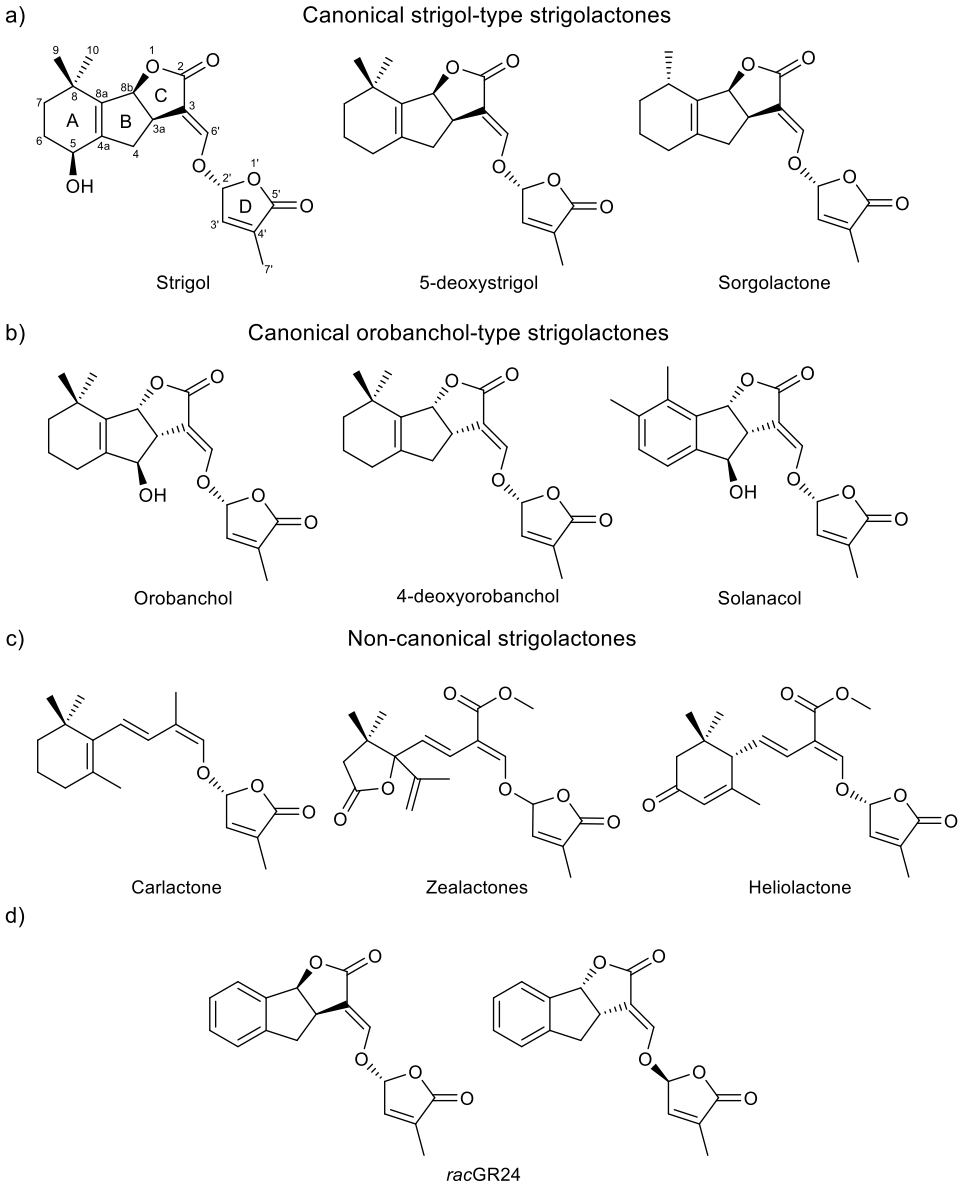

Figure 1.3: Chemical structure of strigolactones (SLs). Naturally occurring SLs can be divided into two families, a) the strigol family and b) the orobanchol family, based on stereochemistry around the BC rings. Chemical differences within a family are related to substitutions on the A or B rings. All naturally occurring SLs found to date display C2'-(R) stereochemistry via the enol-ether bridge that connects the C and D rings. c) 'Non-canonical' SLs (lacking the tricyclic lactone). d) GR24, shown as its two stereoisomers, is the most used synthetic SL.

1.2.3 *Strigolactone biosynthesis*

Recently, great progress has been made in elucidating key steps of SL biosynthesis and signal transduction, enabled by the availability of corresponding mutants from different plant species (Jia *et al*., 2018).

Owing to structural similarities, SLs were originally considered to belong to the sesquiterpene lactones (Akiyama *et al*., 2005; Butler, 1995), a widespread family of compounds formed from the cytosolic compound farnesyl diphosphate. However, the lack of SLs in carotenoid-deficient mutants and the reduced levels of SLs in exudates of plants treated with inhibitors of carotenoid biosynthesis suggested that SLs are derived from carotenoids (Matusova *et al*., 2005). Genetic analyses and enzymatic studies demonstrated that SLs originate from all-*trans*-β-carotene (Fig. 1.4) in a pathway that involves three ancient enzymes, the all-*trans*-/9-*cis*-β-carotene isomerase DWARF27 (D27) and carotenoid cleavage dioxygenase 7 (CCD7) and 8 (CCD8) (Jia *et al*., 2018; Machin *et al*., 2020). The CCD7-mediated, regiospecific and stereospecific double-bond cleavage of 9-*cis*-β-carotene leads to a 9-*cis*-configured intermediate that is converted by CCD8 via a combination of reactions into the central metabolite and SLs universal precursor carlactone (Fig. 1.4) (Alder *et al*., 2012).

These steps of the SL biosynthesis pathway take place in the plastid and the resulting carlactone is then exported into the cytoplasm (Lopez-Obando *et al*., 2015). By catalysing repeated oxygenation reactions that can be coupled to ring closure, CYP711 enzymes then convert carlactone into tricyclic-ring-containing canonical and non-canonical SLs. Modifying enzymes, which are mostly unknown, further increase the diversity of SLs.

Transgenic plants exhibiting reduced CCD7 or CCD8 levels displayed reduced levels of SLs in their exudates and, consistently, increased shoot branching, reduced plant height, increased number of nodes and excessive adventitious root development (Kohlen *et al*., 2012; Vogel *et al*., 2010). These SL mutants constitute a powerful tool to unravel SLs influence and control over plants physiological processes, including responses to nutritional stresses.

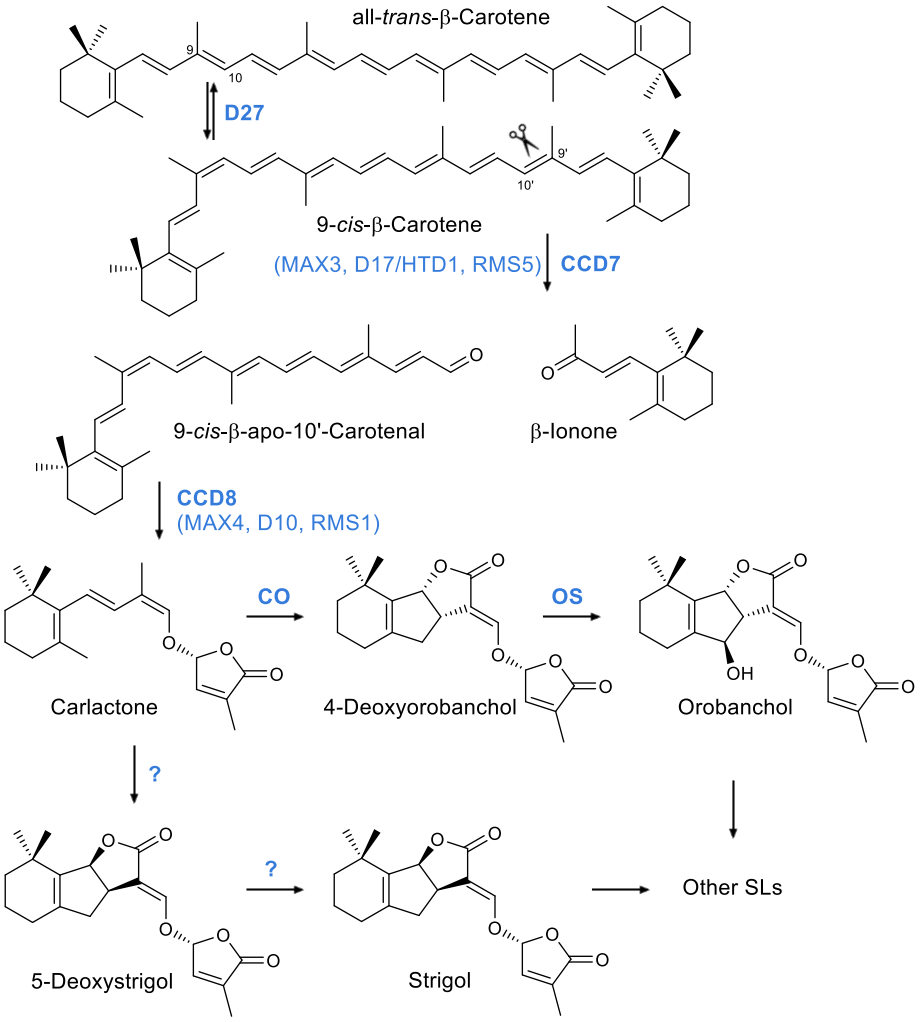

Figure 1.4: Strigolactone (SL) biosynthesis pathway. The carotene isomerase D27 catalyzes the reversible conversion of all-*trans*-β-carotene into 9-*cis*-βcarotene, which is cleaved by the stereospecific carotenoid cleavage enzyme CCD7 at the C9′-C10′ double bond, yielding 9-*cis*-β-apo-10′-carotenal and β-ionone. Then, CCD8 converts 9-*cis*-β-apo-10′-carotenal into carlactone, the central metabolite of the pathway and precursor of canonical and non-canonical SLs. In rice, the MAX1 homolog carlactone oxidase (CO) catalyses repeated oxygenation of carlactone and a stereospecific BC ring closure to form 4-deoxyorobanchol, the parent molecule of orobanchol-like SLs. By introducing a hydroxyl group at the C4 position, a second rice MAX1 homolog, orobanchol synthase (OS), converts 4-deoxyorobanchol into orobanchol. It is assumed that carlactone is also the precursor of 5-deoxystrigol, the parent molecule of the strigol-like SLs. Based on Al-Babili and Bouwmeester, 2015 and Jia *et al.,* 2018.

1.2.4 *Strigolactone production and stability*

Strigolactones are produced by plants at extremely low quantities, and their production is plant dependent. Different plant species and even different varieties within individual crop species produce different SLs and/or mixtures of them (Ćavar *et al*., 2015). Sato and coworkers (2005) showed that average strigol and strigyl acetate production levels in cotton exudates were around 15 and 2 pg/plant/day, respectively, reaching a maximum of exudation after around 5–7 days, while Umehara and coworkers (2008) reported 20 pg/g fresh weight of endogenous 5-deoxystrigol in rice roots. Yoneyama and coworkers (2007a) instead reported around 36 ng/plant of orobanchol in red clover exudates growing in P deficient conditions within 3 days. In addition, the relative amount of SLs in root exudates and tissues is strongly dependent on the plant species and genotype. For instance, the amount of orobanchol was about ten times higher in root tissues extracts than in root exudates of *Pisum sativum* L., 1.4 times higher in *Solanum lycopersicum* L., but less than half in a *Sorghum bicolor* L. cultivar (Floková *et al*., 2020). Strigolactone levels found in roots and in root exudates are also strongly dependent on the availability of nutrients, notably P, and, to a lesser extent, N, that tend to increase SL biosynthesis and exudation (Yoneyama *et al*., 2007; 2012). Rial and coworkers (2019) could detect orobanchol and solanacol (2 µg/L and 60 µg/L, respectively) only in the exudates of P-starved tomato plants, with similar concentration in root extracts, while the same molecules were not detected in the exudates or root extracts of P-replete plants.

The low concentrations at which SLs are produced are not surprising as their activities could be detected at concentrations as low as 10^{-13} M in AM fungi (Akiyama and Hayashi, 2006), 10^{-7} to 10^{-15} M in seeds of parasitic weeds (Xie *et al*., 2010), and 10^{-8} M for GR24 in lateral buds (Gomez-Roldan *et al.*, 2008). The extremely low quantities and their relatively low stability both in aqueous solutions and soil hampered SL isolation and quantification until the development of new sensitive techniques, as described in section 1.2.2. SLs are in fact relatively stable in weakly acidic solutions, but their stability rapidly decreases at alkaline pH (Ćavar *et al*., 2015; Xie *et al*., 2010). Also, they are inherently unstable in soil

and are subjected to hydrolysis, which serves to inactivate and prevent them from accumulating and inducing seed germination in the absence of a suitable host (Zwanenburg and Pospisil, 2013). The SL analogue GR24 exhibited an adequate persistence of 6–8 day in acidic soil (pH 5.0–6.3), whereas of 1–3 days in alkaline soils. The mechanism of hydrolysis follows the addition-elimination pathway reported in Fig. 1.5, analogous to the one generally described for SL signalling (Seto and Yamaguchi, 2014). The hydrolysis involves the enol ether unit and leads to a formilated ABC lactone and 5-hydroxybutenolide (Akiyama *et al*., 2010; Akiyama and Hayashi, 2006; Zwanenburg and Pospisil, 2013).

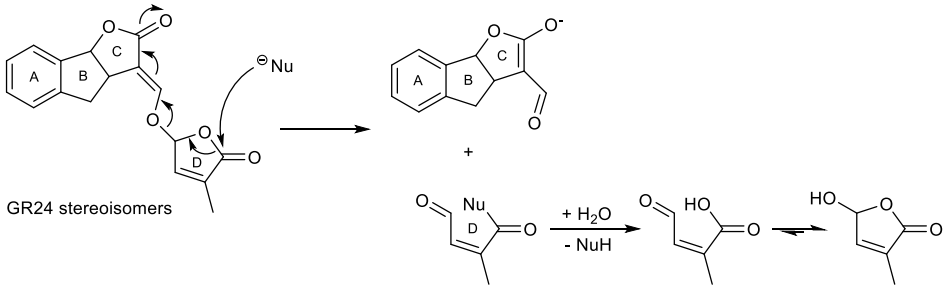

Figure 1.5: Current proposed model for GR24 hydrolysis by nucleophilic attack of the D-ring (based on Flematti *et al*., 2016; Scaffidi *et al*., 2012; Seto and Yamaguchi, 2014). The nucleophilic group attacks the SL butenolide ring leading to the opening of the D-ring and to a formilated ABC lactone. The opened D-ring is then rapidly converted into 5-hydroxybutenolide.

1.3 Phosphorus and strigolactones

The development of a comprehensive understanding of how plants sense P deficiency and coordinate the responses via signalling pathways is a major interest in plant sciences, and a number of signalling players and networks have begun to emerge for the regulation of the P deficiency response (Rouached *et al*., 2010). Accumulating evidence suggests that this response is the result of a complex crosstalk in which a number of hormones, photo-assimilates (sugars), and signals controlling the homeostasis of other ions (e.g., Fe) are involved. Among the many players controlling plant response to P deficiency, SLs are gaining increasing attention since the discovery that low levels of P have a significant stimulatory effect on the production and exudation of SLs by the plant roots (López-Ráez *et al.*, 2008; Yoneyama *et al*., 2007; 2007a).

Apart from being involved in hormonal crosstalk during root development under optimal growth conditions, where they repress lateral roots formation, inhibit adventitious root formation, promote root hair elongation and are positive regulators of primary root (in *Arabidopsis*) (Kapulnik *et al*., 2011; Ruyter-Spira *et al*., 2011), SLs at elevated levels under P-deficiency were shown to increase lateral root formation (Ruyter-Spira *et al*., 2011), affect primary root growth (Niu *et al*., 2013) and promote root hair density (Mayzlish-Gati *et al*., 2012). The involvement of SLs in the regulation of root architecture likely occurs through their crosstalk with the phytohormones auxin and ethylene (Kapulnik *et al*., 2011a; Koltai, 2011; Ruyter-Spira *et al*., 2011). Also, high SL concentrations in plants under P stress are normally accompanied by a suppression of bud outgrowth and shoot branching (Brewer *et al*., 2013; Umehara *et al*., 2010), one of the best characterized phenotypic traits regulated by SLs (see section 1.2.1). Furthermore, the suppression of tiller bud outgrowth in *Oriza sativa* (Umehara *et al*., 2010) and of shoot branching in *Arabidopsis* under P deficient conditions did not occur in SL-deficient and -insensitive mutants (Kohlen *et al*., 2011), highlighting how, in general, mutants defective in the SL pathway are less able to respond to low P conditions (Kohlen *et al*., 2011; Mayzlish-Gati *et al*., 2012; Umehara *et al*., 2008).

In addition to stimulating *de novo* SL biosynthesis, P deficiency can also enhance the exudation of SLs from roots. In fact, some SLs are readily available to be exuded into the rhizosphere after biosynthesis. Experiments on *Trifolium pratense* and tomato revealed that SL exudation negatively correlated with P supply (López-Ráez *et al*., 2008; Yoneyama *et al*., 2007), and dropped after 24 h if plants were transferred to a P sufficient medium (Yoneyama *et al*., 2007). Likely, enhanced SL exudation is in part due to the need to encourage mycorrhizal symbiosis, which helps plants to acquire P from the soil (Yoneyama *et al*., 2007a). In tomato, the increased exudation of such SLs as solanacol, orobanchol, and the didehydro-orobanchol isomers under P starvation correlated with the increased induction of hyphal branching of germinating spores of the AM fungus *Gigaspora margarita* (López-Ráez *et al*., 2008). Interestingly, the stimulation of

SL biosynthesis and exudation under P deficiency is also conserved in plants that are non-host for AM fungi, as *Arabidopsis* (Kohlen *et al*., 2011), even if the physiological function of this exudation remains unclear.

1.4 Aim of the work

Tomato (*Solanum lycopersicum* L.), beyond being a valuable crop worldwide, has become an important model species for research on SLs. The blend of the major SLs produced by this species has been determined, with orobanchol, the two isomers of didehydro-orobanchol and solanacol being the most characteristic, even if the presence of several additional SLs in root exudates and extracts was reported (Kohlen *et al*., 2013; López-Ráez *et al*., 2008). The prompt increase of SL biosynthesis in roots in response to P starvation has been confirmed (López-Ráez *et al*., 2008: Rial *et al*., 2019), and the shoot phenotype of SL-depleted tomato plants was revealed to be consistent with the conserved role of SL in plant development (Kohlen *et al*., 2013; Koltai *et al*., 2010; Vogel *et al*., 2010). Recent studies have also shown that SL biosynthesis is repressed in the roots of tomato plants under drought stress conditions (Ren *et al*., 2018; Rodriguez *et al*., 2010), suggesting that an efficient activation of SL biosynthesis is triggered in response to osmotic stress, activating SL signalling and regulating the tolerance of plants to these adverse conditions (Yang *et al*., 2019). However, whether and how SLs affect the overall plant response to P deprivation in tomato has not been thoroughly investigated.

In the context of the Horizon 2020 European project named TOMRES (***"****A novel and integrated approach to increase multiple and combined stress tolerance in plants using tomato as a model"*), aimed at enhancing tomato plants resilience to combined water and nutrient stress in tomato, the overarching aim of this PhD thesis was to determine how SLs affect the morphological, physiological and molecular processes activated in tomato by P stress and contributing to resilience (Fig. 1.6a). In particular, we investigated the interactions of below-ground traits with P stress resilience, with a special focus on root system architecture and exudate production and composition.

To gather a detailed picture of tomato plants response to diverse P deficiency levels, in the experiments described in the first part of the thesis (**Part I**, including Chapters 2 and 3) P was provided at different concentrations as directly-available inorganic phosphate (Pi), and P stress was applied since the beginning of the experiment or after an acclimation period. More specifically and building upon the existent knowledge on SL-induced root architecture modification in P-deprived plants, in **Chapter 2** we aimed at understanding the impact of SLs on tomato macro- and micro-scopic root features as a response to P starvation, by contrasting wild-type plants with a SL-depleted transgenic line (SL mutants displaying reduced production of SLs). The results showed that, depending on whether plants were grown under totally P-deprived conditions or in suboptimal P levels, SLs significantly affected those root traits associated with nutrient acquisition and that allow for enhanced soil exploration by the roots. In addition, phenotypic differences between the two genotypes were evident at the root morphology and especially at the tip anatomy, providing further evidence in support of the biological role of SLs in mediating plant acclimation responses to P nutritional levels.

To complete the picture of tomato plants acclimatization to P stress, in **Chapter 3** we assayed biomass production, P uptake and accumulation, root exudation kinetics of dissolved organic C, protons, and organic acid anions, root Pi-solubilizing enzymes activity, and PHTs expression in roots of wild-type and SL-depleted tomato plants grown under P-deficient or P-repleted conditions in a hydroponic system. The aim was to evaluate whether impaired SL production may shift P acquisition strategies of plants toward changes in amount and profile of root exudate, and/or in PHT expression, along with the duration of P-shortage. The concentration of available soil Pi seldom exceeds 10 μM in the soil solution (Bieleski, 1973), meaning that most of the P found in soil is not readily available for plant uptake, due to the many fixation processes described in section 1.1.1. Even though adsorption and precipitation are well-known processes contributing to the retention of Pi in soil, it was shown that coprecipitation with Fe significantly contribute to Pi retention, although the retention mechanisms involved in this

process are not fully understood. Furthermore, little is known about the mechanisms of organic P retention during coprecipitation. For these reasons, the second part of the thesis (**Part II**, including Chapters 4 and 5) was devoted to the study of those mechanisms, in particular coprecipitation, leading to reduced P bioavailability in soils and to assay the capacity of tomato plants to scavenge P from sparingly-available P forms, and whether this ability was influenced by SLs.

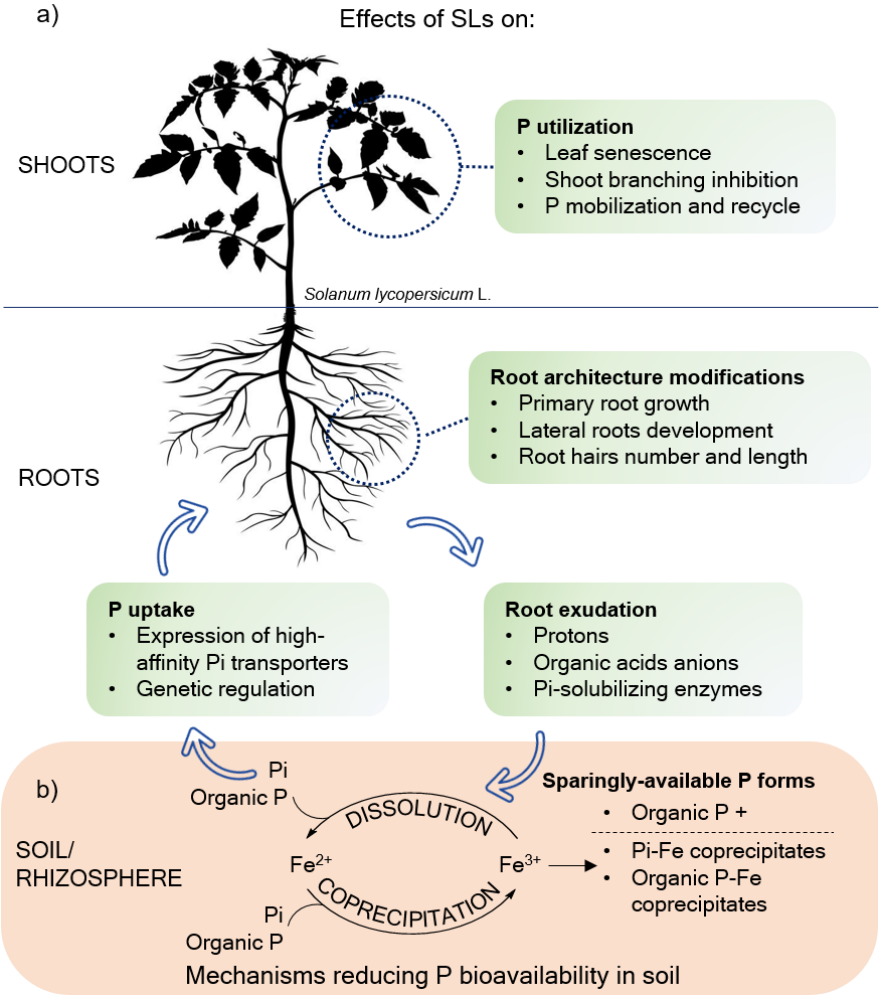

Figure 1.6: General aims of this PhD thesis were a) to determine how SLs affect the morphological, physiological and molecular processes activated in tomato by P stress and b) to study the mechanisms, in particular coprecipitation, leading to reduced P bioavailability in soils and the capacity of tomato plants to scavenge P from sparingly-available P forms, and whether this ability was influenced by SLs.

In detail, in **Chapter 4** we investigated the role of coprecipitation in inorganic and organic P retention through the evaluation of reaction kinetics and properties of the coprecipitates formed during Fe(II) oxidative precipitation in the presence of Pi and phytate (*myo*-inositol hexaphosphate), which constitutes up to 50% of the total organic P in soil and a considerable source of P for plants (Fig. 1.6b). For comparative purposes, we also studied the adsorption of these two P compounds on ferrihyrdrite.

In **Chapter 5** we finally evaluated the adaptation strategies of wild-type and SL-depleted tomato plants when grown in a hydroponic system in the presence of Pi and organic P (in the form of *myo*-inositol hexaphosphate) in the nutrient solution or provided as sparingly-available P in the form of coprecipitates. These adaptation strategies were evaluated in terms of biomass accumulation, P acquisition, enzymatic activity, C and organic acid anion exudation and rhizosphere acidification.

The data presented in Chapter 2 and 4 have been published in:

- Santoro, V., Schiavon, M., Gresta, F., Ertani, A., Cardinale, F., Sturrock, C.J., Celi, L., Schubert, A. (2020). Strigolactones control root system architecture and tip anatomy in Solanum lycopersicum L. plants under P starvation. *Plants* **9**, 612.
- Celi, L., Prati, M., Magnacca, G., Santoro, V., Martin, M. (2020). Role of crystalline iron oxides on stabilization of inositol phosphates in soil. *Geoderma* **374**, 114442.
- Santoro, V., Martin, M., Persson, P., Lerda, C., Said-Pullicino, D., Magnacca, G., Celi, L. (2019). Inorganic and organic P retention by coprecipitation during ferrous iron oxidation. *Geoderma* **348**, 168-180.

Chapter 2 and 4, on which these articles are based, present the main materials and methods, results and discussions which allow for the best interconnection among chapters and overall comprehension of the whole work.

The manuscript presenting the data described in Chapter 3 has recently been submitted (Santoro, V., Schiavon, M., Visentin, I., Constán-Aguilar, C., Cardinale, F., Celi, L. “Strigolactones affect phosphorus acquisition strategies in tomato plants”), while the manuscript discussing the data presented in Chapter 5 is currently under preparation.

Part I
CHAPTER 2

Strigolactones control root system architecture and tip anatomy in *Solanum lycopersicum* L. plants under P starvation

2.1 Introduction

Strigolactones involvement in plant responses to nutrients deprivation, especially P, is now well established (Koltai, 2013; López-Ráez *et al*., 2011; Mayzlish-Gati *et al*., 2012). P is absorbed and assimilated by plants as phosphate anion (Pi), which occurs at fairly low concentrations in the soil solution, typically in the 1–10 µM range (Aziz *et al*., 2014), that is well below the critical level of tens of µM required for optimal plant growth (Hinsinger, 2001). In section 1.1.2 we extensively reported how slight variations of P concentration during plant growth can bring about evident differences in the overall plant development (Wissuwa *et al*., 2005). Dramatic effects on root architecture are reported, for instance, when Pi available for plant uptake is lower than 50 µM (López-Bucio *et al*., 2003). These effects are apparently dependent on the intensity of P deficiency (Schroeder and Janos, 2005; Shen *et al*., 2018).

Previous studies have indicated a major role for SLs as signalling molecules able to trigger morphological, physiological and biochemical responses associated with plant acclimation to P deficiency conditions (Czarnecki *et al*., 2013; Mayzlish-Gati *et al*., 2012; Umehara *et al*., 2010). In P-starved *A. thaliana* plants especially, SLs have been proposed to suppress bud outgrowth and shoot branching to reduce internal P utilization, while initial reports have suggested that SLs promote lateral root development and root hair formation to increase the root surface area in contact with soil, while inhibiting the primary root growth (Czarnecki *et al*., 2013; Kapulnik *et al*., 2011).

Even though the role of SLs as regulators of root development is well-established thanks to detailed investigation on model plants as *Arabidopsis*, pea, petunia and on central crops as rice (Koltai, 2011; Rasmussen *et al*., 2013), **whether SLs**

affect morphological adjustments to P deprivation in tomato has not been thoroughly investigated yet. With this study we therefore **aimed at understanding the impact of SLs on macro- and microscopic root features, as a response to P starvation**. We hypothesized that **even slight variations of Pi concentration in the growing medium or the occurrence of an acclimation period previous to P stress could have significant impacts on tomato roots architecture modification, and that these modifications could be mediated by SLs.** Therefore, we first investigated the effect of exogenous SL on wild-type plants under moderate P deprivation, and further contrasted a wild-type with a SL-depleted transgenic line, assessing primary and lateral root growth under conditions of continuous P deprivation - either complete or moderate. We then assayed the effects of progressively decreasing P supply, to better mimic P availability to plants in field conditions. Finally, we studied in detail the morphology and root tip anatomy of these genotypes under progressive P deficit.

2.2 Materials and methods

2.2.1 *Plant material*

In this study, tomato (*Solanum lycopersicum* L.) M82 was used (wild-type, WT) and contrasted with line 6936, hereafter called SL-depleted (Vogel *et al*., 2010). In this genotype, the key SL-biosynthetic gene *SlCCD7* is knocked down by RNAi and production of the major SLs is thus reduced by about 80–90% compared to its wild-type M82. Both SL-depleted and M82 plants have been previously characterized in terms of SL biosynthesis, shoot branching and mycorrhiza-induced apocarotenoid formation (Vogel *et al*., 2010). Plants were grown under different P conditions and using different substrates, depending on the type of analysis performed, as described below. In all experiments, seeds were surface sterilized in 70% (v/v) ethanol for 2 min, then in 3% sodium hypochlorite for 20 min and washed five times for 10 min with deionized water. Unless otherwise stated, seeds were pre-germinated on wet Whatman filter paper in Petri dishes (10 cm diameter) inside a growth chamber at 22°C and in the dark for 4 days and then grown in growth chambers with a 16/8 h light/dark cycle, air temperature of 22°C and 50–75% relative humidity with a light intensity of 100 µmol $m^{-2}s^{-1}$.

Phosphorus concentrations were chosen based on preliminary results revealing those more effective in causing the most pronounced differences under each experimental set-up.

2.2.2 *Root system architecture changes in response to exogenous application of the synthetic SL analogue* rac-*GR24*

The dependence of root architecture features on SL availability was studied in tomato seedlings grown in vitro. WT seedlings were grown in square Petri dishes (12x12 cm) containing either a full Murashige and Skoog (MS) medium (Murashige and Skoog, 1962) as a positive control (high P, 625 µM) or a modified MS medium with low levels of KH_2PO_4 (low P, 6.25 µM). For each P condition, the synthetic SL analogue *rac*-GR24 was dissolved in 0.1% acetone at 5 µM final concentration (SL-treated groups) while comparable amounts of acetone solution were added to the control groups for mock treatment. Pre-germinated seeds of WT plants were sown (6 seeds per plate, 1 plate per treatment; each seedling a biological replicate) and the Petri dishes were placed vertically in a walk-in growth chamber. Two weeks after sowing, the length of the primary root and the number of lateral roots were evaluated by scanning the plates and analyzing the images using the software ImageJ. Fresh shoot and root biomass were also quantified at the end of the trials. To confirm results, this experiment was repeated twice.

2.2.3 *Root system architecture phenotyping of WT and SL-depleted plants grown under continuously medium or no P conditions*

After germination, WT and SL-depleted seeds were transferred to columns (5 cm diameter x 12 cm height) containing quartz sand (<1 mm) and placed inside a growth chamber (Conviron A1000, Canada). Plants were watered daily with a modified Hoagland nutrient solution containing either 80 µM KH_2PO_4 (medium P) or no KH_2PO_4 (no P). After 10 days of growth, each column was placed into a scanner (GE v|tome|x M 240 kV) and scanned using X-ray energy settings of 140 kV and 160 µA, in “FAST” mode. Three individual scans were required to image the entire column depth at a resolution of 35 µm. Scanned radiograph images were then reconstructed and combined in DatosX REC software (GE

Measurement & Control, Germany) and 3D images were visualized with VGStudioMax v2.0 (Volume Graphics GmbH, Germany). The following root traits were recorded: total root length, primary root length, root surface area, root volume, average lateral root length, root tip number (indicative of total root number). Root trait data were obtained with Rooth software (Mairhofer *et al*., 2017).

2.2.4 *Root system architecture phenotyping of WT and SL-depleted plants grown under increasing levels of P starvation*

To evaluate the effect of increasing P nutritional stress on both root system architecture and anatomy of WT and SL-depleted tomato plants, pre-germinated seeds of the two lines were transferred to square Petri dishes (10x10 cm) filled with a modified half-strength MS medium (Murashige and Skoog, 1962), containing either medium (80 µM) or low (10 µM) KH_2PO_4, at a density of 5 seeds per plate, and allowed to grow for 10 days inside a growth chamber. Representative WT and SL-depleted plants grown under medium or low P were then transferred for one week to sterile boxes (13 cm length x 20 cm height x 2 cm depth), at a density of 3 plants per box, containing the same MS medium as described previously, with either 80 µM KH_2PO_4 (medium P) or no KH_2PO_4 (no P), respectively. Specifically, WT and SL-depleted plants previously given with 80 µM of KH_2PO_4 were grown under the same P concentration, while WT and SL-depleted plants initially treated with low P were transferred to MS medium without P. To obtain a full picture of the root system, root scanning was performed using an Epson Expression 10000XL 1.0 system (Regent Instruments Company, Canada) (Ding *et al*., 2014). The following parameters were recorded with a root image analysis system using the software WinRHIZO: root length (cm), surface area (cm^2), volume (cm^3), average diameter (mm), number of tips (referred to roots with a diameter < 2mm) and lateral roots (referred to roots with a length varying from 0 to 4.5 cm).

2.2.5 *Stereo and light microscopy*

Roots were further analyzed via microscopy. The root tip of WT and SL-depleted plants initially grown with either high or low P and further transferred to either medium P (80 µM KH_2PO_4) or no P (0 µM KH_2PO_4) were first subjected to observation under a stereomicroscope (Leica Microsystems). Root tip segments were collected for additional analyses of root anatomy, fixed in 6% glutaraldehyde and processed for light microscopy as previously described (Bonghi *et al.*, 1993). Thin sections (1 µm thick) were cut with an Ultracut Reichert-Jung ultramicrotome, stained with 1% toluidine blue and 1% tetraborate (1:1, v/v), and observed and photographed under a Leitz Ortholux microscope.

2.2.6 *Statistics*

For all datasets, the analysis of variance (one-way ANOVA) was performed using the SPSS software version 18.0 (SPSS, Chicago, IL, USA), and was followed by pair-wise post-hoc analyses (Student-Newman-Keuls test) to determine which means differed significantly at $p < 0.05$ (± SE). Figures were created using SigmaPlot ver. 12.5 software (Systat, San Jose, CA, USA), with means presented with standard errors.

2.3 Results

2.3.1 *Exogenous SLs increase primary root length and lateral root number under continuously low P availability*

As a first step to assess whether SLs affect root morphology depending on the P status, we scored root biometrics on M82 seedlings grown in vitro in the presence or absence of 5 µM exogenous SL (in the form of the synthetic analogue *rac*-GR24), under high and low P conditions. No significant differences in primary root length were observed following treatment with *rac*-GR24 in high P seedlings; conversely, *rac*-GR24 treatment significantly increased primary root length of low P seedlings (Fig. 2.1a). The lateral root number also increased in *rac*-GR24-treated seedlings only at low P (Fig. 2.1b). Accordingly, root fresh weight increased following SL treatment at low P compared to high P *rac*-GR24-treated seedlings, suggesting that the effects of *rac*-GR24 treatment on root diameter

depend on the P status (Fig. 2.1c). No appreciable changes in shoot biomass were observed under any condition (Fig. 2.1d).

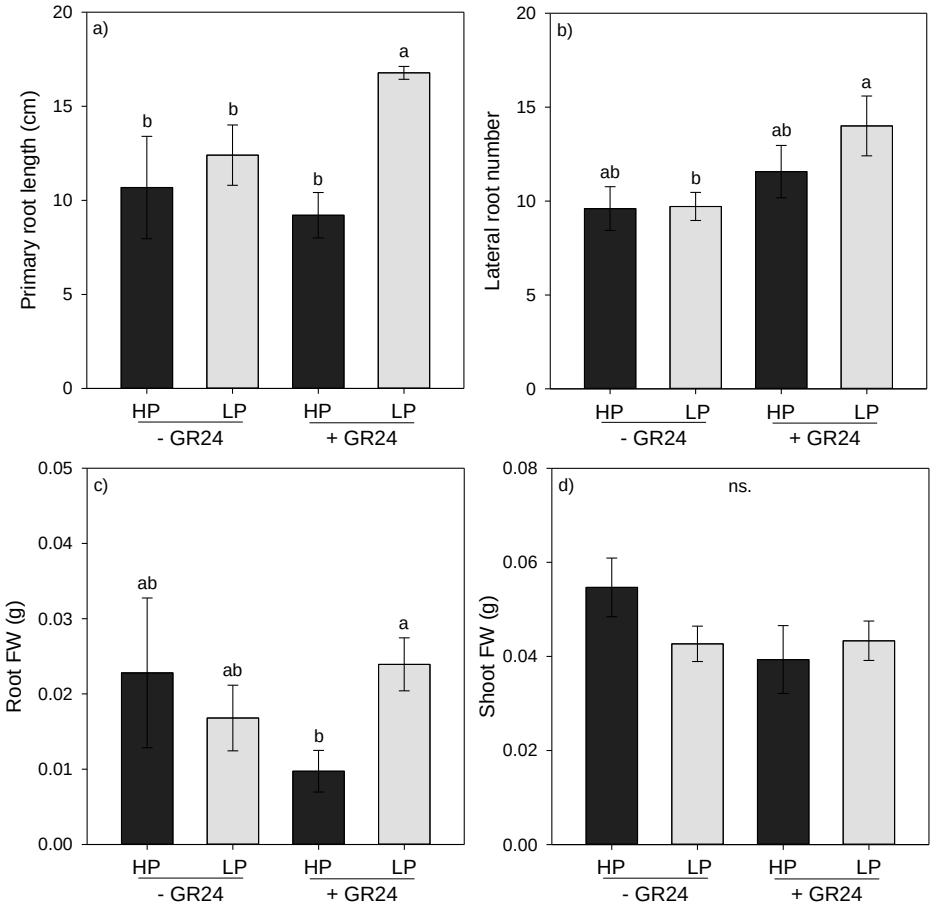

Figure 2.1: Main biometrics of two-week-old wild-type (WT) seedlings grown either in a standard MS medium (high P, HP) or in P-deprived conditions (low P, LP), with (+GR24) or without (–GR24) 5 µM *rac*-GR24: a) primary root length; b) number of lateral roots; c) root fresh biomass; d) shoot fresh biomass. Each column represents the average of three (c,d) to six seedlings (a,b) (± SE). Statistical significance of differences between means is indicated by different letters above bars ($p < 0.05$).

2.3.2 *Strigolactone depletion alters primary and lateral root growth under continuously high or no P conditions*

In order to confirm data obtained with exogenous SLs, we contrasted the response of a WT genotype (M82) with a SL-depleted transgenic line grown under conditions of zero P (no P addition) and medium P (80 µM Pi) using X-ray computed tomography (CT) (Fig. 2.2a). Differences in root traits were evident between WT and SL-depleted plants, both under zero P and medium P conditions (Fig. 2.2b-g). Total root length (Fig. 2.2b) strongly correlated with the average lateral root length (R^2=0.995). Average lateral root length, root surface area, volume and lateral root number (Fig. 2.2c,e-g), followed a similar trend, whereby impairment of SL synthesis weakly decreased these parameters under both P regimes. On the contrary, in this experimental set up, primary root length was not affected by impairment of SL biosynthesis under either P supply status (Fig. 2.2d).

Figure 2.2 (following page): a) Image of tomato plants root architecture displayed by X-ray CT; b-g) root growth-associated parameters of wild-type (WT) and SL-depleted plants (SL–) grown for 10 days inside columns filled with quartz sand and daily watered with modified Hoagland solution containing either medium P (MP) or no P (–P). Data represent the means of measurements on 3 independent replicates per genotype and condition (± SE) obtained via X-ray CT. Different letters above bars indicate significant differences between treatments ($p < 0.05$).

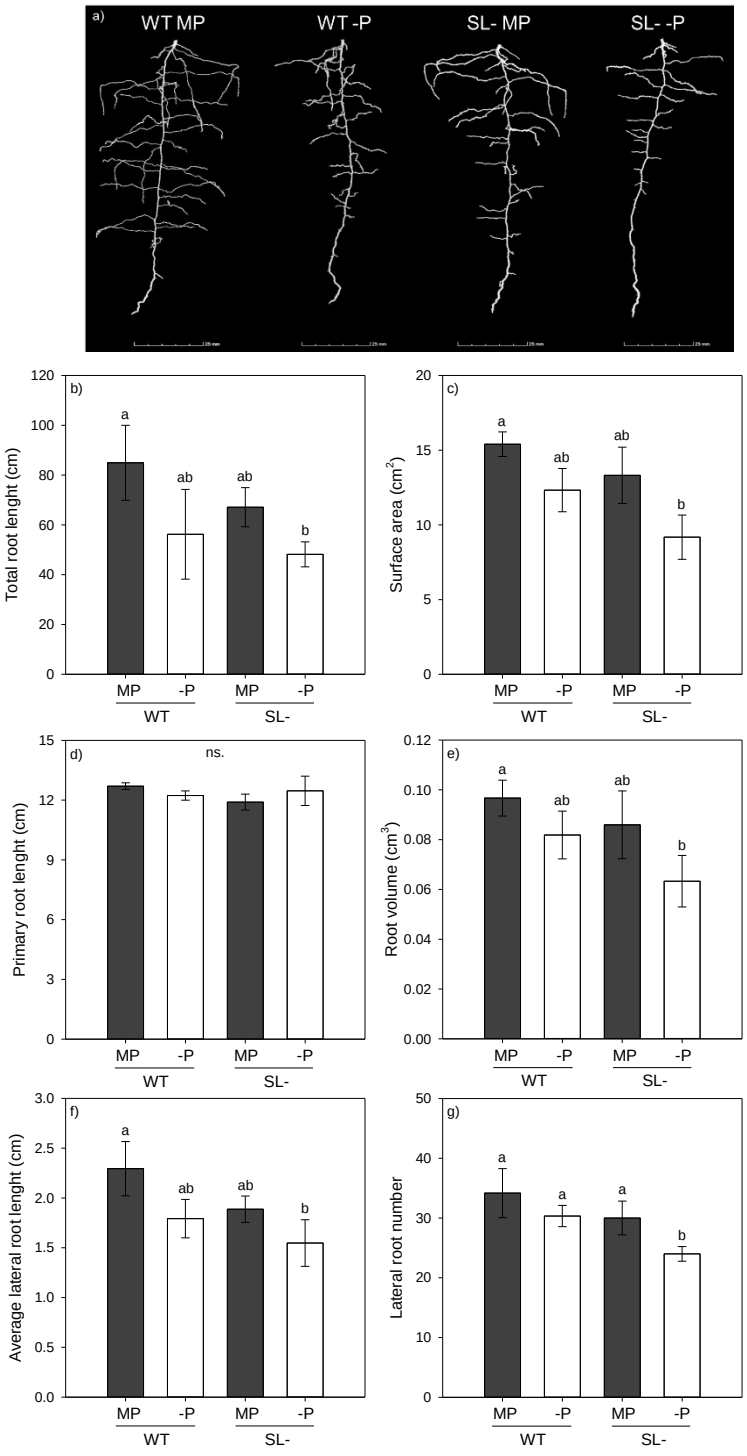
a)
WT MP
WT -P
SL- MP
SL- -P
b)
Total root lenght (cm)
c)
Surface area (cm²)
d)
ns.
Primary root lenght (cm)
e)
Root volume (cm³)
f)
Average lateral root lenght (cm)
g)
Lateral root number
MP
-P
WT
SL-

2.3.3 *Strigolactone depletion affects root system architecture of plants grown under increasingly severe P starvation*

Constant P provision or sudden P unavailability may not be common conditions for plants in field environments, as P availability in soils can be progressively reduced due to plant uptake or fixation processes. Thus we set up an experiment where WT and SL-depleted plants were first grown in vitro for 10 days under low or medium P supply; then, medium-P plants were transplanted to an agar medium with the same P concentration, while low P plants were transplanted onto agar medium containing no P. After 10 days of growth in low P, WT plants displayed higher values of total root length compared to SL-depleted plants (Fig. 2.3a). No differences in root length were observed between WT and SL-depleted plants under medium P supply. This trend was similar as for root surface area (although not significantly in this case, Fig. 2.3b) and root tip number (Fig. 2.3c). Root volume (Fig. 2.3d) and diameter (Fig. 2.3e) only significantly decreased in SL-depleted plants under low P conditions with respect to medium P. No significant variation in lateral root number was revealed between plants under any conditions (Fig. 2.3f). When WT and SL-depleted plants were transferred to new agar plates to either maintain medium P or further decrease low P to no P status (hereby called zero P), differences in root traits became more prominent (Fig. 2.4). Specifically, total root length of plants grown at zero P was substantially lower in SL-depleted than in WT while still no differences were recorded between genotypes under medium P (Fig. 2.4a). The root tip number (Fig. 2.4c) and the root volume (Fig. 2.4d) showed the same behaviour, with values significantly increasing in WT plants under no P, but not in SL-depleted plants. This trend was similar for root surface area, although with no significant differences in this case (Fig. 2.4b). Differences were not significant for root diameter (Fig. 2.4e), while lateral root number decreased significantly in SL-depleted plants at zero P reinforcing a non-significant trend observed also in WT plants (Fig. 2.4f). This suggests that acclimation to zero P (in terms of greater root volume and higher lateral root number) is promoted by a period of growth on low P, and that such acclimation process is favoured by SLs.

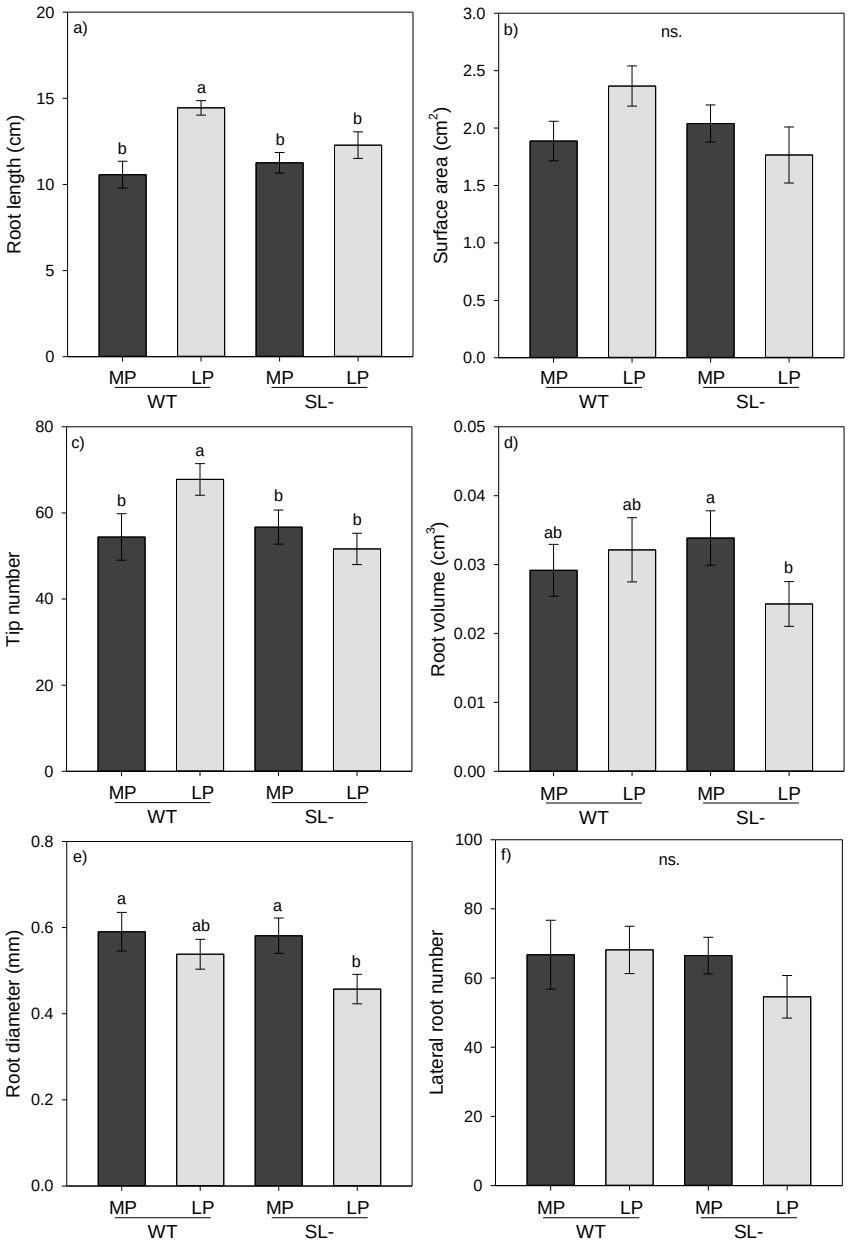

Figure 2.3: Root growth-associated parameters of wild-type (WT) and SL-depleted plants (SL–) grown for 10 days in MS medium with either medium P (MP) or low P (LP). a) Root length; b) surface area; c) tip number; d) root volume; e) root diameter; f) lateral root number. Data represent the means of 14 measurements per treatment (± SE) obtained via WinRHIZO. Different letters above bars indicate significant differences between treatments ($p < 0.05$).

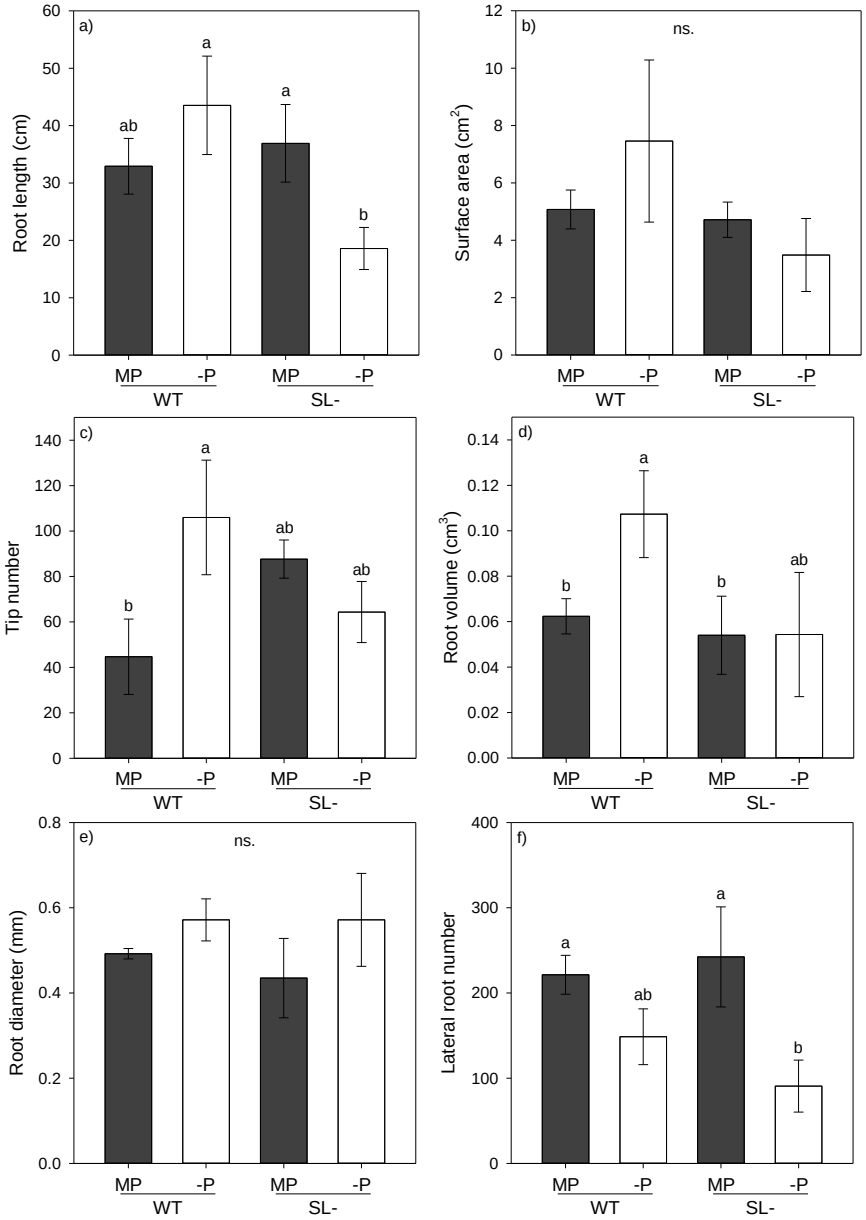

Figure 2.4: Root growth-associated parameters of wild-type (WT) and SL-depleted plants (SL–) grown for 10 days in MS medium with either medium P or low P and further transferred for one week to MS medium containing either medium P (MP) or no P (–P), respectively. a) Root length; b) surface area; c) tip number; d) root volume; e) root diameter; f) lateral root number. Data represent the means of 3 measurements per treatment (± SE) obtained via WinRHIZO. Different letters above bars indicate significant differences between treatments ($p < 0.05$).

2.3.4 *Strigolactone depletion alters root tip morphology and anatomy under different P availability*

As SL depletion was shown to reduce root growth under low P availability, we hypothesized that this may be linked to anatomical modifications. We thus analyzed root tip morphology and anatomy in WT and SL-depleted plants grown under the same experimental set-up as in the previous experiment, i.e., either with medium P or no P supply, in the latter case after transfer from low P (acclimation period). The root tips of WT plants were similar in shape, irrespective of P supply (Fig. 2.5a,b), with abundant root hairs along the differentiation zone without visible differences in length (Fig. 2.5e,f). However, WT plants seemingly produced more root rhizodeposition at the area of cell division and along the elongation zone when grown at zero P after an acclimation period on low P than when kept under medium P conditions. This is suggested by the more abundant rhizodeposition on the fine hairs of WT plants under zero *vs* medium P (Fig. 2.5a,b). In SL-depleted plants, the undifferentiated zone of the root tip was shorter compared to WT plants, with a different shape compared to WT plants and depending on P supply (Fig. 2.5c,d,k). Specifically, the root tip was clearly cone-shaped in SL-depleted plants under medium P (Fig. 2.5c,k), but club-shaped and rounder under zero P (Fig. 2.5d). Under zero P, the root tip in SL-depleted plants was abundantly coated by root exudates and displayed shorter root hairs (Fig. 2.5h,j) compared with plants gown at medium P (Fig. 2.5g) and with WT plants under either P condition (Fig. 2.5e,f,i). Conversely, root hairs in SL-depleted plants were only slightly shorter compared to WT plants under medium P conditions, but their density seemed to be higher than in the WT under any condition and especially under zero P.

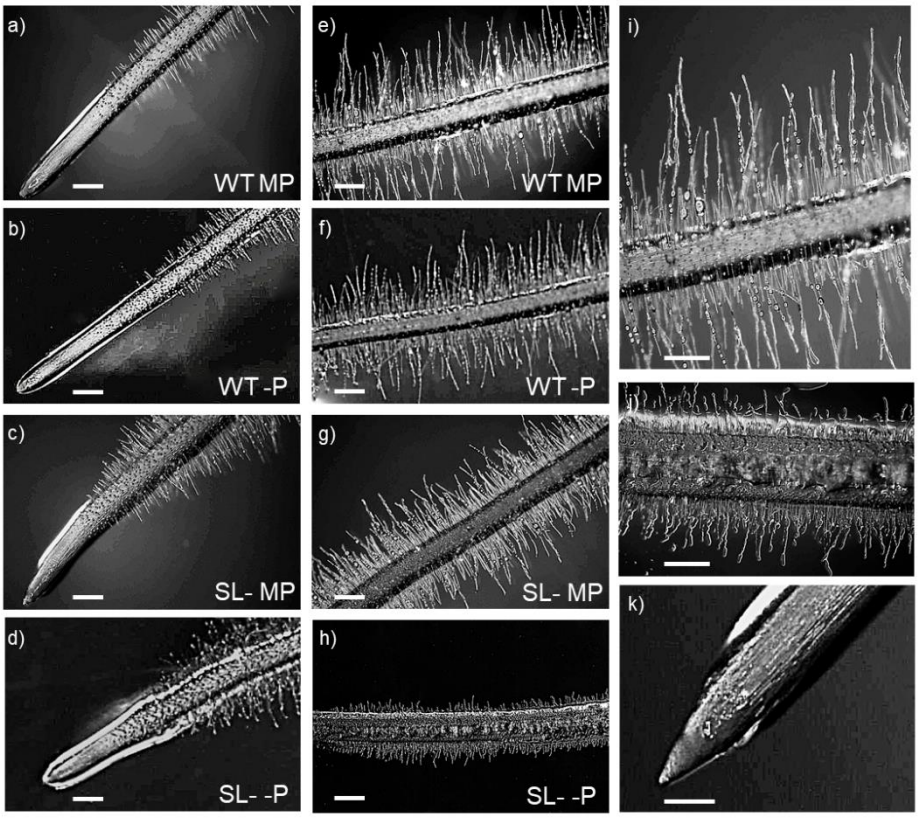

Figure 2.5: Root tip morphology of wild-type (WT) and SL-depleted plants (SL–) grown for 10 days in MS medium with either medium P or low P and further transferred for one week to MS medium containing either medium P (MP) or no P (–P), respectively. a-d) Root primary morphology, differentiation zone and tip of plants: a) WT under MP; b) WT under –P; c) SL– under MP; d) SL– under –P. e-h) Zoom-in on the root differentiation zone of plants: e) WT under MP; f) WT under –P; g) SL– under MP; h) SL– under –P. i) Higher magnification of WT MP differentiated root primary structure; j) higher magnification of SL– –P differentiated root primary structure; k) higher magnification of SL– MP root tip. Scale bars: a-h) 200 µm; i-k) 1 mm.

These observations were further confirmed by transmission light microscopy analyses (Fig. 2.6 and 2.7). The root tips of WT plants grown under medium P conditions showed the expected anatomical organization (Fig. 2.6). The meristematic apex at the root tip consisted of small cells with isodiametric shape and a large nucleus in the center. The meristematic zone was longitudinally shorter compared to that observed at the root tip of P-starved WT plants. In the

elongation zone, cells showed juvenile characteristics with diffuse vacuolization suggesting ongoing differentiation processes.

In the differentiation zone, cells larger in size were evident, each one enclosing a prominent central vacuole, which is a typical feature of adult cells (Fig. 2.6 and 2.7b). Phosphorus starvation caused anatomical changes in the root tips of WT plants, such as the extension of the meristematic zone along the longitudinal axis. This zone was, however, well organized, characterized by typical small cells, each one with a large nucleus in the centre (Fig. 2.6 and 2.7c,d). In the elongation zone, cells maintained the nucleus in central position with several vacuoles scattered in the cytoplasm, which is typical of cells that are differentiating, but are not yet adult. The formation of large adult cells containing one or few vacuoles was clearly delayed compared to WT plants under medium P conditions.

In roots of SL-depleted plants supplied with medium P, the tip and meristematic apex were cone-shaped, consistent with stereomicroscopy evidence (Fig. 2.5k and 2.6), and a number of cells in the cap contained several small vacuoles (Fig. 2.6 and 2.7e). Also, numerous cells displayed isodiametric shape, large central nucleus and intense vacuolization above the meristematic apex, along the root longitudinal axis (Fig. 2.6 and 2.7f). As observed for WT plants under no P, the acquisition of adult cell features was delayed compared to WT under medium P supply. Finally, the root tips of SL-depleted plants swell under no P, consistently with the club-shaped morphology observed under stereomicroscopy, and showed significant signs of tissue disorganization (Fig. 2.6 and 2.7g). At the level of the meristematic apex and cap, cells contained a central nucleus and several small vacuoles, showing signs of differentiation. Above them, several more cells showed diffused vacuolization. Also, a restricted group of cells with meristematic traits was visible, while the root cap was inconspicuous. The differentiation zone, which is formed by typical adult cells, was maintained (Fig. 2.6 and 2.7h).

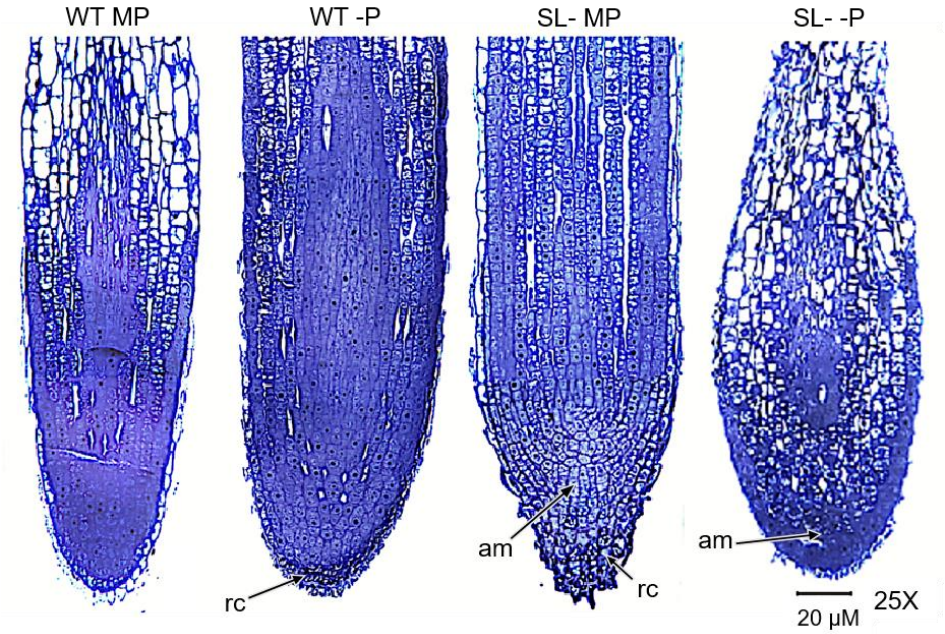

Figure 2.6: Light micrographs of longitudinally sectioned root tips of wild-type (WT) and SL-depleted (SL–) plants grown for 10 days in MS medium with either medium P or low P and further transferred for one week to MS medium containing either medium P (MP) or no P (–P), respectively. In WT MP plants, the postmitotic isodiametric growth zone is reduced in length compared to WT –P plants, and the cells acquire an elongated shape closer to the apical meristem (am). In WT –P plants, an extended postmitotic isodiametric growth, with cells maintaining their isodiametric shape, is visible throughout the root tip. Note the wider root tip diameter compared to WT MP plants. In SL– MP plants, note the root cap (rc) with cells enclosing several small vacuoles, the cone shape of the root apex, and the maintenance of cells with meristematic features along the root longitudinal axis. Above the apical meristem are many cells with isodiametric shape and several vacuoles scattered in the cytoplasm. The root tip of SL– –P plants is swollen and displays high levels of disorganization. A small apical meristem is visible in the center. Above it, most cells are elongated, with a large central vacuole. Below it, cells are isodiametric with several small vacuoles.

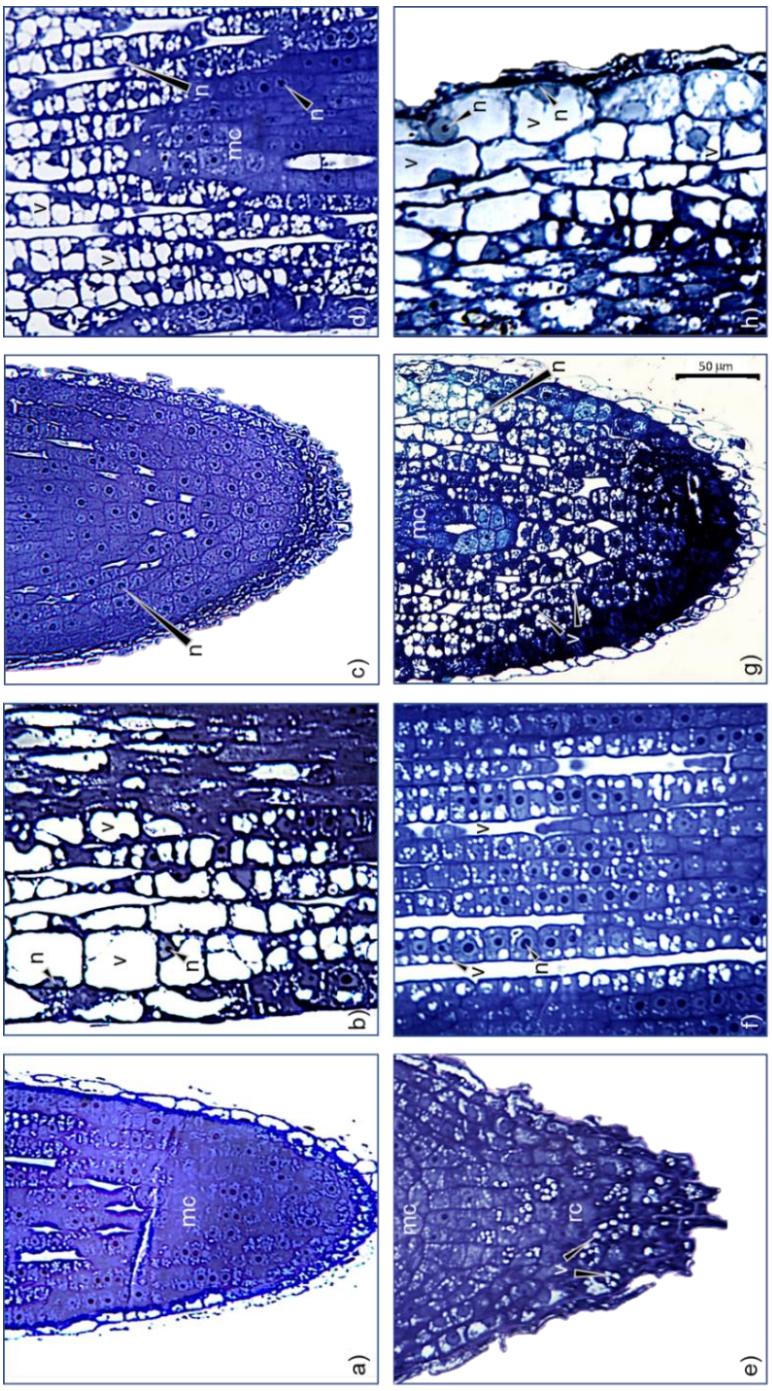
a)
b)
c)
d)
e)
f)
g)
h)
mc
n
v
rc
50 µm

Figure 2.7 (previous page): Light micrographs of selected areas of longitudinally sectioned root tips of wild-type (WT) and SL-depleted (SL–) plants grown as in Fig. 2.5 and 2.6. High magnification images of a) the root apex (mc: meristematic cells) and b) elongation/differentiation zones of WT MP plants (about 100 µm above the apical meristem); c) the root apex and d) elongation zone (about 200 µm above the apical meristem) of WT –P plants. Cells have a big central nucleus (n), isodiametric shape, and some are still dividing; e) the root cap (rc) and f) elongation zone (about 200 µm above the apical meristem) of SL– MP plants. Note the presence of numerous vacuoles (v). The cells show very juvenile characteristics, with large nuclei and numerous small vacuoles scattered in the cytoplasm; g) the root apex of SL– –P plants. Note the small cells enclosing numerous vacuoles in the root cap and below the root apex; h) the area about 100 µm above the apical meristem in SL– –P plants. Note the transition from cells with several vacuoles to cells bigger in size with one central vacuole.

2.4 Discussion

In the current study, we investigated the effects of SLs on root growth and architecture, morphology and anatomy by comparing WT and SL-treated or SL-depleted tomato plants under different P supplies. We first examined the effects of the exogenous application of *rac*-GR24 on root development of WT plants grown under either P-sufficiency or low P conditions. Then, we assayed the effects of impaired SL synthesis on architecture and anatomy of roots adjusting to different P nutrition supply during growth.

rac-GR24 is the most widely used synthetic SL analogue, with similar biological activity to that of endogenous SLs (Gomez-Roldan *et al*., 2008; Umehara *et al*., 2008). In this study, *rac*-GR24 application to WT tomato plants grown under P-limiting conditions increased the primary root length and number of lateral roots, and favoured biomass allocation to the roots (Fig. 2.1). Conversely, WT plants grown at high P were apparently not sensitive to exogenous *rac*-GR24 with respect to such traits. *rac*-GR24-induced root elongation was previously observed in tomato (Koltai *et al.*, 2010) and *A. thaliana* (Ruyter-Spira *et al*., 2011) plants, and was ascribed to the increase in number and length of cells located in the root meristem and transition zone, according to the auxin status of the plants (Koltai *et al.*, 2010a; Ruyter-Spira *et al*., 2011). In *A. thaliana*, primary root elongation was accompanied with a decrease of lateral root density and delayed development (Kapulnik *et al*., 2011a; Mayzlish-Gati *et al*., 2012; Ruyter-Spira *et al*., 2011). In these studies, SLs were proposed to act as modulators of the auxin

flux, thus altering the auxin optima for lateral root formation. Therefore, under low P conditions, changes in root system architecture were attributed to increased sensitivity to auxin (Koltai *et al*., 2010a; Ruyter-Spira *et al*., 2011). Interestingly, *rac*-GR24 application was reported to determine not completely overlapping effects in P-deprived rice plants, where it decreases primary root length and increases lateral root density (Sun *et al*., 2014). However, it is noteworthy that P shortage inversely modulates these parameters in rice compared to *A. thaliana*, by increasing primary root length and reducing lateral root density (Arite *et al*., 2012; Pérez-Torres *et al*., 2008; Sun *et al*., 2014). In both species, variation in primary root length and lateral root density were ascribed to the (either promoting or inhibiting) effects of SLs on auxin transport within the root (Koltai *et al*., 2010a; Sun *et al*., 2014; 2019). In our study, we suppose that exogenous *rac*-GR24 may have acted in roots of tomato plants via a crosstalk with auxin similarly to other species, and we suggest that, in tomato, SLs contribute to adjust those root traits that may favour better soil exploration under low P availability. Additional mechanisms governing SL effects on root development of tomato plants growing under P shortage, including the interaction of SLs with key molecular players in the phosphate starvation response and/or other phytohormones than auxins, cannot be excluded (Koltai, 2013; Ma *et al*., 2003; Villaécija-Aguilar *et al*., 2019). As a final note on this subset of data, it is worth noting that the racemic mixture we employed contains two stereoisomers, one of which can stimulate the KAI2-dependent pathway in *Arabidopsis* (Scaffidi *et al*., 2014). This same pathway was recently proven to influence specific root traits in this plant (Villaécija-Aguilar *et al*., 2019), with a possible confounding effect that is, however, still unproven in tomato.

The important role of SLs in modifying root traits of tomato plants during acclimation to P limiting conditions was also confirmed by the comparison between WT and SL-depleted plants grown with medium P, no P, or low P levels. Plants continuously grown under no P since soon after germination, as in the X-ray CT experiment (Fig. 2.2), had an overall less developed root system; the typical responses to sudden or gradual P stress, such as decreased length of

primary root, increased lateral root length and topsoil foraging (Lynch, 2011; Péret *et al*., 2011; 2014) were not visible in either genotype. This apparent lack of response to nutritional stress both in the WT and the SL-depleted plants may be due to the fact that full root growth could not be supported in the complete absence of P, hence preventing also meaningful morphological adjustments to stress in the WT (Wissuwa *et al*., 2005). Furthermore, a study with tomato suspension cells revealed that P shortage induced elevated expression of a phosphatase that catalyzed internal P remobilization, allowing tomato seedlings to use stores of phytic acid and preventing the onset of the typical morphological and biochemical symptoms of P-deficiency during the first 10 days of growth (Bozzo *et al*., 2005). When WT plants were grown under low P conditions, instead, their total root length and tip number were increased compared to WT plants supplied with medium P levels, as expected; such response was not displayed by SL-depleted plants (Fig. 2.3). Our experiments also indicate that, in tomato, low SL synthesis affects the ability of roots to respond to more gradual P decrease when plants are transferred from low P to no P, i.e., when they are allowed to acclimate before being exposed to complete P deprivation (Fig. 2.4). Under these settings, a significant decrease in total root length was observed in P-starved SL-depleted plants compared to both SL-depleted plants and WT plants receiving higher P. This decline was not due to less primary root elongation, but rather to a decline in lateral root number and length. These results provide further evidence of the role of SLs as regulators of lateral root formation and development, consistent with observations reported in the *A. thaliana* SL-biosynthesis mutant *max4-1* (Mayzlish-Gati *et al*., 2012). As for SL-dependent morphological responses at the root level reported in other plant species (Ruyter-Spira *et al*., 2011; Sun *et al*., 2019) these may happen via the modulation of auxin fluxes and localized auxin levels along the root axis of tomato as well.

Root hair development is under hormonal control (Omoarelojie *et al*., 2019) and increasing the amount of root hairs is a common strategy adopted by P-deprived plants to enhance the capacity of their roots to explore the rhizosphere for P scavenging (Aziz *et al*., 2014; Lynch, 2007). A SL-auxin crosstalk has been

proposed to regulate root hair formation and elongation, with SLs triggering the increase in auxin accumulation in root epidermal cells through modulation of auxin flux from the root (Czarnecki *et al*., 2013; Kapulnik *et al*., 2011a; Koltai *et al*., 2010a; López-Bucio *et al*., 2003). However, these reports were reassessed recently, leading to the conclusion that the sibling pathway initiated by KAI2 is instead responsible for root hair elongation in *Arabidopsis* (Villaécija-Aguilar *et al*., 2019). Whether this holds true in tomato as well has not been addressed. In this work, we observed that, in addition to the reduction of lateral root growth (a trait that was confirmed to depend on SL in *Arabidopsis*), SL-depleted plants grown under P starvation exhibit a dramatic decrease in root hair elongation compared to the WT (Fig. 2.5). Thus, we propose that lower SL levels in tomato roots prevent root hair elongation under P deficiency, possibly by altering auxin levels in epidermal cells. It is noteworthy that, although root tips of SL-depleted, P-sufficient plants were characterized by only slightly shorter root hairs compared to WT plants, their density was apparently higher.

If, on the one hand, root hairs are important to increase the root surface area and the portion of soil explored by roots, on the other hand root tips are of primary importance in nutrient sensing. The physical contact with low P media is necessary to reprogram the whole root architecture (Abel, 2011; Svistoonoff *et al*., 2007), with inorganic P itself acting as a signalling molecule (Ticconi *et al*., 2004). Therefore, analyzing changes in root tip morphology and anatomy could help in elucidating the overall plant response to nutrient stress. Clear alterations of root tip anatomy in SL-depleted, P-starved plants were visible (Fig. 2.6 and 2.7), which may explain why these plants were less efficient in developing their roots under P starvation when compared to the WT. The root tip was indeed characterized by extensive cell and tissue disorganization, possibly due to unbalanced levels not only of SLs, but also other hormones known to control cell division and differentiation processes at the root apex (Niu *et al*., 2013). Tomato seems hypersensitive to P-limitation stress when SL biosynthesis is reduced. This hypothesis is supported by the observation that, in P-sufficient plants, low SLs caused moderate anatomical changes in the root tip, which were similar to

those observed in WT plants shifted to no P supply after acclimation at low P. In the latter group, the root meristem was more developed than in WT under adequate P, thus indicating that division processes of WT plants were not affected by P deficiency under our experimental conditions, at least at the root apex. Additionally, the processes of cell differentiation and maturation were clearly delayed compared to WT plants kept under medium P conditions. Instead, the root apex of SL-depleted plants was markedly altered under P stress. Low SL biosynthesis along with P starvation, and complex cross-talks of SLs with other hormone pathways could be responsible for such observed alterations. Strigolactones indeed proved to promote crown root elongation by stimulating meristematic cell division, via modulation of the local auxin concentrations controlling meristem cell number (Arite *et al*., 2012). Auxins could further interact with the cytokinin signalling pathway that impacts stem cells patterning. The overall shape was different and peculiarly club-shaped; the internal anatomy showed some hallmarks of the determinate developmental reprogramme that is induced by P starvation in *Arabidopsis* (Sánchez-Calderón *et al*., 2005). Previous studies have shown indeed that the rates of cell division at the root meristem and of root cell elongation decline in *A. thaliana* with decreasing P availability, and concomitantly the number of cells within the elongation zone is reduced while early differentiation and meristem reduction is observed (Rouached *et al*., 2010). The activity of meristems within a plant is tightly coordinated to optimize root growth in response to environmental conditions and many mobile signals, including auxin, cytokinins, and possibly SLs can modulate cell growth and differentiation, as well as meristem shape (Brewer *et al*., 2015; Niu *et al*., 2013). Interestingly, SL-depleted plants under P-replete conditions exhibited a cone-shaped root tip, coated by a prominent root cap formed by cells with diffuse vacuolization, which could contribute to rhizodeposition. Intense rhizodeposition in SL-depleted plants was most pronounced under P starvation, where root tips presented not only vacuole-rich cells in the root cap but also below/around the apical meristem. Rhizodeposition seemingly was also greater in WT plants in P deprivation compared to non-stressed WT, as revealed by stereomicroscopy.

Despite the effects of defective SL production combined with P starvation being clear and consistent at the root level, differences between genotypes were in general not significant under adequate P conditions. These results suggest that, at least when abundant P is available, SL-depleted plants maintain their capacity to acquire P from the external medium to sustain their growth.

CHAPTER 3

SL-silencing reprograms P acquisition strategies in tomato (*Solanum lycopersicum* L.) plants

3.1 Introduction

In Chapter 2, we reported the hypersensitive behaviour of tomato plants to P-limitation when SL biosynthesis was impaired. Some root traits functional for the acquisition of P were severely affected in these plants, and root tip anatomy revealed extensive cell and tissue disorganization. In light of these findings, the next step was to understand whether, how and when SLs may modify the canonical P starvation markers and PSRs in this crop.

Strigolactones have been shown to mediate physiological and biochemical changes as part of the adaptation strategies to optimize plant growth under P deficiency (Brewer *et al*., 2013; Czarnecki *et al*., 2013). Gamir and coworkers (2020) indicate SLs as early modulators of tomato plant responses to low P availability, by promoting the expression of P-related key regulatory genes after 1 h pulse of 2'-*epi*-GR24, among which miR399 and *PHO2* play a role in the modulation of high-affinity transporters belonging to the PHT1 family. In wheat, the expression profile of the *TaPht1;2a/b* Pi transporter was described as a fast-responsive P marker, while the expression of *TaPht1;10* was initially low and increased with time (Grün *et al*., 2017), indicating that both the capacity and extent of P acquisition may be indirectly kinetically controlled by SLs. The root metabolic profile to support plants coping with P starvation also appears to be controlled by SLs (Gamir *et al*., 2020). However, this effect could be masked by the large variability of exudates, being continuously and simultaneously subjected to processes of production and degradation.

Based on these considerations, we hypothesized that **P acquisition and allocation as well as exudates production may be SL-mediated in quantitative terms according to specific kinetics.**

Therefore, in this chapter **we aimed at evaluating the influence of SLs on P acquisition in WT and SL-depleted tomato plants, grown with or without Pi**

supply, in terms of biomass accumulation, P allocation, expression of high-affinity Pi transporters and transcripts of their regulators (miR399 and *PHO2*). In addition, **we assessed the short- and long-term kinetics of P uptake as well as exudates release kinetics in terms of proton extrusion, dissolved organic C (DOC) and organic acid anion exudation.**

3.2 Materials and methods

3.2.1 *Plant material*

The plant material used in this study was the same as the one described in Chapter 2 (section 2.2.1.).

3.2.2 *Plant growth conditions*

WT and SL-depleted tomato seeds were surface sterilized as described in Chapter 2 (section 2.2.1). Seeds were germinated on wet Whatman filter paper in Petri dishes (10 cm diameter) inside a growth chamber at 25°C and in the dark. After 5 days, germinated seeds were transferred to plastic pots filled with silica sand and allowed to grow for 45 days inside a growth chamber with a 16/8 h light/dark cycle, air temperature of 25°C and relative humidity ≥70%, with a light intensity of 100 µmol $m^{-2}s^{-1}$. The silica sand was washed with 10% H_2SO_4 prior to using it, in order to obtain a background P concentration below the detection limit (0.1 mg P kg^{-1} sand). Plants were watered with a modified Hoagland nutrient solution [$MgSO_4$ (1 mM), $Ca(NO_3)_2$ (1 mM), KNO_3 (250 µM), KH_2PO_4 (80 µM), FeNaEDTA (20 µM), H_3BO_3 (9 µM), $MnCl_2$ (1.8 µM), $ZnSO_4$ (0.2 µM), $Al_2(SO_4)_3$ (0.075 µM), $Co(NO_3)_2$ (0.2 µM), $NiSO_4$ (0.2 µM), $CuSO_4$ (0.2 µM)] every day (~ 100 mL). The initial pH of the nutrient solution was adjusted to 6.0.

3.2.3 *Phosphorus nutritional conditions and collection of root exudates*

Aerated hydroponic systems were setup to assess modifications in root exudates' composition and to investigate other strategies activated by the two genotypes to respond to P deficiency. After 45 days of growth in sand, WT and SL-depleted plants were gently removed from culture boxes and roots were thoroughly washed with deionized water, in order to remove any sand and residue. Plants were then transplanted to 250 mL flasks, one for each flask, each containing 200

mL of the nutrient solution previously described. The flasks were covered with aluminium foils to prevent light from interfering with root growth and reduce photodegradation of labile organic compounds. The nutrient solution was continuously aerated using an air pump. Plants were kept with the full nutrient solution for 2 days to acclimatize and, before the application of the P treatments, roots were gently rinsed with deionized water several times. Half the plants were then kept in a P-free (–P, 0 µM KH_2PO_4) nutrient solution (KCl replaced KH_2PO_4 in the –P solution to provide plants with the same amount of K), while the remaining plants were supplied with the complete nutrient solution containing a medium P concentration (80 µM KH_2PO_4), hereafter called +P. Such a P concentration was decided based on previous experiments, to induce responses in the high affinity range of Pi transporters. Hydroponic solutions were constantly aerated during the experiment. Each treatment was replicated four times for each genotype. The solution was collected at different times for 13 days, in concomitance with the replacement of the nutrient solution. Immediately after sampling, the solutions containing root exudates were filtered using 0.22 µm nylon membrane filters and stored at –20°C until further analyses. On day 13, three plants per genotype and treatment were sampled and their roots were rapidly frozen with liquid N_2 and stored at –80°C for gene expression of Pi transporters and the transcripts of miRNA399 and *PHO2* (see section 3.2.4.2). The rest of the plants was moved to 250 mL flasks containing deionized water in order to generate osmotic stress and stimulate further exudation. Root exudates solutions were collected after 1, 4, 8, and 24 h, then plants were harvested, separated in shoots and roots, and the fresh biomass was recorded. Furthermore, the number of internodes was counted, and the weight of senescent leaves collected along the experiment was recorded. Root subsamples were frozen with liquid N_2 and stored at –80°C for enzymatic analysis, while the remaining roots and shoots were dried at +40°C. Dry root and shoot samples were ground separately, passed through a 0.5 mm mesh sieve and used for elemental analyses.

3.2.4 *Plant analysis*

3.2.4.1 *Elemental analysis*

Total C and N contents were determined by dry combustion (UNICUBE, Elementar Analysensysteme GmbH, Langensenbold, Germany). Concentration of total P in plant tissues was determined colorimetrically on dry plant material (50 mg) after sulfuric-perchloric digestion using the malachite green method (Ohno and Zibilske, 1991). P-acquisition efficiency (PAE) values were calculated as the ratio of P accumulated in tissues to exogenously supplied P during both plant growth in sand and the hydroponic experiment, while P-utilization efficiency (PUtE) was calculated as the ratio of plant dry biomass to P content in plant tissues (Neto *et al.*, 2016).

3.2.4.2 *Gene transcript and microRNA quantification*

To determine the levels of *PHO2* and PHT gene transcripts, and of mature mir399, RNA was extracted from individual root samples of wild-type and strigolactone-depleted plants grown in hydroponics with either 80 µM KH_2PO_4 or no KH_2PO_4 as described above. Total RNA was extracted by using Spectrum™ Plant Total RNA Kit (Sigma-Aldrich), and treated with DNase I (ThermoScientific) at 37°C for 30 min to remove residual genomic DNA. First-strand cDNA was synthesized from 500 ng of purified total RNA using the High-Capacity cDNA Reverse-Transcription Kit (Applied Biosystems, Monza, Italy) according to the manufacturer's instructions. A modified protocol with a stem-loop primer (Pagliarani et al., 2017) was followed for targeted miR399 cDNA synthesis. For transcript quantification of target genes, the quantitative reverse-transcriptase PCR (qRT-PCR) reactions were carried out in a StepOnePlus system (Applied Biosystems) using the SYBR Green (Applied Biosystems) method. Transcript concentrations were normalized on *SlEF-1α* or *SlsnU6* transcripts as endogenous controls. Three independent biological replicates were analysed as a minimum, and each qRT-PCR reaction was run in technical triplicates. Transcript amounts were quantified through the $2^{-\Delta\Delta Ct}$ method.

3.2.4.3 *Enzyme activity*

Enzymatic activity was assayed following the methodology reported in Hayes and coworkers (1999). Root material was ground in 15 mM MES buffer (pH 5.5) containing 0.5 mM $CaCl_2 \cdot H_2O$ and 1 mM EDTA. The extract was centrifuged, and the supernatant subjected to gel filtration at 4°C on Sephadex G-25 columns. To assay total acid phosphatase activity, the enzyme extract was incubated at 26°C in 15 mM MES buffer (pH 5.5) with 1 mM EDTA, 5 mM cysteine and 10 mM *p*-nitrophenyl phosphate (*p*NPP). The assays were conducted for 30 min and the reactions stopped by addition of 0.25 M NaOH. The concentration of *p*-nitrophenol (*p*NP) was determined by measuring the absorbance at 412 nm against standard solutions. Phytase activity was measured on the same root extracts and under the same conditions as described above, except that *p*NPP was replaced with 2 mM *myo*-inositol hexaphosphate (*myo*InsP6). Assays were conducted for 60 min and the reactions stopped by addition of ice-cold 10% trichloroacetic acid (TCA). Solutions were subsequently centrifuged to remove precipitated material and phosphate concentration determined by the malachite green method (Ohno and Zibilske, 1991).

3.2.4.4 *Phosphorus concentration in the nutrient solution and exudate analysis*

Concentration of P in the nutrient solution was determined as described above previous every root exudates sampling in order to evaluate the amount of P absorbed by plants, and expressed as µmol P L^{-1} of exudate solution.

Root exudates were then analyzed for dissolved organic C, protons, and organic acid anions. Dissolved organic C (DOC) was determined using Pt-catalysed, high-temperature combustion (850°C) followed by infrared detection of CO_2 (VarioTOC, Elementar, Hanau, Germany), after removing inorganic C by acidifying to pH 2 and purging with CO_2-free synthetic air. The concentration of protons in the nutrient and water solutions was monitored using a pH-sensitive electrode (inoLab pH 7110, WTW GmbH, Weilheim, Germany) and was expressed as the cumulative amount of H^+ ions released at each sampling time. Organic acid anions were analyzed by Dionex DX-500 Ion Chromatography system (Sunnyvale, CA, USA) equipped with a dimensional-exclusion column (Ion PAC ICE-AS6) and an electrochemical detector (Dionex ED40). The anions

in the samples were identified by comparison with the retention times of pure standards including oxalic, tartaric, malic, lactic, acetic, maleic, citric, succinic and fumaric acid anions.

Dissolved organic C, protons and organic acid anions data at different time intervals were fitted with a proper mathematical equation (as reported in Tables 3.3, 3.4 and 3.5, respectively) in order to obtain the relative exudation kinetic parameters.

3.2.5 *Statistics*

The analysis of variance (one-way ANOVA) was performed using the SPSS software version 26.0 (SPSS, Chicago, IL, USA), and was followed by pair-wise post-hoc analyses (Student-Newman-Keuls test) to determine which means differed significantly at $p < 0.05$ (± SE). In addition, to evaluate the effect of plant genotype, P treatment and the combination of the two on the measured parameters, we used a linear mixed-effect ANOVA model performed with the statistical programming language R (R Core Team, 2020). Figures were created using SigmaPlot ver. 12.5 software (Systat, San Jose, CA, USA), with means presented with standard errors.

3.3 Results

3.3.1 *Shoot and root growth*

Under normal growing conditions (+P), SL-depleted plants displayed a marked increase in shoot branching when compared to the WT, whose internodes were more spaced along the stem (Fig. 3.1, Table 3.1). The number of nodes was higher in SL-depleted plants and strongly influenced by the plant genotype ($p < 0.001$). Plant height of +P SL-depleted plants was also slightly reduced. Nevertheless, such a trait was more pronounced under P deficiency. No variation in shoot biomass was observed in WT plants depending on exogenous P, and typical symptoms of severe P deficiency (i.e., purple leaves due to anthocyanin accumulation) were not visible at the aboveground parts of plants except for leaf senescence and drop, which were restricted to P-depleted WT plants (Table 3.1).

Plant fresh weight and dry root biomass were comparable between WT and SL-depleted plants, regardless of P supply (Table 3.1). However, +P SL-depleted plants were inclined to produce less root biomass in favour of higher resource allocation to the shoot. Accordingly, these plants displayed the lowest root to shoot (R/S) ratio, while P-deficient plants, either WT or SL-depleted, promoted root over shoot growth, resulting in greater R/S ratios (Table 3.1). +P and –P WT plants had yet comparable R/S ratios, although values were basically higher under P shortage. Substantial differences in R/S ratios were conversely evident between +P and –P SL-depleted plants, the latter displaying 2-fold-higher values. However, the R/S ratios were only significantly affected by P treatment ($p < 0.001$) and not by the plant genotype.

Leaf senescence was mainly observed in WT plants and was influenced by the plant genotype only ($p < 0.001$). The highest amount of senescent leaves was exhibited by P-starved WT plants, immediately followed by the same genotype under +P conditions (Table 3.1). P-starved SL-depleted plants lost around one third of the weight lost by –P WT plants by dropping senescent leaves, while under +P they lost five time less weight than +P WT plants.

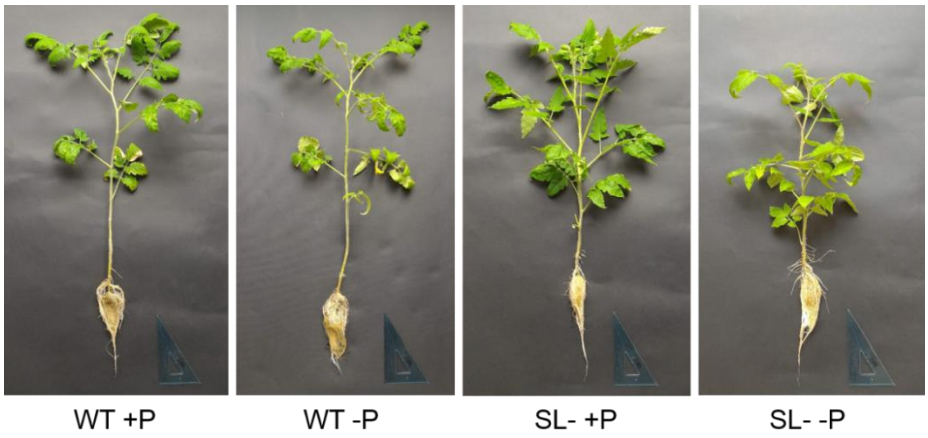

Figure 3.1: Wild-type (WT) and SL-depleted (SL–) tomato plants developmental response to P treatments. Plants were grown in quartz sand for 45 days with a nutrient solution containing 80 µM Pi, then transferred to hydroponic culture with (+P, 80 µM) or without (–P, 0 µM) Pi for 13 days, followed by 24 h in deionized water.

Table 3.1: Effect of P treatments on fresh and dry biomass, root/shoot ratio (R/S), number of nodes and senescent leaves of wild-type (WT) and SL-depleted (SL–) tomato plants after 13 days of hydroponic culture with (+P, 80 µM) or without (–P, 0 µM) Pi, followed by 24 h in deionized water. Abbreviations: FW, fresh weight; DW, dry weight. Each value represents the mean of four replicates (± SE). Different letters indicate significant differences between treatments ($p < 0.05$).

	WT +P	WT –P	SL– +P	SL– –P
Plant FW (g)	12.9 ± 1.1	12.4 ± 0.9	15.6 ± 1.1	10.9 ± 1.5
Root DW (g)	0.22 ± 0.04	0.27 ± 0.07	0.20 ± 0.05	0.26 ± 0.09
Shoot DW (g)	1.07 ± 0.11 ^{ab}	1.03 ± 0.24 ^{ab}	1.39 ± 0.30 ^{a}	0.91 ± 0.22 ^{b}
R/S	0.20 ± 0.02 ^{ab}	0.27 ± 0.03 ^{a}	0.15 ± 0.01 ^{b}	0.28 ± 0.03 ^{a}
Number of nodes	6.25 ± 0.25 ^{b}	7.25 ± 0.25 ^{b}	11 ± 0.91 ^{a}	10.75 ± 0.62 ^{a}
Senescent leaves DW (g)	0.63 ± 0.16 ^{ab}	0.70 ± 0.19 ^{a}	0.11 ± 0.00 ^{bc}	0.02 ± 0.00 ^{c}

Even if no differences were observed in the C content of the two genotypes under both P conditions, SL-depleted plants accumulated more N under +P than –P conditions, while N content of WT plants did not vary along with P treatment (Table 3.2).

Wild-type and SL-depleted plants showed similar capacity of P root to shoot translocation, but +P plants accumulated about five times more P in their shoot than their relative –P genotype (Fig. 3.2a). SL-depleted plants contained more P in their shoot than the WT, consistently with their higher shoot biomass, being this trait significantly influenced by both P treatment ($p < 0.001$) and the combination of P treatment and plant genotype ($p < 0.01$).

Under P shortage, P content was similar in the shoots of the two genotypes. Considering P content in roots, the differences were only due to the P treatment ($p < 0.001$), resulting in higher P content in the roots of +P WT plants, while no significant differences were observed under –P conditions. P-acquisition efficiency (PAE) was comparable under –P conditions in both genotypes but higher in SL-depleted plants under +P conditions (Fig. 3.2b), being strongly influenced by the P treatment ($p < 0.001$), plant genotype ($p < 0.01$) and the combination of the two factors ($p < 0.05$). On the contrary, P-utilization efficiency (PUtE, Fig. 3.2c) was only dependent on P treatment ($p < 0.001$) and higher under –P than under +P conditions, irrespective of the plant genotype.

C/P and N/P ratios were higher under –P conditions for both genotypes (Table 3.2), reflecting the lower P content of plant tissues. While in SL-depleted plants a significant decrease in N content was observed under P starvation, this was not the case of WT plants.

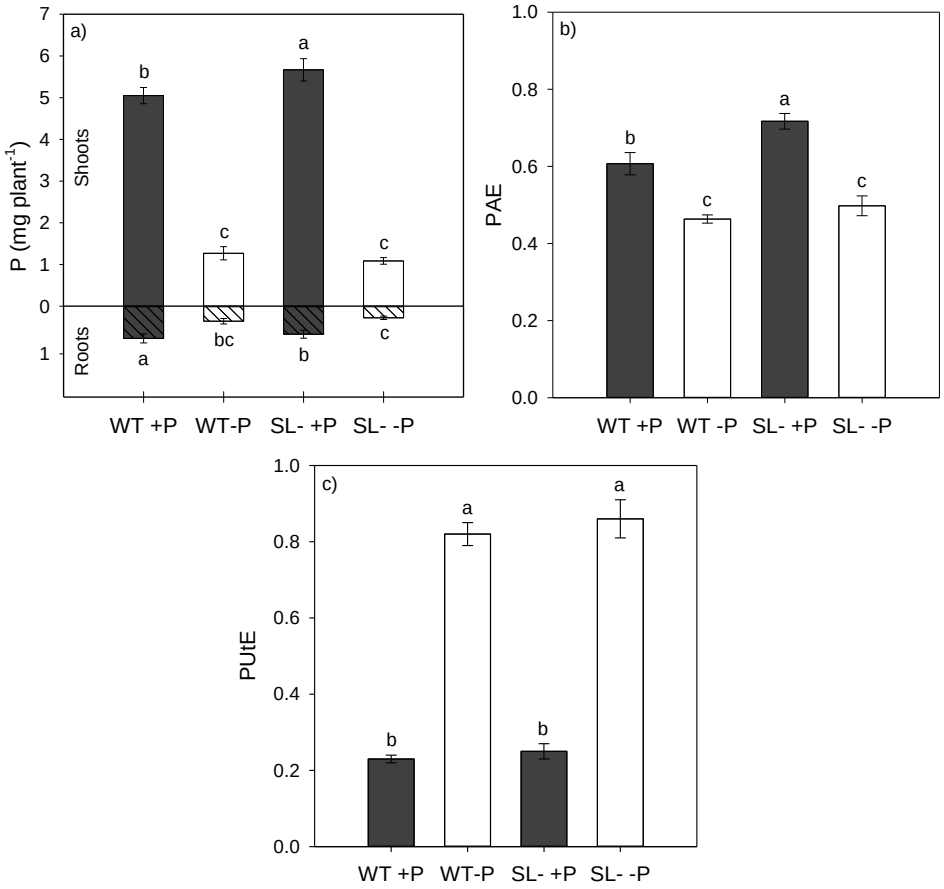

Figure 3.2: a) Roots and shoots P content, b) P-acquisition efficiency (PAE) and c) P-utilization efficiency (PUtE) of wild-type (WT) and SL-depleted (SL–) tomato plants after 13 days of hydroponic culture with (+P, 80 µM) or without (–P, 0 µM) Pi, followed by 24 h in deionized water. Each value represents the mean of four replicates (± SE). Different letters above bars indicate significant differences between treatments ($p < 0.05$).

Table 3.2: Carbon (C) and nitrogen (N) content and C/P and C/N ratios of wild-type (WT) and SL-depleted (SL–) tomato plants after 13 days of hydroponic culture with (+P, 80 µM) or without (–P, 0 µM) Pi, followed by 24 h in deionized water. Each value represents the mean of four replicates (± SE). Different letters indicate significant differences between treatments ($p < 0.05$).

	C content (g plant^{-1})	N content (mg plant^{-1})	C/P	N/P
WT +P	0.89 ± 0.07	92.94 ± 5.54 ^{ab}	157 ± 8 ^{b}	16.2 ± 0.5 ^{b}
WT –P	0.91 ± 0.11	89.91 ± 8.71 ^{ab}	569 ± 23 ^{a}	56.9 ± 1.8 ^{a}
SL– +P	1.14 ± 0.13	112.73 ± 9.76 ^{a}	181 ± 17 ^{b}	17.9 ± 1.2 ^{b}
SL– –P	0.77 ± 0.08	75.53 ± 10.08 ^{b}	568 ± 23 ^{a}	56.6 ± 3.8 ^{a}

The kinetic of P depletion (Fig. 3.3) underlined a greater P consumption by SL-depleted plants compared to the WT. Such a behaviour was evident in the first seven days, when the nutrient solution was replaced every day (in correspondence of the arrows), restoring the original P concentration (80 µM).

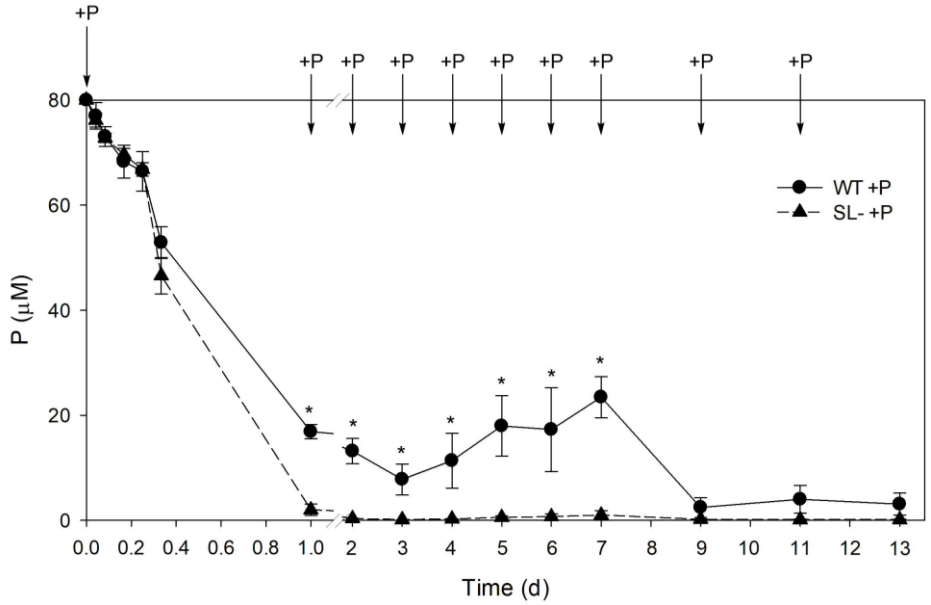

Figure 3.3: Residual P content in exudates solution of wild-type (WT) and SL-depleted (SL–) tomato plants during the 13 days of hydroponic treatment with a nutrient solution containing 80 µM Pi. Arrows indicate the substitution of the nutrient solution and restoration of the original P concentration (80 µM). Values are expressed as µmol of P L^{-1} of exudate solution. Each value represents the mean of four replicates (± SE). Significant differences between treatments ($p < 0.05$) were indicated with an asterisk.

Thereafter, when the nutrient solution was replaced every two days, P was almost completely removed by WT plants and completely taken up by SL-depleted plants. No P was detected in both WT and SL-depleted solutions corresponding to the –P conditions.

3.3.2 *High-affinity Pi transporters expression and regulators*

High-affinity Pi transporters were generally up-regulated under P shortage in both genotypes, with maximum values of relative gene expression displayed by SL-depleted plants (Fig. 3.4).

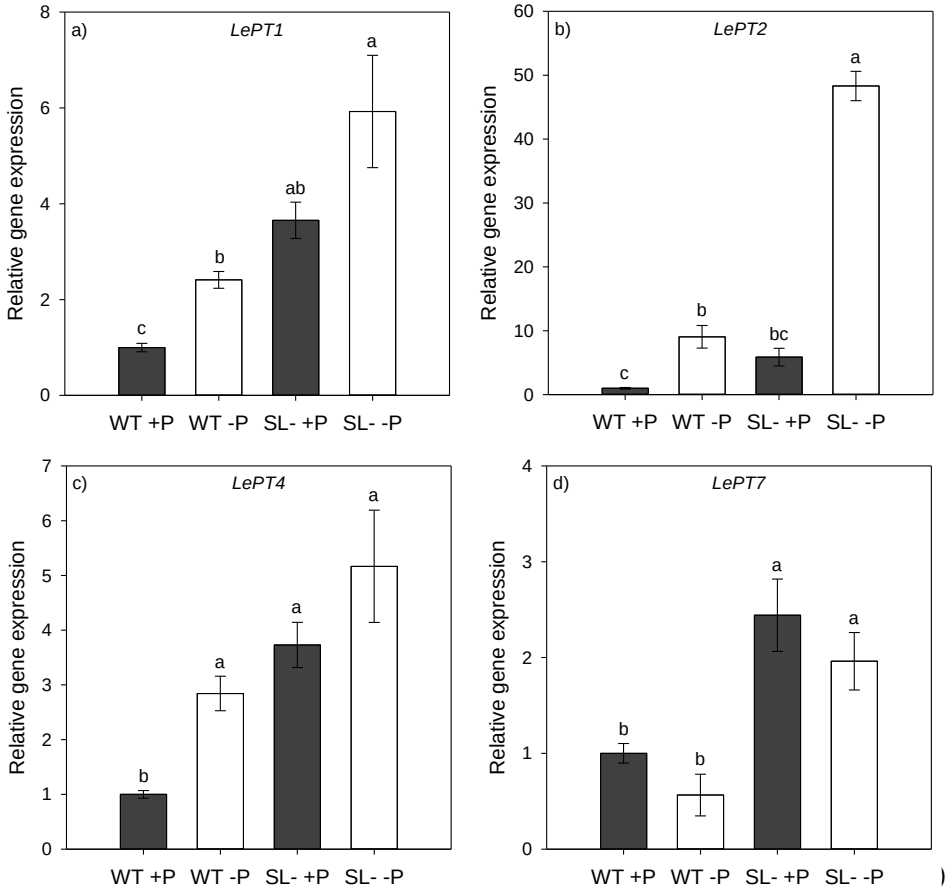

LePT4, d) *LePT7* in roots of wild-type (WT) and SL-depleted (SL–) tomato plants after 13 days of hydroponic culture with (+P, 80 µM) or without (–P, 0 µM) Pi, followed by 24 h in deionized water. Each value represents the mean of three replicates (± SE). Different letters above bars indicate significant differences between treatments ($p < 0.05$).

When plants were P-provided, the expression of *LePT1*, *LePT2, LePT4* and *LePT7* was significantly higher in SL-depleted than in WT plants. In both genotypes, *LePT7* was apparently not transcriptionally up-regulated by P shortage (Fig. 3.4c). The amounts of mature miR399 and *PHO2* transcripts diverged in our samples (Fig. 3.5a). *PHO2* transcription was down-regulated in roots of plants containing the highest amounts of Pi transporters' transcript (SL-depleted and P-starved WT roots). Conversely, the concentration of mature miR399 was the lowest in P-replete wild-type plants, and higher in –P wild-type and strigolactone-depleted plants under both P conditions (Fig. 3.5b).

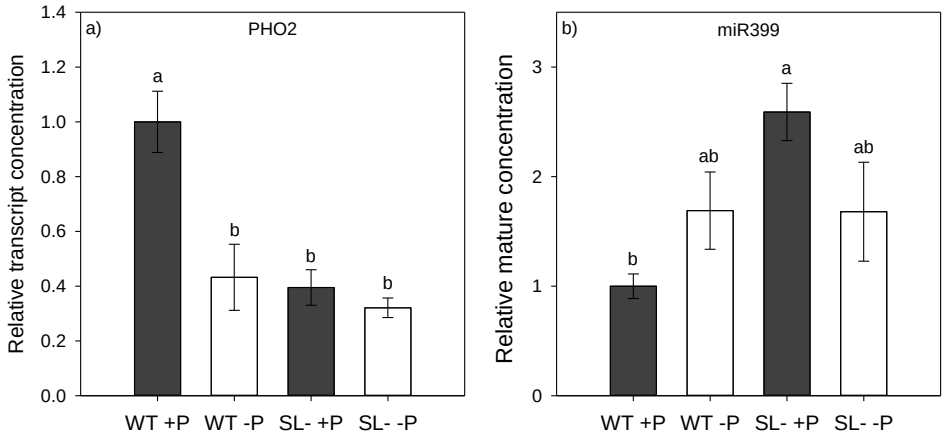

Figure 3.5: a) Relative *PHO2* transcript concentration and b) mature miR399 concentration in roots of wild-type (WT) and SL-depleted (SL–) tomato plants after 13 days of hydroponic culture with (+P, 80 µM) or without (–P, 0 µM) Pi, followed by 24 h in deionized water. Each value represents the mean of three biological replicates (± SE). Different letters above bars indicate significant differences between treatments ($p < 0.05$).

3.3.3 *Root enzymatic activity*

Phosphatase activity was the lowest in WT plants receiving P, and slightly increased in the same genotype starved of P (Fig. 3.6a). In SL-depleted plants, values were significantly higher than the WT under +P, and remained stable under –P. Phytase activity in P-starved plants was higher than in P-repleted (Fig. 3.6b). Although only slight differences were evident between genotypes under the two P conditions, the phytase activity in SL-depleted plants was generally greater than in WT plants.

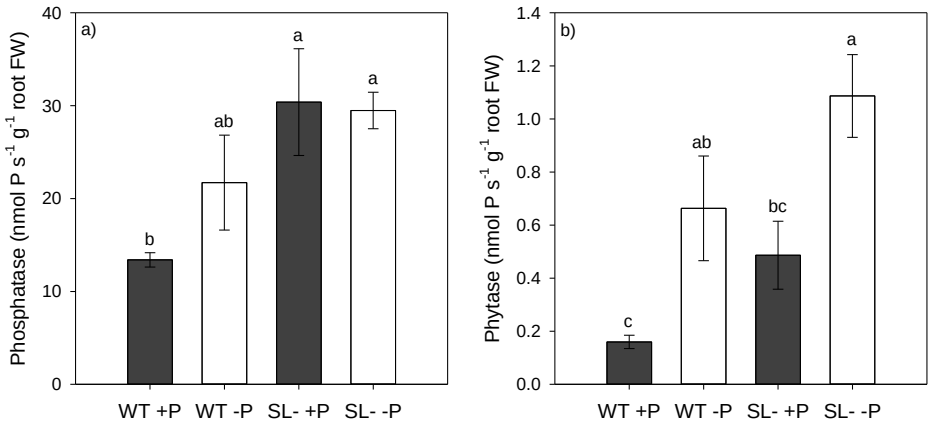

Figure 3.6: a) Phosphatase and b) phytase activity in roots of wild-type (WT) and SL-depleted (SL–) tomato plants after 13 days of hydroponic culture with (+P, 80 µM) or without (–P, 0 µM) Pi, followed by 24 h in deionized water. Each value represents the mean of four replicates (± SE). Different letters above bars indicate significant differences between treatments ($p < 0.05$).

3.3.4 *Exudation kinetics and characterization*

3.3.4.1 *Dissolved organic C and proton exudation*

Figure 3.7 depicts the content of dissolved organic C (DOC) and protons (H^+) in the exudates of WT and SL-depleted plants during the hydroponic growth. Specifically, Fig. 3.7a and 3.7d depict the DOC and proton cumulative release during the first 24 h of +P and –P treatment, while Fig. 3.7b and 3.7e represent the cumulative values throughout the two weeks-experiment, under +P or –P conditions. Fig. 3.7c and 3.7f instead show the cumulative amount of DOC and proton exudation during the 24 h in water at the end of the hydroponic experiment. Cumulative data were fitted with kinetic equations whose parameters are reported in Tables 3.3 and 3.4.

During the first 24 h of hydroponic experiment, the amount of DOC in the solution reached a plateau. P-provided SL-depleted plants steadily exuded a lower amount of organic C than under –P conditions, reaching a plateau of 2.13 ± 0.01 mg C g^{-1} plant in 24 h, with a kinetic comparable to that of P-depleted WT plants (Table 3.3). Within the same time interval, the exudation of C by –P SL-depleted plants and by both +P and –P WT plants attained a similar plateau, at ~ 3.4 mg

C g^{-1} plant (Table 3.3). However, the lower *b* values observed for –P WT plants and +P SL-depleted plants indicated a faster release kinetics and a faster plateau achievement (Table 3.3).

In the long term, values of C exudation were comparable between –P SL-depleted and WT plants under both P conditions, although the former started displaying a higher capacity to release C after about 9 days (Fig. 3.7b). In this time interval, the amount of C did not reach a plateau but constantly increased along the experiment, requiring a hyperbolic equation to fit the data (Table 3.3). The net concentration increase, described by the *c* parameter, was comparable between +P and –P WT plants, while it was slightly higher for –P SL-depleted plants (Table 3.3), reflecting the final increase in C exudation (Fig. 3.7b). Under +P conditions, SL-depleted plants kept exuding the lowest amount of organic C, with the lowest increase during time (lowest *c* value, Table 3.3).

Once transferred to water without any nutrient, plants exuded less C if compared to the first 24 h (Fig. 3.7c). In addition, P-depleted plants released more DOC than the respective +P genotype. Also in this case, C exudation did not reach a plateau, and data were fitted using a power equation (Table 3.3). The highest amount of DOC was exuded by P-depleted WT plants (Fig. 3.7c), with a *b* value comparable to that of –P WT and SL-depleted plants, while the slowest C exudation was measured for +P SL-depleted plants (Table 3.3).

Similarly to DOC, proton release achieved a plateau during the first 24 h of P treatment in all cases (Fig. 3.7d), with the highest values at this point displayed by –P WT plants (8.47 ± 0.58 µmol H^+ g^{-1} root, Table 3.4). The lowest plateau values were determined for –P SL-depleted plants (4.87 ± 0.21 µmol H^+ g^{-1} root, Table 3.4), with a fast kinetic, as similar as that of +P plants (both WT and SL-depleted). Comparable and intermediate plateau values were obtained for the two genotypes under +P condition, at roughly 7 µmol H^+ g^{-1} root (Table 3.4).

Within the two-week interval, such a trend of higher proton release by –P WT plants was confirmed, with values slightly but constantly increasing until the end of the experiment (Fig. 3.7e). On the contrary, proton release by –P SL-depleted plants appeared to reach a steady state after 4 days, but then started increasing

quickly (highest *c* value, Table 3.4), thus reaching a final value that was comparable to that of +P WT and SL-depleted plants, which instead reached a plateau for proton extrusion (~ 8 µmol H^+ g^{-1} root) already after 1 and 7 days, respectively (Fig. 3.7e).

When plants were transferred to water without the addition of any nutrient, proton release exponentially increased in 24 h without approaching the plateau (Fig. 3.7f). The fastest kinetics was that of –P SL-depleted plants, which also released the highest amount of protons, followed by the same genotype in +P (Table 3.4, Fig. 3.7f). In the case of WT plants, proton release was more intense under –P conditions, even if the difference between the two P treatments was not as sharp as for SL-depleted plants, and the release kinetics were comparable (Fig. 3.7f, Table 3.4).

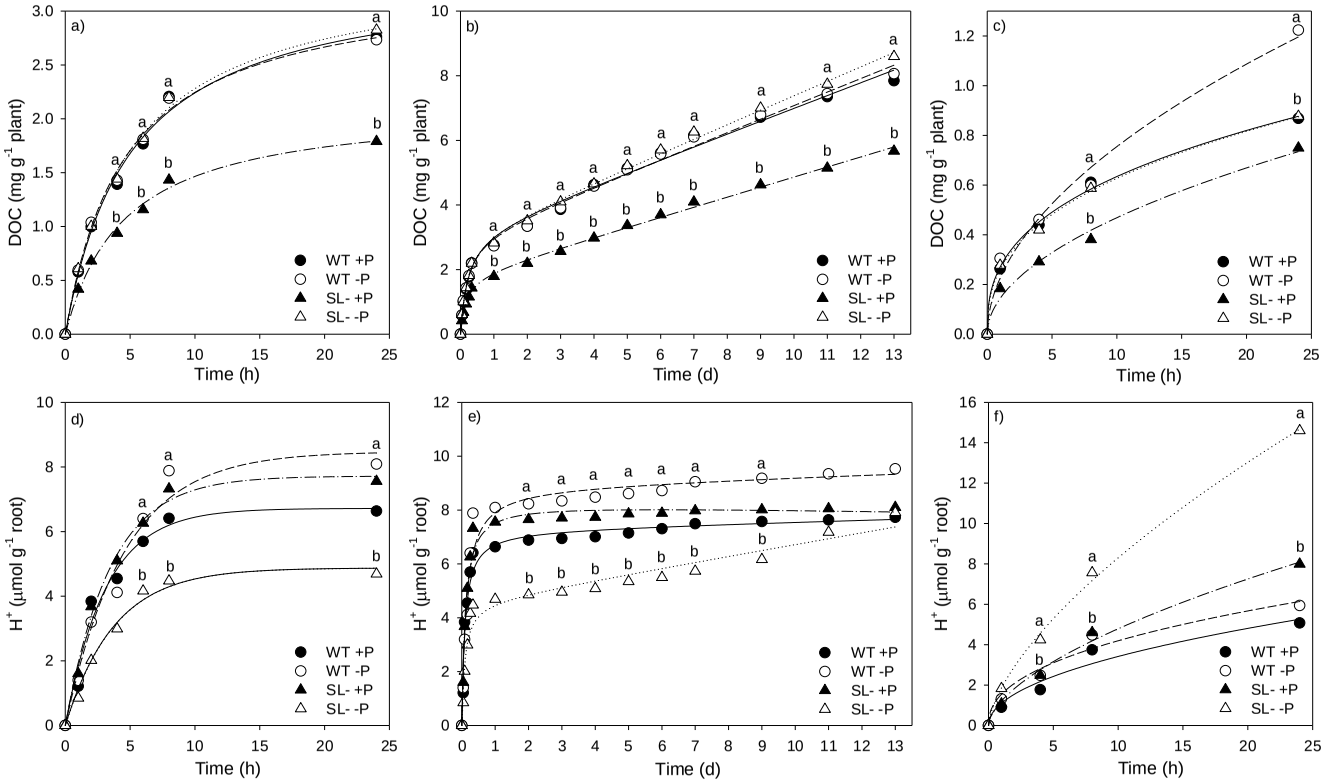

Figure 3.7: Dissolved organic C (DOC) and proton (H^+) content in the exudates of wild-type (WT) and SL-depleted (SL–) tomato plants during a,d) the first 24 h and b,e) the 13 days of hydroponic culture treatment with (+P, 80 µM) or without (–P, 0 µM) Pi. c,f) DOC and H^+ exudation during the 24 h in deionized water. Values are expressed as cumulative pools and each value represents the mean of four replicates. Different letters above points indicate significant differences between treatments ($p < 0.05$). For the sake of graph readability, SE are not reported.

Table 3.3: Parameters of the mathematical functions fitted to cumulative dissolved organic C (DOC) data, as reported in Fig. 3.7a-c.

Time interval	Fitted equation	Plant type and treatment	Function parameters			R^2	p
			a	*b*	*c*		
0 – 24 h	$^{\alpha}\, y = \frac{ax}{b+x}$	WT +P	3.37 ± 0.14	5.05 ± 0.56	-	0.993	< 0.0001
		WT –P	3.29 ± 0.12	4.63 ± 0.44	-	0.995	< 0.0001
		SL– +P	2.13 ± 0.01	4.58 ± 0.49	-	0.994	< 0.0001
		SL– –P	3.43 ± 0.11	5.04 ± 0.02	-	0.997	< 0.0001
0 – 13 d	$^{\beta}\, y = \frac{ax}{b+x} + cx$	WT +P	3.15 ± 0.18	0.22 ± 0.04	0.39 ± 0.02	0.992	< 0.0001
		WT –P	3.00 ± 0.14	0.19 ± 0.03	0.41 ± 0.02	0.995	< 0.0001
		SL– +P	1.82 ± 0.07	0.16 ± 0.02	0.31 ± 0.01	0.998	< 0.0001
		SL– –P	3.02 ± 0.09	0.19 ± 0.02	0.44 ± 0.01	0.998	< 0.0001
0 – 24 h (water)	$^{\gamma} y = ax^b$	WT +P	0.27 ± 0.01	0.37 ± 0.02	-	0.998	< 0.0001
		WT –P	0.23 ± 0.03	0.53 ± 0.06	-	0.985	0.0008
		SL– +P	0.14 ± 0.02	0.51 ± 0.05	-	0.990	0.0004
		SL– –P	0.26 ± 0.01	0.38 ± 0.02	-	0.998	< 0.0001

$^{\alpha}$ a, asymptotic DOC maximum; b, initial rate of DOC release.
$^{\beta}$ a, asymptotic DOC maximum; b, initial rate of DOC release; c, net DOC increase in the linear range of the equation.
$^{\gamma}$ a, initial rate of DOC release; b, asymptotic DOC value.

Table 3.4: Parameters of the mathematical functions fitted to cumulative proton (H^+) exudation data, as reported in Fig. 3.7d-f.

Time interval	Fitted equation	Plant type and treatment	Function parameters			R^2	p
			a	*b*	*c*		
0 – 24 h	[α] $y = a(1 - e^{-bx})$	WT +P	6.71 ± 0.37	0.31 ± 0.05	-	0.976	< 0.0001
		WT –P	8.47 ± 0.58	0.22 ± 0.04	-	0.971	< 0.0001
		SL– +P	7.72 ± 0.25	0.29 ± 0.03	-	0.992	< 0.0001
		SL– –P	4.87 ± 0.21	0.27 ± 0.03	-	0.990	< 0.0001
0 – 13 d	[β] $y = \frac{ax}{b+x} + cx$	WT +P	7.27 ± 0.28	0.09 ± 0.01	0.03 ± 0.03	0.992	< 0.0001
		WT –P	8.89 ± 0.44	0.13 ± 0.02	0.04 ± 0.05	0.968	< 0.0001
		SL– +P	8.28 ± 0.28	0.09 ± 0.01	0.02 ± 0.03	0.979	< 0.0001
		SL– –P	4.59 ± 0.29	0.08 ± 0.02	0.22 ± 0.04	0.964	< 0.0001
0 – 24 h (water)	[γ] $y = ax^b$	WT +P	1.10 ± 0.28	0.49 ± 0.09	-	0.960	0.0035
		WT –P	1.54 ± 0.29	0.44 ± 0.07	-	0.971	0.0021
		SL– +P	1.20 ± 0.16	0.60 ± 0.06	-	0.993	0.0002
		SL– –P	1.86 ± 0.14	0.65 ± 0.03	-	0.998	< 0.0001

[α] a, asymptotic H^+ maximum; b, initial rate of H^+ release.
[β] a, asymptotic H^+ maximum; b, initial rate of H^+ release; c, net H^+ increase in the linear range of the equation.
[γ] a, initial rate of H^+ release; b, asymptotic H^+ value.

3.3.4.2 *Organic acid anion exudation*

Qualitative and quantitative analyses of organic acid anions revealed variable amounts of several types of these compounds in the root exudates of both WT and SL-depleted plants, including oxalic, succinic, malic, citric, glycolic, lactic and acetic anions.

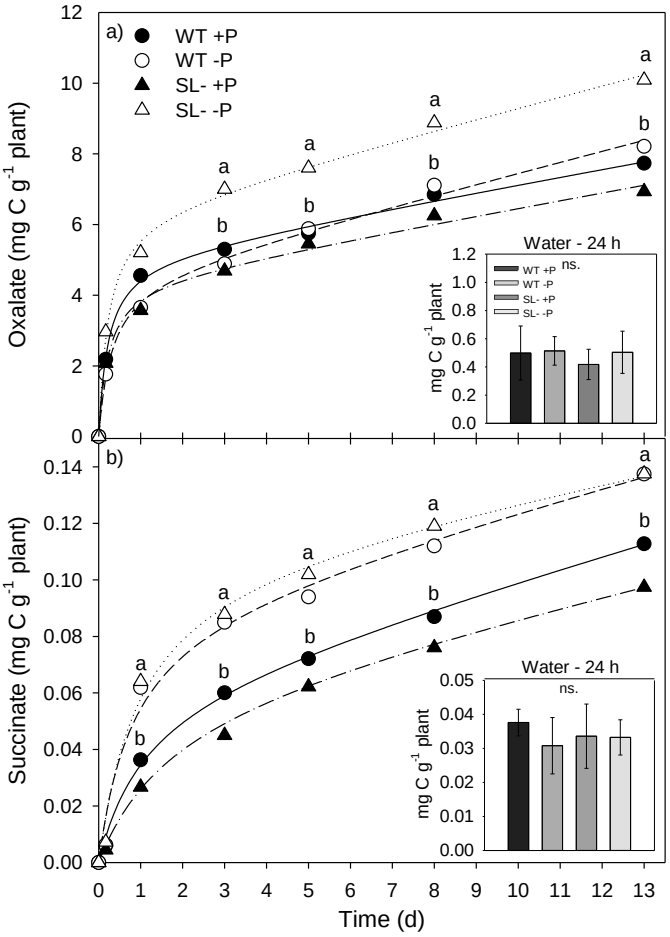

Figure 3.8: Oxalate (a) and succinate (b) content in root exudates of wild-type (WT) and SL-depleted (SL–) tomato plants during the 13 days of hydroponic culture treatment with (+P, 80 µM) or without (–P, 0 µM) Pi. Values are expressed as cumulative pools of exuded C, in mg g^{-1} of plant DW. Different letters above points indicate significant differences between treatments ($p < 0.05$). For the sake of graph readability, SE are not reported. Small boxes: average concentration of the respective anions in the root exudates of WT and SL-depleted plants after 24 h in deionized water. Each value represents the mean of four replicates (± SE). No statistically significant differences were observed.

Among them, the most abundant were oxalate and succinate (Fig. 3.8), while the other anions were present in traces. Similar to the trend reported for DOC flow from roots, cumulative exudation of oxalate and succinate increased along time, without reaching a plateau. Also, the content of these two anions was lower in +P SL-depleted plants compared to the same –P genotype and to WT plants. P-deficient SL-depleted plants exuded the highest amount of oxalate and with a faster kinetics than the other plants (Table 3.5), with values significantly higher after a few hours since the beginning of the experiment (~ 4h, Fig. 3.8a). +P and –P WT plants conversely released comparable amounts of this compound during the whole experiment. In addition, no significant differences in oxalate content of root exudates were evident between SL-depleted and WT plants after 24 h of water treatment (Fig. 3.8a, small box), even if the amount exuded under previous –P was slightly higher than previous +P conditions. With respect to succinate, its content in root exudates of P-starved was higher than in P-repleted plants since 1 day (Fig. 3.8b), while the exudation was comparable between the two genotypes at the two P levels both in terms of quantity and exudation kinetics (Table 3.5).

Table 3.5: Parameters of the hyperbolic function $y = \frac{ax}{b+x} + cx$, fitted to cumulative organic acid anion exudation data reported in Fig. 3.8. *a*, asymptotic anion maximum; *b*, initial rate of anion release; *c*, net anion increase in the linear range of the equation.

	Function parameters			R^2	p
	a	*b*	*c*		
Oxalate					
WT +P	5.08 ± 0.21	0.22 ± 0.03	0.21 ± 0.02	0.997	< 0.0001
WT –P	4.54 ± 0.30	0.30 ± 0.08	0.30 ± 0.03	0.997	< 0.0001
SL– +P	4.41 ± 0.29	0.22 ± 0.06	0.21 ± 0.03	0.994	< 0.0001
SL– –P	6.35 ± 0.30	0.21 ± 0.04	0.31 ± 0.03	0.997	< 0.0001
Succinate					
WT +P	0.06 ± 0.01	1.09 ± 0.36	$4.0 \cdot 10^{-3} \pm 7 \cdot 10^{-4}$	0.999	0.0015
WT –P	0.09 ± 0.03	0.81 ± 0.62	$3.9 \cdot 10^{-3} \pm 2 \cdot 10^{-5}$	0.987	0.0128
SL– +P	0.06 ± 0.01	1.72 ± 0.35	$3.3 \cdot 10^{-3} \pm 4 \cdot 10^{-5}$	0.999	0.0004
SL– –P	0.11 ± 0.03	0.96 ± 0.57	$2.7 \cdot 10^{-3} \pm 2 \cdot 10^{-4}$	0.991	0.0092

3.4. Discussion

3.4.1 *Plant response to P supply*

The reduced SL production due to *CCD7* silencing triggered the expected modifications of shoot shaping. SL-depleted plants exhibited the typical dwarf and bushy phenotype (Gomez-Roldan *et al*., 2008; Umehara *et al*., 2008) previously reported for tomato (Koltai *et al*., 2010) and SL-synthesis and -signalling mutants of other species, as rice, *Arabidopsis* and grapevine (Mayzlish-Gati *et al*., 2012; Ren *et al*., 2020; Sun *et al*., 2014; Yamada *et al*., 2014). SL-dependent inhibition of shoot branching in WT plants was consistent with the hypothesized role for SLs in plant shaping and development (Gomez-Roldan *et al*., 2008; Umehara *et al*., 2008), and has been widely demonstrated by restored phenotype upon exogenous application of the synthetic SL analogous *rac*GR24 to SL mutants (Barbier *et al*., 2019; Kohlen *et al*., 2011; Rameau *et al*., 2015; Vogel *et al*., 2010). SL silencing prevented leaf senescence symptoms in SL-depleted plants, while SLs promoted internode elongation and induced early leaf senescence especially in P-starved WT plants, probably to facilitate internal P reallocation under P shortage. Supporting this hypothesis, SLs are considered positive regulators of leaf senescence by activating the ethylene-mediated senescence-signalling pathway that may support plants in reallocating nutrients from old to developing younger tissues (Czarnecki *et al*., 2013; Ueda and Kusaba, 2015; Yamada *et al*., 2014; Yang *et al*., 2019).

Under +P condition, the R/S ratio was similar between genotypes, despite the slightly higher shoot biomass of SL-depleted plants. However, the similar biomass partitioning and capacity to optimize P usage to create biomass (given the similar P-utilization efficiency) displayed by the two genotypes were not reflected by a similar P allocation in tissues. In fact, SL-depleted plants preferentially allocated P in the aerial part, indicating a greater translocation to the shoots, possibly to sustain and maintain the more shoot-branched phenotype. The higher P content of SL-depleted plants under normal P provision was related to the greater consumption of P from the nutrient solution compared to the WT, as reflected by the higher PAE. These plants were in fact capable of consuming most of the P that was present in the nutrient solution within 24 h, as observed along the whole experiment. On the contrary, WT plants consumed 80% of

provided P during the first day of experiment and, on average, between 70 and 90% of the 80 µM P when the nutrient solution was renewed every day. When it was replaced every 48 h, WT plants consumed more than 95% of the provided P, without displaying the typical symptoms of P deficiency, as purple colouring of leaves. The higher, time-dependent demand of P by SL-depleted plants may be due to altered perception of exogenous P and/or to disturbance of the systemic PSR control, consistent with the altered responses to this nutrient and the changes in root system architecture and tip anatomy in Chapter 2. Coherently with better P removal from the nutrient solution, gene transcripts of the root high-affinity Pi transporters *LePT1*, *LePT2*, *LePT4* and *LePT7* were more concentrated under +P in SL-depleted plants than in the WT. *LePT1* and *LePT4* were induced by P starvation in WT plants, but not in SL-depleted plants, while *LePT7* behaved differently, as it was not up-regulated by P starvation in either plant genotype. Interestingly, *LePT2* showed significant transcript accumulation also in SL-depleted plants instead. These transporters belonging to the PHT1 family are in fact abundantly induced by P starvation in tomato as well as in other species from Solanaceae and other plants families as Leguminosae and Brassicaceae (Chen *et al*., 2014a). In particular, among the eight PHT1 transporters in *S. lycopersicum*, *LePT1* and *LePT7* are ubiquitously expressed in plant tissues, especially roots and leaves and under low P conditions, while *LePT4* is usually strongly activated in the roots colonized by AM fungi under low P (Chen *et al*., 2014a), highlighting an indirect influence of SLs on mycorrhizal colonization. Our results are partly in agreement with the findings of Gamir and coworkers (2020), as far as inducibility of *LePT2* by P starvation in the WT. However, they are apparently in contrast with their observation that the transcriptional induction of *LePT2* and of the PSR regulator miR399, and the down-regulation of *PHO2*, were compromised in the tomato SL-depleted line *SlCCD8*-RNAi L04 when compared to the WT under low P. However, the very different conditions under which these apparently contrasting results were obtained (80 *vs* 800 µM Pi for P-sufficient condition, and 0 vs 200 µM Pi for the P-depleted condition in our work and in Gamir and coworkers (2020),

respectively) highlight how the regulation of Pi transporters in SL-depleted plants is strongly dependent on the levels of P provision and is modified when growth conditions resemble the more realistic concentrations of P in soils (around 80 µM Pi). Such differences in P supply may have triggered diverse signals in plants in response to decreased P availability, especially in the high-affinity range of Pi transporter activity and induction (µM range). Given that the P-utilization efficiency is promoted by SLs, it is conceivable that the lower P concentrations applied to plants in our study amplified the sensitivity of SL-depleted plants to P-deficiency, also resulting in the activation of the core PSR module at P levels that are still perceived as sufficient by WT plants. Consistently with the higher PHT transcript abundance in the roots of SL-depleted plants under both P conditions, we indeed observed higher miR399 and coherently lower *PHO2* levels, which constitute one of the best-understood systemic signalling pathways activated under P stress (Bari *et al*., 2006; Pant *et al*., 2008).

The hypothesized higher susceptibility to P-shortage displayed by SL-depleted plants and consequent altered regulatory mechanisms is further supported by the higher enzymatic activity in their roots, under both P conditions. A higher phosphatase activity might in fact be indicative of more intense P release from P-containing cellular constituents, such as membrane phospholipids, to promote P remobilization inside cells and the whole plant, being phosphatases involved in many P-related metabolic routes (Bozzo *et al*., 2005; Vance *et al*., 2003). On the other side, elevated activity of phytases in the roots of SL-depleted plants suggests an attempt to mine P from inositol hexaphosphate, which represents one of the major organic P forms found in soils, or to use the internal phytate-derived P, being phytate the principal storage form of P in many plant tissues (Baldwin *et al*., 2001; Brinch-Pedersen *et al*., 2002; Hayes *et al*., 2000). Given the strong positive correlation between P and N content (Pearson correlation coefficient $\rho = 0.619$, $p < 0.01$), it is possible that the remarkable enzymatic activity of SL-depleted plants is related to the use of this element to build-up enzyme molecules (de Groot *et al*., 2003). Under –P conditions, the response of SL-depleted plants in terms of enzymatic activity was comparable to that of WT

plants, even if the low N content of these plants could indicate the exudation of these enzymes by roots, in the attempt to release P from soil organic P-esters (Vance *et al*., 2003). However, this result highlights that, even if under +P conditions SL-depleted plants activate the typical PSRs, possibly because of an altered perception of this nutrient, under –P the onset of these same responses was not as intense as conceivable from the elevated necessity of P under optimal growth conditions. The R/S ratio and P-utilization efficiency were in fact comparable to those of P-stressed WT plants. The modification of resource distribution in favour of belowground biomass production over shoot growth negatively correlated with the plant P content ($\rho = 0.867$, $p < 0.01$), and is a typical response to P starvation intended to increase soil exploration by roots to enhance P uptake (Aziz *et al*., 2014; Niu *et al*., 2013; Ramaekers *et al*., 2010). Additionally, the expected increase in R/S ratio induced by P starvation was observed in both WT and SL-depleted plants, confirming that the differences between these genotypes observed in Chapter 2 were likely due to differences in root topology rather than biomass allocation. Also the expression of the high-affinity Pi transporters was higher than in WT plants, but comparable to the same genotype under +P conditions, in line with our last hypothesis.

3.4.2 *Root exudation*

The results discussed so far suggest that, when the concentration of P in the nutrient solution resembles that found in soil, SL-depleted plants activate some of the strategies that are usually adopted to respond to P shortage, as increased expression of high-affinity Pi transporters and enzymatic activity, resulting in a higher P consumption from the nutrient solution and consequently higher P concentration in tissues, especially in the more-developed aerial part. This altered sensing of external P is consistent with the morphological and microscopic data of Chapter 2, and was not reflected by an equally intense response under real P stress (–P conditions). The strongly reduced SL production by this genotype attested in Vogel and coworkers (2010) could therefore be responsible for the disorganized response to normal P conditions and missing or unoptimized reaction to P stress, the latter possibly deriving from an altered perception caused

by the anatomical disorganization at the root tips.

In light of these results, we sought to understand whether this increased P demand by SL-depleted plants was also translated in a different capacity of organic acid anions and proton exudation, representing the major expression of P acquisition strategies.

Our kinetic study of exudation clearly highlighted a time-depending response in terms of both organic C exudation and proton release. In the short term (0-24 h), organic C content in the solutions of both genotypes under either P conditions reached a concentration plateau, that was lower in the case of +P SL-depleted plants and comparable between this genotype under –P conditions and WT plants. Phosphorus-starved SL-depleted plants in fact exuded more organic C than the same +P genotype since the very beginning of the experiment (1 h), while DOC exudation from roots of WT plants was not altered by P supply. Based on kinetic assays, WT plants under –P exuded C faster than under +P conditions and –P SL-depleted plants, that in any case achieved a slightly higher exudation plateau. In the long term, instead, C concentration steadily increased with time maintaining the same exudation trend, with +P and –P SL-depleted plants exuding the lowest and highest C amount, respectively, while WT plants exuded a similar intermediate amount regardless of the P conditions, in line with other studies carried out on tomato (Neumann and Römheld, 1999). In addition, the ratio of DOC release between –P and +P SL-depleted plants remained almost steady throughout the experiment, suggesting that differences in organic C exudation in this genotype were established early during P deficiency, while the low DOC exudation observed in +P SL-depleted plants might be in part due to a feedback repression exerted by higher P accumulation in the shoot. When plants were moved to water to stimulate further exudation, C release increased with increasing time, and –P WT plants resulted in the highest exudation levels, while +P SL-depleted plants confirmed the trend of lower exudation. The increased C exudation by P-depleted WT plants could be the result of a forced release of re-accumulated organic acid, as discussed later (Tiziani *et al*., 2020). Organic acid anions analysis revealed that the majority of this C was constituted by oxalate,

whose exudation kinetics clearly matched the one of C. In particular, SL-depleted plants released oxalate anions faster than WT plants under either P conditions during the first 24 h, while the concentration increase in the long term proceeded specularly to WT plants, but resulted in significantly higher oxalate content in the exudates of –P SL-depleted plants.

Another strategy usually adopted by P-starved plants and in this case shared by –P WT and SL-depleted plants was the increase of proton release by roots. Rhizosphere acidification is a well-known response activated by P-starved plants to enhance the bioavailability of soil P (Shen *et al*., 2011). Root-induced acidification can decrease the rhizosphere pH by 2 or 3 units relative to the bulk soil, resulting in substantial dissolution of sparingly available soil P (Marschner, 1995). Depending on the plant species, rhizosphere acidification is due to either enhanced net release of protons via stimulation of the plasma membrane H^+-ATPase activity, or increased release of organic acids (Marschner, 1995; Siao *et al.,* 2020). Because the amount of organic C (and therefore of oxalate) in the exudates of WT plants was almost the same regardless of the P treatment applied, we conclude that the acidification of the nutrient solution in this study was restricted to proton release. Consistent with our findings, many authors exclude that H^+-ATPase activity coincides with increased exudation of organic acid anions in tomato under P stress (Neumann and Römheld, 1999; Yu *et al*., 2016). As observed in the case of C exudation, during the first 24 h of P treatment, the amount of released protons fastly increased until reaching a plateau for both genotypes and P conditions. In this case, the highest plateau was reached by P-depleted WT plants, that differentiated from the other cases after around 5 hours since the beginning of the experiment, highlighting how WT plants responded more promptly to P-starvation through the strategy of nutrient solution acidification. In the long term instead, both +P WT and SL-depleted attained a plateau of proton release at a comparable value, while –P plants constantly increased solution acidification. More specifically, –P WT plants released the highest amount of protons, almost double than the corresponding +P plants. Conversely, the initially lower exudation by SL-depleted plants under –P was

followed by an increase after 4 days, reaching values comparable to the plateau attained by +P plants. This could be due to a delayed activation of factors acting in parallel with SLs in the signalling pathway activated under –P. In fact, although the loss of sensitivity of plant response to low P by SL mutants was reported in rice (Sun *et al*., 2014) and *Arabidopsis* (Mayzlish-Gati *et al*., 2012), at least in terms of root architecture modifications, it was also shown that the SL mutants *max*2-1 and *max*4-1 were able to increase root hair production in response to low P over time, eventually reaching WT levels (Mayzlish-Gati et al., 2012). In addition, proton extrusion from P-deficient SL-depleted plants strongly intensified when they were transferred to water. Possibly, if these plants showed an altered sensitivity to P stress as we hypothesize, they suffered more than WT plants when all other nutrients were no longer available. Therefore, they significantly promoted protons release in the attempt to get nutrient foraging.

Taken together, all these results highlight how, as observed previously, even if SL-depleted plants appeared to be more P-demanding than WT tomato plants, under P stress conditions they were not able to efficiently activate the mechanism usually adopted to increase P uptake, despite the up-regulation of Pi transporters and the elevated activity of Pi-solubilizing enzymes. The reduced SL biosynthesis had therefore negative effects under both the applied P conditions. Under +P, SL-depleted plants activated many physiological responses to sustain the elevated P uptake, as if they were under P shortage, with a great C cost to build up transporters and enzymes possibly resulting in lower C exudation. Under –P conditions, where an accentuation of PSRs could be expected, these plants resulted less efficient at responding to P shortage than WT plants. Despite the great differences in proton release by WT plants under –P than +P conditions, only small changes in C exudation and organic acid anions amount were evident along the experiment, while differences were more accentuated in SL-depleted plants where, on the other hand, proton extrusion did not differ between P treatments. This result confirms our hypothesis on the independence of rhizosphere acidification from organic anion exudation. Among all exuded organic acids, oxalic was clearly the most abundant, with values largely exceeding those

of succinic, citric and malic. Oxalate is the simplest dicarboxylic acid, with high-acidity (pK_{a1}= 1.23) and strong chelating capacity for Ca^{2+}, Al^{3+}, Fe^{3+} (Ryan *et al.,* 2001). It is widely distributed in the plant kingdom and may account for 6-10% of tissue dry weight in many plant species, and its elevated exudation could be related to the fact that its release is energetically favoured as less C and energy are consumed when being exuded, and it is easier to metabolically engineer since it is not an intermediate metabolite like citrate and malate (Zhao *et al*., 2014). In addition, due to its strong adsorption and affinity for soil components and synthetic Fe oxides, it is one of the most effective anions in displacing P anions from poorly-available systems (Hinsinger, 2001). Nevertheless, for WT plants, we cannot exclude that tomato plants re-acquired organic acids occurring in root exudates under P deficiency in order to recycle C sources, a process recently reported by Tiziani and coworkers (2020) using ^{13}C-labelled molecules. However, other studies carried out other species like white lupin, alfalfa, oilseed rape and chickpea indicated a trend of increased exudation of organic anions under P deficiency (Aziz *et al*., 2014; Neumann and Römheld, 1999). It is also possible that the P dosages applied did not allow discriminating differences in organic acid exudation or that plants preferred to activate concomitant alternative strategies to acquire P to prevent excessive C losses.

Part II
CHAPTER 4

Retention of inorganic and organic P through adsorption on ferrihydrite and coprecipitation during ferrous iron oxidation: extent and mechanisms

4.1 Introduction

In the experiments described in Part I, P was directly available to plants in the nutrient solution in the form of soluble potassium phosphate. However, the concentration of available Pi in soil seldom exceeds 10 µM (Bieleski, 1973), which is much lower than P concentration in plant tissues, ranging approximately from 5 to 20 mM (Raghothama, 1999). This is due to abiotic reactions that seize P in the solid phase decreasing its availability to plants, and to the fact that up to 80% of total soil P occurs as organic P, which requires mineralization prior to acquisition (Turner *et al*., 2002).

These abiotic processes involve adsorption and precipitation reactions and are related to the different affinity of organic P compounds for Fe and Al species and to the solubility of their salts (Celi *et al.*, 2003; 2020; Ognalaga *et al.*, 1994; Zhang *et al.*, 1994). In addition, P retention through coprecipitation with Fe following changes in pH, redox potential or ionic strength is a common process occurring in water and sediment environments. The oxidation of Fe(II), released into the soil solution during mineral weathering and/or reductive dissolution under anoxic conditions, and precipitation of Fe (hydr)oxides is indeed known to contribute significantly to the retention of Pi (Senn *et al*., 2015; van der Grift *et al*., 2016; Voegelin *et al.,* 2010; 2013) and other inorganic and organic anions (Gorra *et al.,* 2012; Mikutta *et al*., 2014; Senn *et al.,* 2015). However, the retention mechanisms involved in Pi coprecipitation with Fe are not fully understood, and little is still known about the mechanisms of organic P retention during coprecipitation.

Therefore, this chapter aims at **providing new insights into the role of coprecipitation in inorganic and organic P retention, to further investigate how plants may modify their strategies to acquire these scarcely-available**

P forms. To achieve this goal, we studied the reaction kinetics and properties of the formed Fe-P systems during *myo*-inositol hexaphosphate (*myo*InsP6) coprecipitation with Fe(II). Based on previous considerations, we hypothesized that **i) coprecipitation retains more P than adsorption; ii) the kinetics of P retention and Fe(II) oxidative precipitation depend on the type of organic P compound involved and the initial P/Fe ratio; iii) the type of organic P compound influences the mineralogy, morphology and surface properties of the formed coprecipitates.** We tested these hypotheses by synthesizing a series of Fe-P coprecipitates with increasing P/Fe ratios at near-neutral pH. These systems were obtained during the oxidative Fe(II) precipitation in the presence of *myo*InsP6 or inorganic phosphate (Pi). For comparative purposes, we also studied the adsorption of these two compounds on a ferrihydrite synthesized by the same procedure, and obtained the computational geometries of *myo*InsP6 molecule to gain more insights into the possible interaction mechanisms between the molecule and the Fe oxide surface.

4.2 Materials and methods

4.2.1 *Phosphorus-containing compounds*

Potassium dihydrogenphosphate, KH_2PO_4 (≥99.0%, P5655) and dipotassium *myo*-inositol hexaphosphate ($C_6H_{16}O_{24}P_6K_2$, premium quality level, P5681) were analytical grade reagents from Sigma-Aldrich. To minimize the effect of hydrolysis, solutions of *myo*InsP6 were freshly prepared prior to each test. All solutions were prepared in 0.01 M KCl.

4.2.2 *Synthesis of ferrihydrite*

Two-line ferrihydrite (Fh) was prepared by rapidly oxidizing a 2.0 mM $FeCl_2$ solution at pH 6.0 ± 0.2 in a 2 L reagent bottle fitted with an oxygen supply tube (200 mL min^{-1}), a pH probe and a burette tip. During oxidation, the contents were continuously stirred while pH was maintained at 6.0 by progressive addition of 0.25 M KOH by means of an automatic titrator (TTT85 titrator and ABU80 autoburette, Radiometer, Copenhagen, Denmark). The addition of base was continuously recorded during the experiment. After complete oxidation, evaluated

through the disappearance of Fe(II) from solution, the reaction volume was reduced by centrifugation and removal of the supernatant, while the concentrated suspension was stored at 4°C until further use. Iron concentration of the suspension was measured by atomic absorption spectrometry (PerkinElmer AAnalyst 1400, Norwalk, CT, USA) after acidic dissolution.

4.2.3 *Synthesis of Fe-P adsorbed and coprecipitated systems*

Ferrihydrite-P surface adsorbed systems (ADS) with increasing P loadings were prepared by mixing solutions of Pi and *myo*InsP6 having different P concentrations (0.05–2 mM P) with suspensions of Fh (previously prepared as described above) at pH 6.0 to obtain initial solution molar P/Fe ratios [$(P/Fe)_0$] of 0.05, 0.1, 0.5 and 1.0. $(P/Fe)_0$ ratios were chosen in accordance with the relative abundance and speciation of P compounds in soils (Magid *et al*., 1996) and based on the Langmuir adsorption coefficients determined by preliminary adsorption isotherm experiments (Table 4.1).

Table 4.1: Langmuir coefficients of adsorption isotherms of $H_2PO_4^-$ (Pi) and *myo*-inositol hexaphosphate (*myo*InsP6) on ferrihydrite.

P form	Isotherm	Coefficients
Pi	Langmuir $Q_a = \frac{Q_{max} \cdot C_e \cdot K_L}{1 + K_L \cdot C_e}$	Q_{max} = 1.34 µmol m^{-2} K_L = 89.3 L $mmol^{-1}$ R^2 = 0.817
*myo*InsP6	Langmuir	Q_{max} = 2.59 µmol m^{-2} K_L = 67.3 L $mmol^{-1}$ R^2 = 0.805

Fe-P coprecipitates (COP) with the same $(P/Fe)_0$ ratios as the adsorbed systems were prepared by oxidizing a 2 mM $FeCl_2$ solution in the presence of increasing amounts of P, using the same procedure as described for the preparation of Fh above. All batch preparations (2 L total volume) were performed in triplicate and maintained under vigorous stirring for 1 h at 25°C and subsequently allowed to equilibrate for 23 h at 4°C. The suspensions were then centrifuged (10,000 rpm for 10 min) and the supernatant analyzed for Fe, P and pH after filtration through a 0.20 µm nylon membrane filter. The amount of P retained was determined as the difference between initial and equilibrium P concentrations. The synthesized

materials were washed with deionized water, dialyzed through a 14 kDa membrane, freeze-dried and stored in a desiccator until analysis.

4.2.4 *Coprecipitation kinetics*

During the synthesis of Fh and coprecipitates, a small aliquot of the suspension was sampled at regular time intervals, filtered through a 0.20 µm nylon membrane filter and analyzed to follow changes in the concentrations of Fe(II), Fe(III) and P over time. Dissolved Fe(II) concentrations were measured colorimetrically immediately after sampling using the 1,10-phenanthroline method (Loeppert and Inskeep, 1996) and the total Fe in the solution was measured by atomic absorption spectrometry (PerkinElmer AAnalyst 1400, Norwalk, CT, USA). Fe(III) concentrations were then calculated as the difference. Dissolved P concentrations were measured colorimetrically using the malachite green method (Ohno and Zibilske, 1991) for Pi while, for *myo*InsP6, dissolved P concentrations were measured colorimetrically after sulfuric-perchloric digestion (Martin *et al*., 1999). At each sampling time, the volume of OH^- added by the automatic titrator was recorded and used to calculate the H^+ ions released during Fe(II) oxidation and hydrolysis. All concentrations were corrected for the volume of KOH added and the change in the reaction volume with successive sampling.

4.2.5 *Characterization of Fe-P adsorbed and coprecipitated systems*

Iron and P contents in the obtained coprecipitates were determined by dissolving 1 mg of each sample in 2 mL of 6 M HCl, neutralizing with 10 M NaOH using 4-nitrophenol as pH indicator, and quantifying Fe and P concentrations as described above. The specific surface area (SSA) and porosity of the Fe-P systems were determined by N_2 adsorption-desorption isotherms performed at 77 K. The SSAs were estimated by applying the Brunauer-Emmett-Teller (BET) equation (Brunauer *et al*., 1938), whereas microporosity was calculated by the t-plot method (Gregg and Sing, 1982) and the mesopore size distribution by the Barrett-Joyner-Halenda (BJH) analysis (Barrett *et al*., 1951). The zeta potential (ζ) was calculated from the electrophoretic mobility determined on a 0.2 mL suspension of freshly synthesized material diluted with 5 mL of its supernatant by

Laser Doppler Velocimetry coupled with Photon Correlation Spectroscopy (LDV-PCS) using a spectrometer (DELSA 400, Beckman Coulter Inc., Hialeah, FL) equipped with a 5 mW He-Ne laser (632.8 nm). X-ray diffraction (XRD) patterns of powder samples were acquired in Bragg-Brentano geometry, using an X'Pert PRO MPD diffractometer (PANalytical, The Netherlands) equipped with Cu anode, ultrafast detector and working at 45 kV and 40 mA. The acquisition was performed between 10 and 80°, with a step size of 0.02° and a 3 s step time. Transmission electronic microscopy (TEM) was conducted in the bright field modality with a 300 kV ultrahigh resolution JEOL-JEM-3010 Transmission Electron Microscope (Tokyo, Japan), equipped with a LaB_6 filament and an Energy Dispersive X-ray Spectrometer (EDS) detector. Samples for TEM observations were prepared by depositing ground powder samples on a carbon coated copper grid (200 mesh). X-ray photoelectron spectroscopy (XPS) measurements were carried out using a PHI X-tool Automated XPS Microprobe (ULVAC-PHI, Inc., USA) applying monochromatic Al Kα-radiation. Samples were deposited on a double-stick tape that was placed on the sample holder. Except for drying the sample, no other pre-treatment was performed. For each sample, an XPS survey scan was acquired confirming the presence of P, oxygen (O), Fe and C in all samples. In addition, narrow scans around the C 1s (278–298 eV), O 1s (523–543 eV), P 2p (123–143 eV) and Fe $2p_{3/2}$ (702–727 eV) were acquired. Before determining the position of the peaks, a background subtraction was performed and the spectra were calibrated to C 1s excitation at BE of 284.8 eV from adventitious C, which was present on all surfaces. Data were collected and analyzed with the Multipack Software from Physical Electronics. Diffuse reflectance infrared (DR-IR) spectra were acquired between 4000 and 400 cm^{-1} at a resolution of 4 cm^{-1} with a Bruker Vertex 80v vacuum FT-IR Spectrometer (Bruker Scientific Instruments, Billerica, MA, USA) and a praying mantis diffuse reflectance attachment (Harrick Sci., Inc.). All samples were ground and prepared by mixing 10 mg of sample with 390 mg of finely powdered KBr (Merck, spectroscopic grade).

4.2.6 *Computational studies*

For the computational calculations, the two *myo*InsP6 chair conformations (1-axial/5-equatorial and 5-axial/1-equatorial) were considered, as reported in Barrientos and Murthy (1996). The two structures were drawn with the use of the software GaussView 5.0.9 (Gaussian Inc., Wallingford, CT 06492 USA) then their geometry was investigated at the Hartree-Fock (HF) level of theory employing the 3-21G basis set, with Gaussian ® 09 W software (Gaussian Inc., Wallingford, CT 06492 USA). The distances among the P and O atoms belonging to the six phosphate groups were then measured for the two conformers, with the help of Moldraw software (Ugliengo *et al*., 1993; http://www.moldraw.unito.it).

4.3 Results

4.3.1 *Phosphorus retention by adsorption and coprecipitation*

Inorganic phosphate retention by adsorption on Fh increased with increasing $(P/Fe)_0$, gradually approaching a maximum of P/Fe ~ 0.20 at the largest $(P/Fe)_0$ ratio (Fig. 4.1a). In contrast, molar P/Fe ratios of coprecipitates increased nearly linearly with increasing $(P/Fe)_0$, up to a maximum value of 0.78 over the experimental range evaluated. Adsorption of *myo*InsP6 also approached a maximum P/Fe ratio of around 0.25, while the similarity between coprecipitate P/Fe and $(P/Fe)_0$ ratios suggested a complete retention of *myo*InsP6 over the entire experimental range (Fig. 4.1b).

4.3.2 *Coprecipitation kinetics*

In the absence of P, the disappearance of Fe(II) from solution during oxidation at pH 6.0 was complete within 20 min (Fig. 4.2a). The release of H^+ followed a similar trend with a final H^+/Fe_0 ratio (Fig. 4.2b) that was only slightly greater than the stoichiometric value for the oxidation and hydrolysis of Fe^{2+} ($H^+/Fe_0 = 2.0$). The presence of Pi slowed down the rate of Fe(II) oxidation and precipitation particularly at $(P/Fe)_0 = 0.1$ and the complete disappearance of Fe(II) occurred after approximatively 30 min (Fig. 4.3a). The rate of disappearance of Pi from the solution also tended to decrease with increasing $(P/Fe)_0$ (Fig. 4.3b). Whereas all the added anion was precipitated by the end of the oxidation at $(P/Fe)_0 \leq 0.5$, only 62% of initial Pi was retained by the end of the coprecipitation at $(P/Fe)_0 = 1.0$.

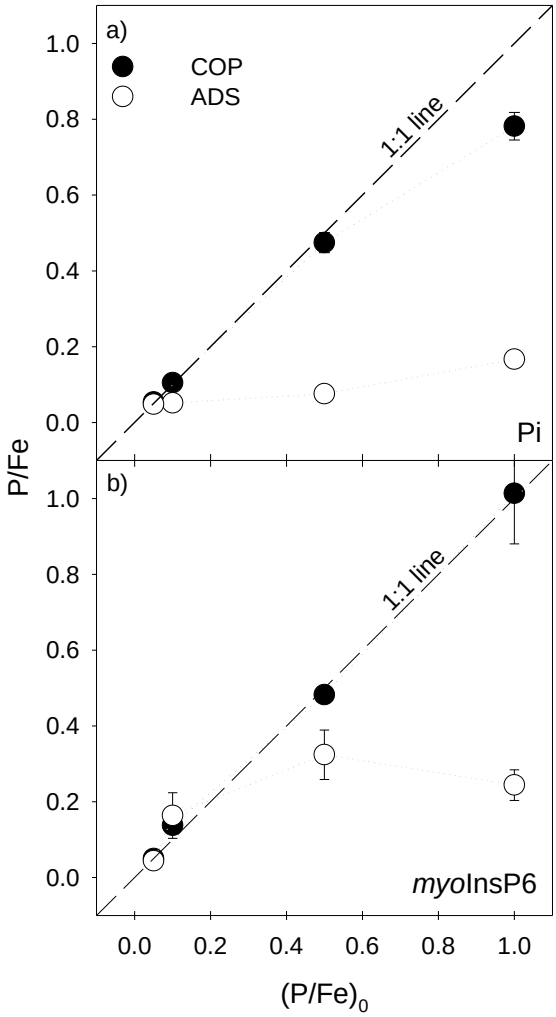

Figure 4.1: P retention by adsorption (open symbols) and coprecipitation (closed symbols) with increasing initial molar $(P/Fe)_0$ ratios of (a) inorganic phosphate (Pi), (b) *myo*-inositol hexaphosphate (*myo*InsP6).

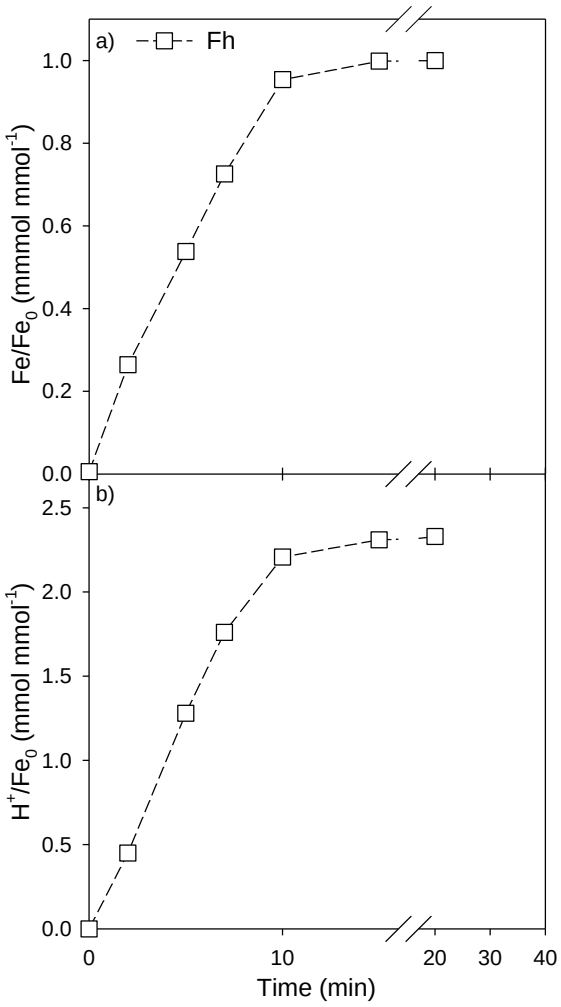

Figure 4.2: Kinetics of Fe precipitation (a) and H^+ release (b) during the oxidative precipitation of Fe(II) in the absence of P. Values, normalized to the initial amount of Fe (Fe_0), represent the mean of three replicates (standard error always <5%).

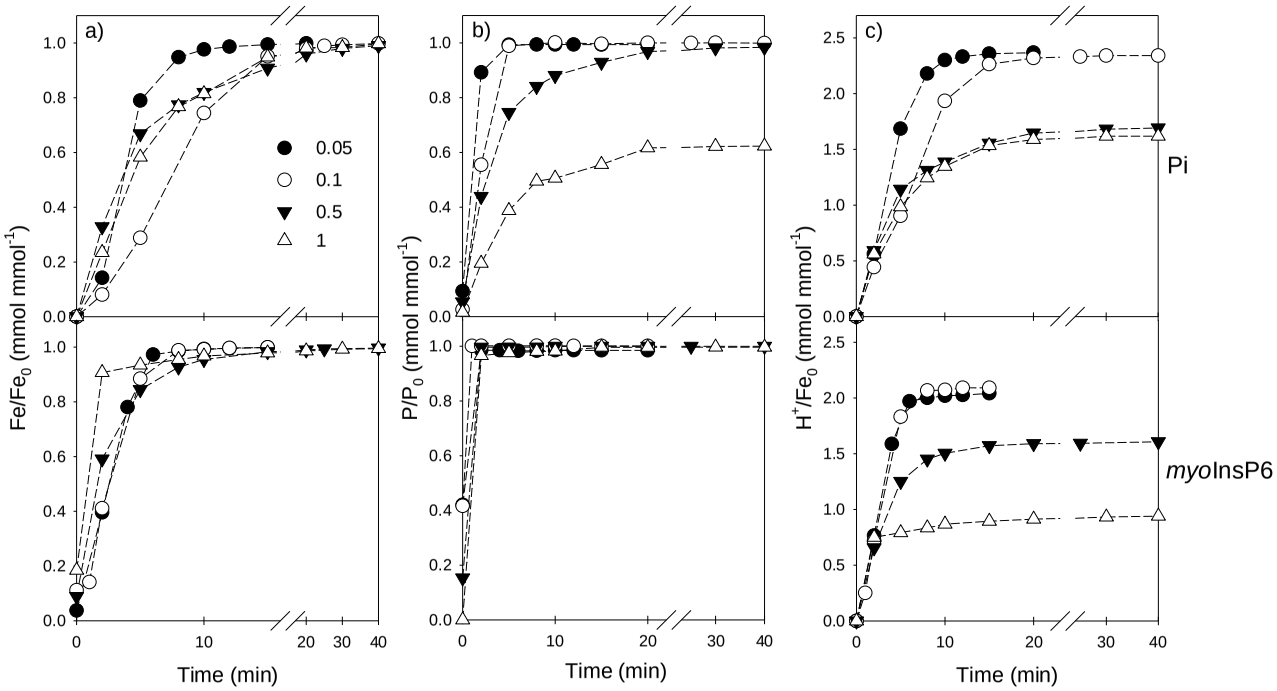

Figure 4.3: Kinetics of a) Fe precipitation, b) P retention and c) H^+ release during the oxidative precipitation of Fe(II) in the presence of inorganic phosphate (Pi) and *myo*-inositol hexaphosphate (*myo*InsP6) as a function of increasing initial molar $(P/Fe)_0$ ratios (different series symbols). Values represent the mean of three replicates (standard error always <5%).

The molar H^+/Fe_0 ratio at the end of the coprecipitation was > 2.0 for $(P/Fe)_0$ < 0.5, while it tended towards 1.5 at greater $(P/Fe)_0$ values (Fig. 4.3c).

The rate of Fe(II) oxidation and precipitation increased in the presence of *myo*InsP6, leading to a complete disappearance of Fe(II) from solution within only 10 min (Fig. 4.3a). The precipitation of *myo*InsP6 was also very rapid and complete, with all P disappearing from solution within the first 5 min for all $(P/Fe)_0$ ratios (Fig. 4.3b). The H^+/Fe_0 ratios at the end of the oxidation reached values around 2.1 in the two systems with lower $(P/Fe)_0$, while it tended towards approximately 1.5 and 1.0 for $(P/Fe)_0$ of 0.5 and 1.0, respectively (Fig. 4.3c).

4.3.3 *Properties of the Fe-P precipitates*

4.3.3.1 *Surface properties*

Coprecipitates obtained with increasing additions of Pi showed a consistent decrease in N_2-SSA, in contrast to the adsorbed systems that only presented a modest variation in N_2-SSA with increasing P loadings (Table 4.2). According to the IUPAC classification of adsorption isotherms (Alothman, 2012), all synthesized materials appeared to be mesoporous. In particular, Pi coprecipitates showed a great increase in pore volume with increasing $(P/Fe)_0$ (Table 4.2). At low $(P/Fe)_0$, pores were 7 to 10 nm wide (mesoporous material), while at greater P contents the pore width increased reaching a value of around 60 nm (microporous material). In contrast, adsorbed Pi samples showed little variation in BET N_2-SSA, pore size and distribution, with an increase in the pore width (from 10 to 15 nm) only observed at the greatest $(P/Fe)_0$ ratio. The ζ potentials of the Fe-Pi systems became less positive with increasing P contents, reaching negative values at $(P/Fe)_0$ = 1.0 (Table 4.2). Similar ζ potentials were obtained for coprecipitated and adsorbed systems, despite the greater P contents in the former (Fig. 4.1). At the lowest $(P/Fe)_0$ ratios, coprecipitation or adsorption of *myo*InsP6 induced a more prominent reduction in N_2-SSA in comparison with Pi, while similar values were observed at greater $(P/Fe)_0$ ratios (Table 4.2). Fe-*myo*InsP6 coprecipitates generally showed lower N_2-SSA values with respect to the adsorbed systems. Mesopore volumes were generally greater in the former, with the widest pore width (60 nm) observed already at $(P/Fe)_0$ = 0.5, while in the

adsorbed systems pore volume and width tended to increase with increasing P loading over the whole $(P/Fe)_0$ range evaluated. Adsorption of *myo*InsP6 also led to a negative surface charge even at the lowest P loadings, while only coprecipitates obtained with $(P/Fe)_0 \geq 0.5$ showed negative ζ potentials.

Table 4.2: Specific surface area (SSA), total mesopore volume, ζ potential and element composition of the coprecipitated and adsorbed systems.

Sample	SSA ($m^2\ g^{-1}$)	Mesopore volume ($mm^3\ g^{-1}$)	ζ potential (mV)	Chemical P/Fe ratio	XPS P/Fe ratio
Fh	385	360	28	-	-
COP 0.05 Pi	333	451	23	0.05	0.14
COP 0.1 Pi	317	446	12	0.11	0.23
COP 0.5 Pi	194	850	2	0.47	1.15
COP 1 Pi	176	1200	–11	0.78	1.53
ADS 0.05 Pi	327	453	22	0.05	0.13
ADS 0.1 Pi	323	490	16	0.05	0.16
ADS 0.5 Pi	307	486	10	0.08	0.25
ADS 1 Pi	293	564	–18	0.17	0.22
COP 0.05 *myo*InsP6	279	448	20	0.05	0.05
COP 0.1 *myo*InsP6	264	516	8	0.11	0.20
COP 0.5 *myo*InsP6	193	882	–38	0.48	0.92
COP 1 *myo*InsP6	191	859	–47	1.01	1.79
ADS 0.05 *myo*InsP6	275	465	–14	0.04	0.13
ADS 0.1 *myo*InsP6	294	397	–38	0.16	0.18
ADS 0.5 *myo*InsP6	301	433	–44	0.33	0.34
ADS 1 *myo*InsP6	272	593	–62	0.24	0.35

4.3.3.2 *X-ray diffraction*

The diffractograms of the adsorbed Pi systems showed two broad signals at around 36° and 63° 2θ, typical of 2-line Fh (Fig. 4.4). Coprecipitation with Pi resulted in a similar 2L-Fh pattern at low $(P/Fe)_0$, while at greater ratios diffractograms were characterized by a broad peak at 30° 2θ and no reflections at wider diffraction angles. Similar patterns were observed for adsorbed and coprecipitated *myo*InsP6 systems, with coprecipitates at greater $(P/Fe)_0$ values showing a single broad peak at around 30° 2θ.

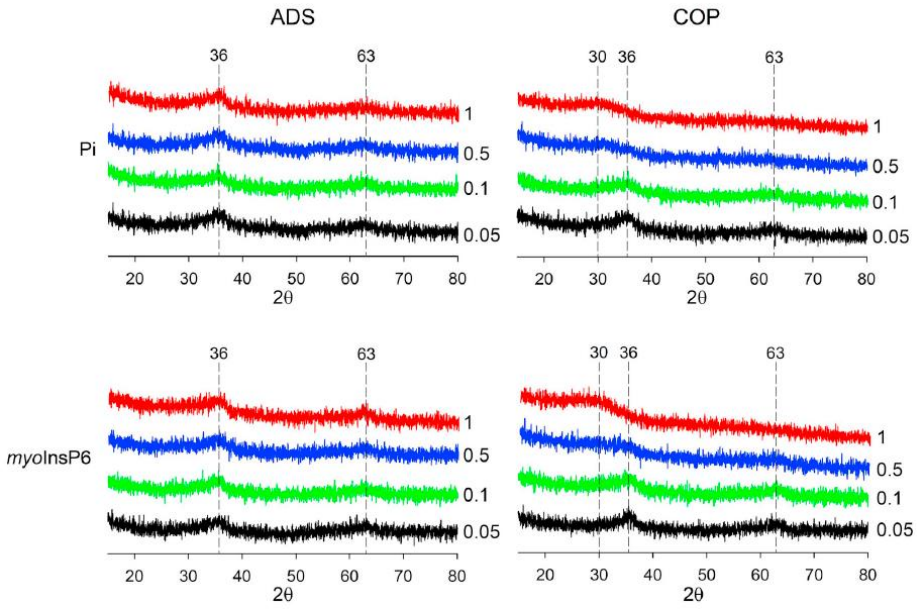

Figure 4.4: X-ray diffractograms of adsorbed (ADS) and coprecipitated (COP) systems. Series labels represent different initial molar $(P/Fe)_0$ ratios. Abbreviations: Pi, inorganic phosphate; *myo*InsP6, *myo*-inositol hexaphosphate.

4.3.3.3 *Infrared spectroscopy*

We focused the analyses of the IR spectra on the 1400–400 cm^{-1} region dominated by bands originating from P-O stretching and bending modes. The main P-O band of the Pi adsorbed systems, centred at ≃1020 cm^{-1}, was asymmetric and composed of at least two overlapping bands (Fig. 4.5). The spectra of the coprecipitated systems showed similar features at the lowest $(P/Fe)_0$. However, this band became more symmetric and shifted from 1020 to 1050 cm^{-1} with increasing $(P/Fe)_0$. The IR spectra of adsorbed *myo*InsP6 systems displayed three partly resolved bands at 1150, 1070 and 990 cm^{-1} (Fig. 4.5), assigned to υ_{as}(P-O), υ_s(P-O) and υ_{as}(P-O-C), respectively (Celi *et al.*, 1999; Guan *et al.*, 2006; Johnson *et al.*, 2012). The same bands were also detected in the spectra of the coprecipitated systems at $(P/Fe)_0 \leq 0.1$. At the greater ratios, the band at 1150 cm^{-1} disappeared and two low-intensity bands formed at 860 and 810 cm^{-1}, attributed to υ_{as}(C-O) and υ_s(C-O), respectively.

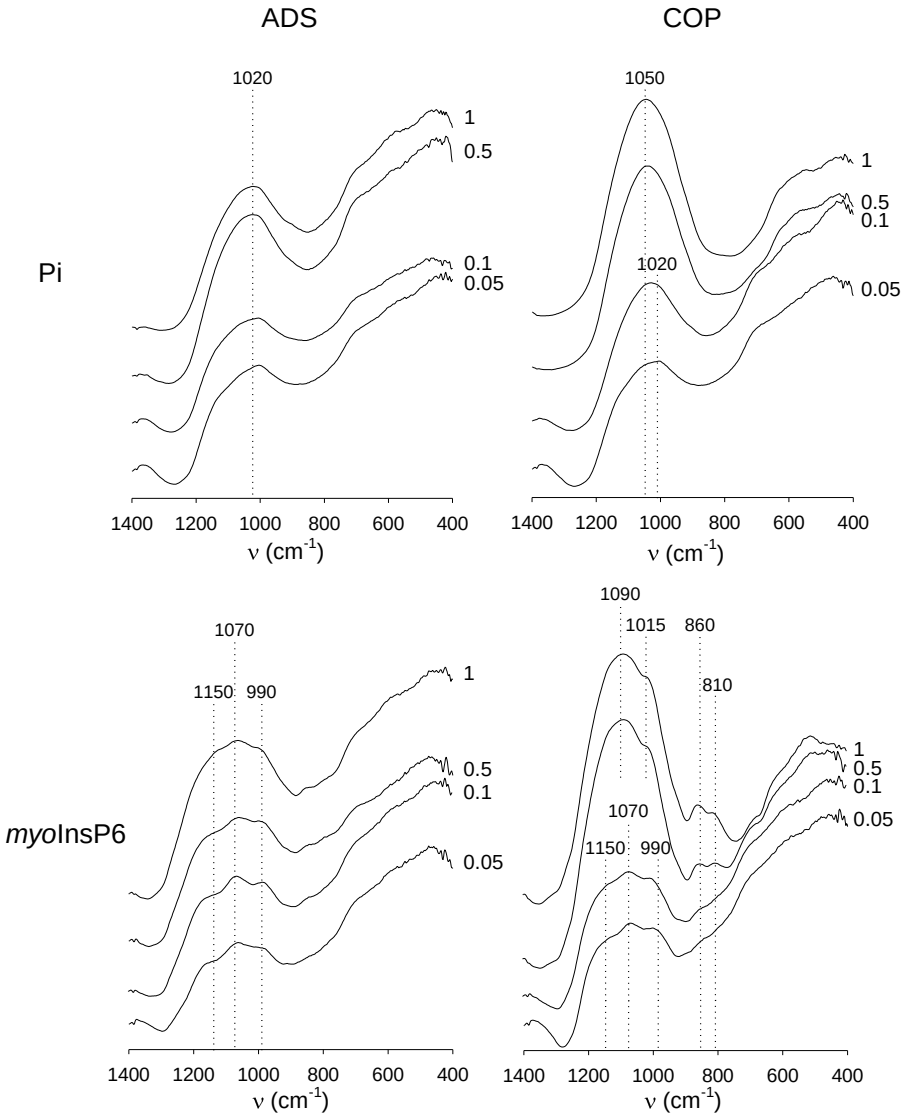

Figure 4.5: FT-IR spectra of adsorbed (ADS) and coprecipitated (COP) systems in the 1400–400 cm^{-1} region. Series labels represent different initial molar $(P/Fe)_0$ ratios. Abbreviations: Pi, inorganic phosphate; *myo*InsP6, *myo*-inositol hexaphosphate.

4.3.3.4 *X-ray photoelectron spectroscopy*

Molar P/Fe ratios were calculated from surface element composition derived from XPS survey spectra (Table 4.2). Comparison with molar P/Fe ratios obtained by acid dissolution was used to evaluate surface enrichment of P during the synthesis of these systems. Adsorption of Pi and *myo*InsP6 resulted in surface molar P/Fe ratios that were slightly greater than molar ratios obtained by acid dissolution. Coprecipitation with Pi resulted in a surface enrichment of P particularly at high P loadings, and a similar surface P enrichment at high $(P/Fe)_0$ ratios was observed for the coprecipitation with *myo*InsP6, although to a lesser extent with respect to Pi.

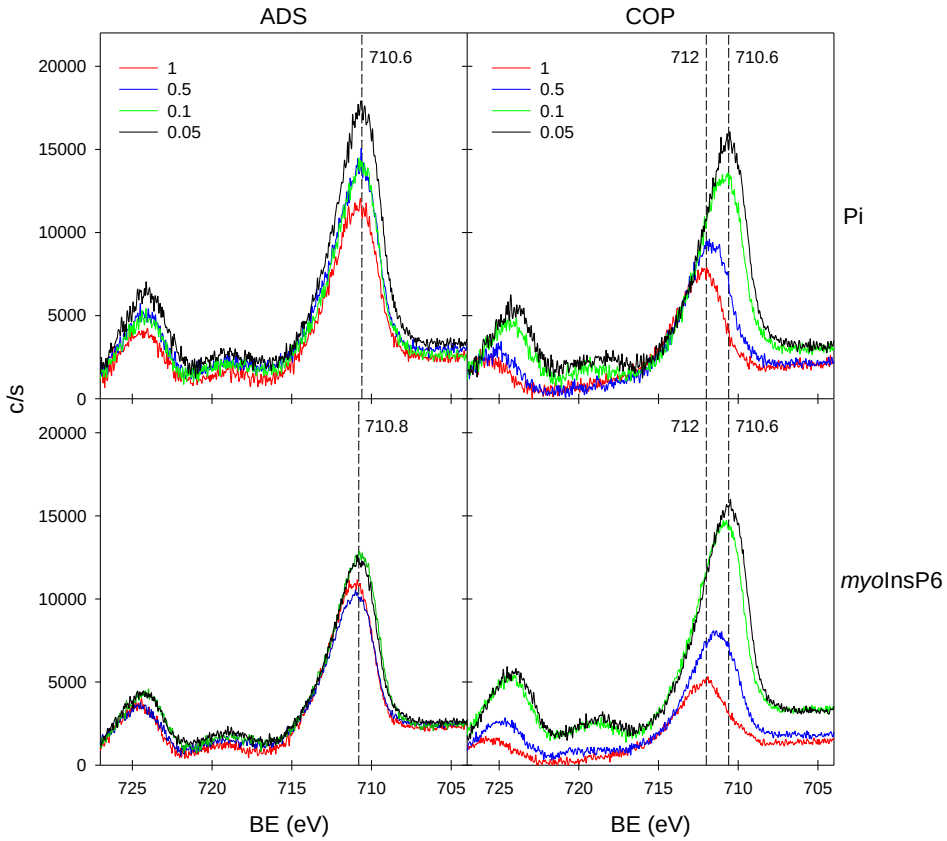

Figure 4.6: XPS spectra (Fe peaks) of adsorbed (ADS) and coprecipitated (COP) systems. Series labels represent different initial molar $(P/Fe)_0$ ratios. Abbreviations: Pi, inorganic phosphate; *myo*InsP6, *myo*-inositol hexaphosphate.

Fe $2p_{3/2}$ XPS spectra of adsorbed Pi systems showed a peak with a binding energy between 711 and 710 eV (Fig. 4.6), corresponding to a Fe (III)-oxide species (Moulder *et al*., 1995), in our case ferrihydrite. The intensity of this peak decreased with increasing P content, suggesting a major coating of P on the (hydr)oxide surface. The Fe $2p_{3/2}$ peak of Pi coprecipitates (Fig. 4.6) not only became less intense with increasing P loading, but also shifted from ~710 to ~712 eV, as a result of a change in Fe chemical state.

Similarly, in *myo*InsP6 adsorbed systems, Fe signals showed a slight decrease in intensity with increasing P content with no peak shift (~710 eV), while the corresponding coprecipitates showed both a decrease in intensity and a shift in Fe $2p_{3/2}$ peaks, from 710 to 712 eV with increasing $(P/Fe)_0$ (Fig. 4.6).

4.3.3.5 *Transmission electron microscopy*

Transmission electron microscopy images of Fh synthesized from the oxidation and hydrolysis of Fe(II) indicate that the (hydr)oxide is composed of particle aggregates that vary from 0.2 to 0.5 μm in size (Fig. 4.7). Particles appear quite small (2–5 nm), well defined and in some regions with an elongated form.

Transmission electron microscopy images of Pi coprecipitates showed an increase in particle size with increasing P content. At low $(P/Fe)_0$ the morphology was similar to the P-free Fh, and the systems appeared to be composed of an amorphous part and of some thin lath-like particles. At greater $(P/Fe)_0$, aggregates appeared to be more compact with bigger individual particles having poorly defined edges and smooth surfaces. Also in *myo*InsP6 coprecipitates aggregation increased with increasing P content with particles ranging from 1 to 3 nm to 5–10 nm at $(P/Fe)_0 = 0.05$ and 1.0, respectively.

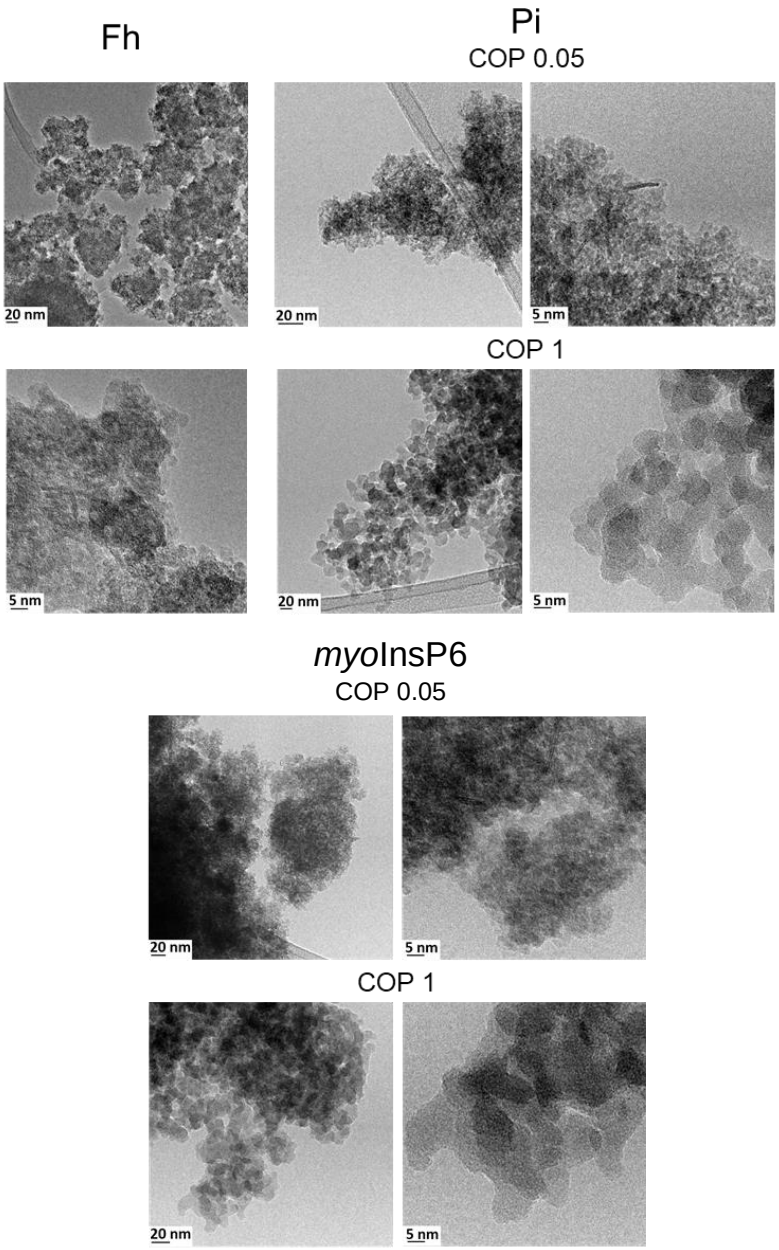

Figure 4.7: Bright field TEM images of ferrihydrite (Fh) and coprecipitated (COP) systems synthesized at lowest and highest initial P/Fe molar ratios. Abbreviations: Pi, inorganic phosphate; *myo*InsP6, *myo*-inositol hexaphosphate.

4.3.4 *Computational results*

The optimized geometries of the two *myo*InsP6 conformations and the distances among O atoms of the six phosphate groups are shown in Fig. 4.8. The sterically unhindered 1-axial/5-equatorial conformer (Fig. 4.8a) was obtained by positioning the phosphate group bound to C2 in axial position and the other five in equatorial position, oriented on the same molecular planes of the inositol moiety. In this conformation, the distances between O atoms of contiguous phosphate groups were in the 0.299–0.363 nm range but increased to more than 0.699 nm between the O atoms of the 2 and 4, 3 and 5, 4 and 6 non-contiguous groups. Conversely, the sterically-hindered 5-axial/1-equatorial conformer (Fig. 4.8b) presented the phosphate group in C2 equatorial and the other five phosphate groups in axial position. The axial 4 and 6 phosphate groups were oriented in a plane opposite to the other four, with respect to the molecular plane of the inositol moiety. In this case, the distances between the O atoms of contiguous and non-contiguous 1, 2, 3 and 5 phosphate groups were in the 0.320–0.380 nm range.

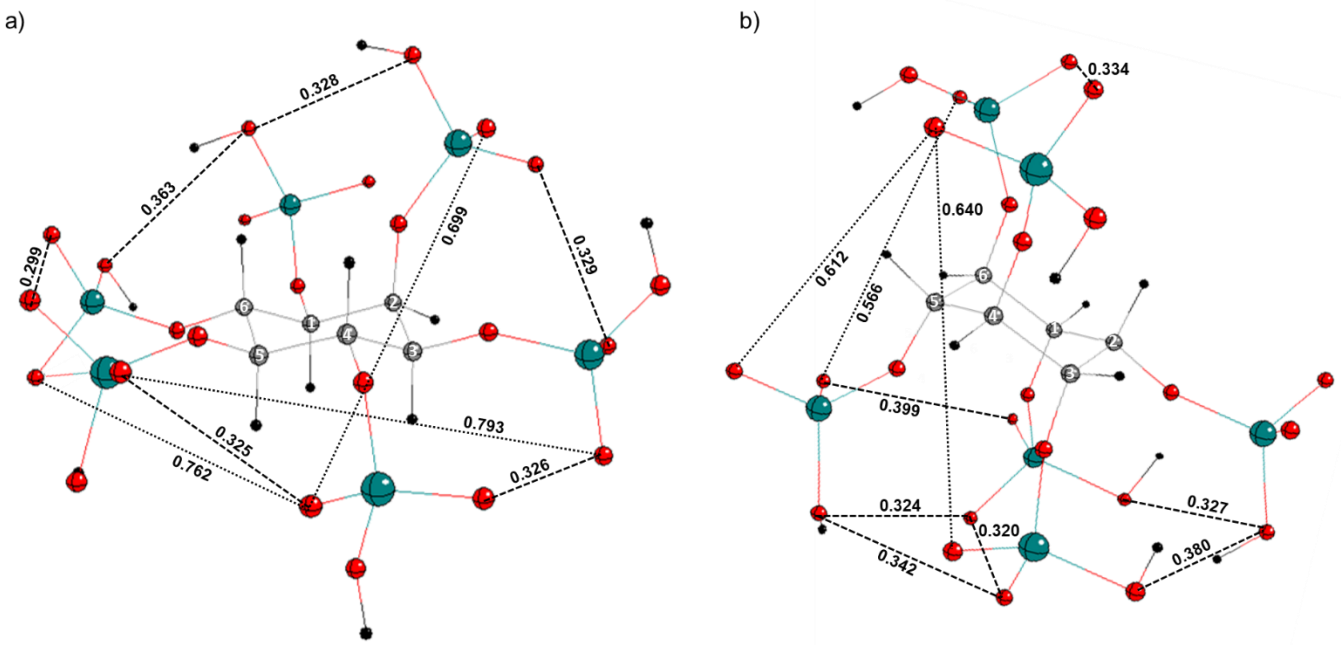

Figure 4.8: Computational a) 1-axial/5-equatorial conformer and b) 5-axial/1-equatorial conformer of *myo*-inositol hexaphosphate (*myo*InsP6). Colors legend: black = hydrogen (H), grey = carbon (C), red = oxygen (O) and dark green = phosphorus (P). Line legend: dashed lines = O bound to contiguous phosphate groups; dotted lines = O bound to non-contiguous phosphate groups.

4.4 Discussion

4.4.1 *Phosphorus retention and kinetics during coprecipitation*

Coprecipitation generally led to a substantially higher retention of both the P forms compared to adsorption, particularly at greater $(P/Fe)_0$.

Inorganic phosphate retained by coprecipitation at the highest P loading was about four times greater than that retained by adsorption. When present in solution at a molar $(P/Fe)_0 \leq 0.5$, the anion was completely removed from solution during coprecipitation (along the 1:1 line in Fig. 4.1), while up to 60% of Pi was retained at $(P/Fe)_0 = 1.0$, in accordance with the findings of Chatellier and coworkers (2013) and Voegelin and coworkers (2013). The presence of Pi slowed down the rate of Fe(II) oxidative precipitation, likely interfering with the formation of crystallization nuclei and subsequent precipitation of Fe (hydr)oxides. This is in agreement with van der Grift and coworkers (2016), who hypothesized that dissolved Pi might affect Fe(II) oxidation either by changing the speciation of dissolved Fe or by affecting the surface speciation of the Fe hydroxyphosphates. The latter may influence the nucleation of Fe precipitates and interfere with surface catalysis. A decrease in reaction rate was also observed in the presence of dissolved organic matter (Chen *et al.,* 2014; Pedrot *et al*., 2011; Shimizu *et al.*, 2013; Sodano *et al.*, 2016), proteins (Kashyap *et al.,* 2014) or other anions such as arsenate (Mikutta *et al*., 2014) and silicate (Voegelin *et al*., 2013). The faster disappearance of Pi from the solution with respect to Fe precipitation and H^+ release at $(P/Fe)_0 = 0.05$ suggests that Fe-phosphate nuclei were rapidly formed. However, the amount of H^+ released by the end of the reaction ($H^+/Fe_0 \approx 2.4$) was similar to that observed in the absence of P ($H^+/Fe_0 \approx 2.2$), suggesting that at low P loading Fe (hydr)oxide precipitation occurred (Eq. (1)) and Pi adsorption on the newly formed mineral surface was mainly responsible for P retention.

$$Fe^{2+} + 0.25O_2 + 1.5H_2O \rightarrow FeOOH_{(s)} + 2H^+ \quad (1)$$

The slightly higher H^+/Fe_0 ratio obtained with respect to the theoretical stoichiometry may be due to other reactions, such as Fe(II) adsorption on the new formed surfaces and generation of reactive oxygen species (Jones *et al*., 2015), which may contribute to modify the production of protons.

At greater P concentrations the mechanisms involved changed and the precipitation of $FePO_4$ (Eq. (2)) contributed significantly to P retention (Voegelin *et al*., 2013).

$$Fe^{2+} + 0.25O_2 + H_2PO_4^- \rightarrow FePO_{4(s)} + H^+ + 0.5H_2O \quad (2)$$

In fact, at $(P/Fe)_0 \geq 0.5$ the measured final $H^+/Fe_0 \approx 1.6$ approached the theoretical stoichiometry of the combined reactions of $FePO_4$ precipitation and FeOOH formation (Eq. (3)), in line with the observations of Chatellier and coworkers (2013):

$$2Fe^{2+} + 0.5O_2 + H_2PO_4^- + H_2O \rightarrow FeOOH_{(s)} + FePO_{4(s)} + 3H^+ \quad (3)$$

These results suggest that Pi retention during coprecipitation at high P loadings mainly involved $FePO_4$ precipitation (up to 50% of the initial P), but the quantitative coprecipitation data (Fig. 4.1) also highlighted other mechanisms including adsorption on the newly formed Fe (hydr)oxide and/or inclusion into particle aggregates.

P retention during coprecipitation in the presence of *myo*InsP6 was up to five times greater than adsorption at the highest $(P/Fe)_0$, and total removal of the P compound was observed over the whole experimental range of $(P/Fe)_0$ values. In contrast to Pi, *myo*InsP6 tended to accelerate Fe(II) oxidative precipitation. An increase in the rate of Fe(II) oxidation has also been observed in the presence of other organic ligands, such as citrate (Pham and Waite, 2008), EDTA and fulvic acids (Jones *et al*., 2015), and is explained by the capacity of these ligands to form strong Fe(II) complexes with greater oxidation rate constants with respect to Fe(II). As *myo*InsP6 is known to have a higher Fe(II) complexation capacity than Pi (Celi and Barberis, 2004 and references therein), Fe-*myo*InsP6 species are expected to form rapidly. Considering the acid dissociation constants of the six phosphate groups (Table 4.3), *myo*InsP6 at pH 6 may be present as $[C_6H_6(HPO_4)_4(PO_4)_2]^{8-}$ and can thus chelate from one to four Fe(II) ions (Eq. (4)):

$$nFe^{2+} + [C_6H_6(HPO_4)_4(PO_4)_2]^{8-} \rightarrow [Fe(II)_n–C_6H_6(HPO_4)_4(PO_4)_2]^{2n-8} \quad (4)$$

This complex may favour the oxidation of Fe(II) in the presence of O_2 according to Eq. (5), and potentially act as crystallization nuclei for the further precipitation of Fe (hydr)oxides:

$$[Fe(II)_n–C_6H_6(HPO_4)_4(PO_4)_2]^{2n-8} + 0.25nO_2 + nH^+ \rightarrow [Fe(III)_n–C_6H_6(HPO_4)_4(PO_4)_2]^{3n-8} + 0.5nH_2O \quad (5)$$

The H^+/Fe_0 ratio of ~ 2.0 observed at the end of the coprecipitation at $(P/Fe)_0 \leq 0.1$ suggests that at low *myo*InsP6 concentrations P retention is determined by the oxidative precipitation of FeOOH and rapid sorption of *myo*InsP6 on the newly formed (hydr)oxide, although the formation and precipitation of Fe(III)-*myo*InsP6 species cannot be completely excluded. As for the adsorption of the molecule on the surface of the forming (hydr)oxide, computational results highlighted how in the 1-axial/5-equatorial conformation that generally occurs at pH < 9 (Murthy, 2006 and references therein), the O atoms of non-contiguous phosphate groups disposed on the same planes of the carbon moiety were at larger distances than those generally found on the surface of Fe oxides (Barrón and Torrent, 1996). Thus, the adsorption reaction possibly requires a ring-ring interconversion from the 1-axial/5-equatorial form to a more sterically hindered 5-axial/1-equatorial conformation, where the distances between the O atoms of both contiguous and non-contiguous groups are more favourable for an interaction with the mineral surface. This conformational change requires energy (Murthy, 2006), possibly accounting for the lower affinity of *myo*InsP6 for Fh with respect to Pi (K_L 67.3 L $mmol^{-1}$ for *myo*InsP6 *vs* 89.3 L $mmol^{-1}$ for Pi, Table 4.1).

At greater *myo*InsP6 concentrations ($(P/Fe)_0 \geq 0.5$), the additional formation and precipitation of $[Fe(III)_4–C_6H_6(PO_4)_6]$ may contribute increasingly to the overall retention of P, leading to the observed decrease in final H^+/Fe_0 ratios from ~ 2.0 to ~1.5 and 1.0 for $(P/Fe)_0 = 0.5$ and 1.0, respectively. Measured proton release for the highest P loading may be hypothetically explained through the formation of FeOOH and Fe(III)-*myo*InsP6 in a stoichiometric ratio of 4:1 by the end of the oxidative precipitation of Fe(II), according to the reaction:

$$8Fe^{2+} + [C_6H_6(HPO_4)_4(PO_4)_2]^{8-} + 2O_2 + 4H_2O$$

$$\rightarrow 4FeOOH + [Fe(III)_4–C_6H_6(PO_4)_6] + 8H^+ \quad (6)$$

In this case, aside from Fe(III)-*myo*InsP6 precipitation, adsorption on FeOOH and inclusion into aggregates consistently contributed to the complete retention of *myo*InsP6.

Table 4.3: Dissociation acid constants of phosphate (Hinsinger, 2001) and *myo*-inositol hexaphosphate (*myo*InsP6) (Costello *et al*., 1976).

Molecule	pK_1	$pK_{2,3}$	$pK_{4,6}$	pK_7	pK_8	pK_9	$pK_{10,11}$	pK_{12}
Phosphate	2.1	7.2	12.3					
*myo*InsP6	1.1	1.5	1.8	5.7	6.9	7.6	10.0	12.0

4.4.2 *Properties of the Fe-P systems*

The complementary surface, microscopic and spectroscopic analyses of this study showed that the mineralogy, structure and surface properties of the obtained coprecipitates differed markedly as a function of the P species and $(P/Fe)_0$ ratios.

4.4.2.1 *Pi coprecipitates*

Aggregative processes occurring during coprecipitation, favoured by the attraction between the negatively charged P anions and the positively charged, newly formed, Fe (hydr)oxide surfaces, were probably responsible for the reduction in N_2-SSA and increase in mesopore volume observed in the presence of Pi. Nanoparticle coprecipitates with a short-range crystalline order were formed at low Pi concentrations, evidenced by the smooth surface texture and broad nature of the XRD peaks (Eusterhues *et al*., 2008; Janney *et al*., 2000; Jia *et al*., 2007), and were very similar to those obtained from P-free solutions. Chatellier and coworkers (2004) hypothesized that during the synthesis of $FePO_4$ systems, the phosphate ligand was likely competing with ferrous ions for adsorption on the lateral planes of the growing crystals resulting in the inhibition of particle growth. The ζ potential measured at $(P/Fe)_0 \leq 0.5$ suggested that the positively charged surface of the Fe (hydr)oxide at pH 6.0 was only partially balanced by the dissociated phosphate groups at this pH (Celi *et al*., 2001). However, surface P/Fe ratios obtained by XPS, approximately two times greater than those obtained by chemical analysis, suggest that phosphate groups were nonetheless

enriched at the surface, possibly due to the adsorption on the lateral planes of the growing FeOOH crystals (Chatellier *et al*., 2004). Increasing P loading led to the formation of more spherical-like particles, consistent with the formation of Fe(III)-phosphate (Kaegi *et al.,* 2010). This was in line with the lower amount of protons released during Fe(II) oxidation and hydrolysis ($H^+/Fe_0 < 2$), and the progressive broadening and disappearance of the main XRD peaks of 2L-Fh, together with the appearance of the reflection at 30° 2θ of amorphous Fe(III)-phosphate (Lai *et al*., 2011; Voegelin *et al*., 2013). In addition, the shift in Fe binding energy from ~710 to 712 eV with increasing $(P/Fe)_0$ reflects a change in Fe chemical state from an oxide-like structure to a Fe-phosphate salt (Mallet *et al*., 2013). Indeed, Grosvernor and coworkers (2004) found that the binding energy associated with Fe (ferrous or ferric) $2p_{3/2}$ peak increases with an accentuation in the ionic bond character between Fe and the ligand, due to the reduction in shielding of the Fe cation by the more electronegative ligands. This effect was not observed in the adsorbed Pi systems, as no change in the chemical state of Fe is expected. Although the contribution of $FePO_4$ precipitation to Pi retention clearly increased with increasing $(P/Fe)_0$, the negative surface charge at the highest P loading (−11 mV) was much lower than that of pure $FePO_4$ (Li and Stanforth, 2000) and closer to that of the adsorbed systems, further indicating that Pi adsorption on the newly formed hydroxide surfaces contributed to total P retention. Additional insights into the retention and nature of interaction between Fe and Pi during adsorption and coprecipitation were obtained by the IR spectra. Adsorption of Pi onto iron octahedral structures at the Fh surface was highlighted by the difference between the peak maxima of the solution P species and the adsorbed ones, confirming the formation of P inner-sphere complexes (Arai and Sparks, 2001). Given the amorphous nature of the substrate, the presence of multiple (slightly) different phosphate complexes at the ferrihydrite surface is not unlikely and leads to a larger variety in the characteristics of surface sites available for phosphate adsorption than in the case of a crystalline oxide such as goethite or haematite (Elzinga and Sparks, 2007), resulting in less symmetrical peaks. The similarity between the IR spectra of the adsorbed systems and of the

low $(P/Fe)_0$ coprecipitates suggests that, although during coprecipitation Fe(III)-phosphate formed first, the final product is characterized by the presence of phosphate accumulated on the surface, in line with XPS results. This is in agreement with Voegelin and coworkers (2013), who suggested a transformation of Fe(III)-phosphate into P-ferrihydrite during Fe(II) oxidation at $(P/Fe)_0 < 0.5$. The one featured peak obtained at greater $(P/Fe)_0$ confirms the formation of the phosphate salt. In addition, under most conditions, Fe(III)-phosphate contains the non-protonated phosphate ion, justifying the broad features centred consistently around 1150–1050 cm^{-1} (Persson *et al.*, 1996).

4.2.2.2 myo*InsP6 coprecipitates*

Similarly to Pi, coprecipitation in the presence of increasing concentrations of *myo*InsP6 led to a reduction in N_2-SSA and an increase in mesopore volume. Coprecipitates formed in the presence of *myo*InsP6 at low $(P/Fe)_0$ ratios were mainly constituted of ferrihydrite particles (1–2 nm) with some needles and laths probably due to lepidocrocite. In contrast to the adsorbed systems that showed a negative surface charge even at the lowest P loadings, the surface charge of coprecipitates unexpectedly remained highly positive, suggesting that the high charge density of *myo*InsP6 was partially neutralized (Celi and Barberis, 2004). This, together with the kinetic features, may support the hypothesis that Fe(III)-*myo*InsP6 species could act as nuclei of crystallization accelerating crystal growth on lateral planes, while including the organic P compound within the structure. At the highest $(P/Fe)_0$ ratios the particles were more aggregated, albeit the negative charge of the particle surface and the strong colloidal dispersion effect exerted by *myo*InsP6 (Celi *et al*., 1999; Wan *et al*., 2016). This may suggest that, as for Pi, simultaneous precipitation of Fe hydroxides and Fe-*myo*InsP6 salts may occur, as well as adsorption of *myo*InsP6 on the newly formed oxide surfaces. The latter may be followed by the further formation of ternary systems with Fe (III), partially neutralizing *myo*InsP6 charge. This can also be deduced from XR diffractograms, showing a progressive broadening and disappearance of the 2L-Fh signals and the appearance of a single signal attributed to the formation of Fe(III)-*myo*InsP6 (Yan *et al.,* 2014). The shift in Fe binding energy in

the XP spectra confirmed a change from a Fe-O to a Fe-O-P like bonding type (Mallet *et al*., 2013). A stronger association of Fe and P atoms of *myo*InsP6 than that found within the structure of some Fe-inorganic P precipitates by EXAFS studies (Chatellier *et al.*, 2013; Senn *et al*., 2015) could be expected due to its unique affinity for Fe (Martin and Evans, 1987). IR spectra suggest that, during adsorption, the phosphate groups of *myo*InsP6 coordinated with metal ion(s) at the hydroxide surface by forming inner-sphere complexes, as the bands corresponding to the vibration of phosphate groups split into two or three bands, and shifted with respect to those of the free compound in solution (Celi *et al*., 1999; Guan *et al*., 2006). The inner-sphere complexes formed via ligand exchange of aquo- and hydroxo-groups can involve a different number of phosphate groups depending on the oxide (Celi *et al*., 1999; Yan *et al*., 2014). The three featured absorption band is again similar in the low $(P/Fe)_0$ coprecipitates, confirming that adsorption on the forming surface dominated Fe(III)-*myo*InsP6 precipitation, as also deduced by XRD and XPS data.

CHAPTER 5

P stress-induced changes in plant root exudation facilitate P mobilization from stable mineral forms

5.1 Introduction

It is clear from Chapters 2 and 3 that P deficiency triggers diverse signals in tomato plants in response to starvation, activating several physiological and morphological changes. We also observed how some of these modifications are mediated by the plant hormones SLs, while others appear to be SL-independent. At the root morphological level, for instance, SL-depleted mutants differentiated from WT tomato plants as many root traits were severely affected by P starvation and extensive cell and tissue disorganization was evident at the root tip when the provision of P was reduced from the most commonly used hundreds of µM (Steiner, 1984) to the 80 µM Pi used in the experiments of Chapters 2 and 3. This concentration better reflects the availability of P in soils and is low enough to induce in SL-depleted plants the onset of many P-deficiency responses that WT plants adopt only under harsh P-stress conditions. In fact, the greater P removal from the nutrient solution, the elevated expression of high-affinity Pi transporters and increased root enzymatic activity observed in SL-mutants even under P-repleted conditions and emphasized under P stress led us to the hypothesis that SL-depleted plants may have altered perception of exogenous P, which could be responsible for the observed altered responses to this nutrient.

As largely observed throughout the previous chapters of this thesis, most studies use soluble Pi salts to assess the response of plants to P limitation, although soil-P occurs also as organic P molecules, including inositol phosphates, DNA and RNA fragments and phospholipids (George *et al*., 2018). Inositol phosphates, in particular, form the largest P component in most soils and *myo*-inositol hexaphosphate is the major P storage sink within the plant seed (Freed *et al*., 2020), thus being a potentially important source of P for the nutrition of plants (Hayes *et al*., 2000). However, how this compound is used by plants that produce SLs remains largely unknown. Moreover, unlike other macronutrients, the

majority of both inorganic and organic P in soil is inaccessible to plants due to many fixation processes, involving pH-dependent complexation with Ca, Fe and Al and adsorption on mineral surfaces. In Chapter 4 we showed how P-bioavailability to plants is also strongly related to the biogeochemical cycle of Fe, making coprecipitation during Fe(II) oxidation and Fe(III)-(hydr)oxides precipitation another significant process responsible for P retention in soil. This mechanism was proven to additionally contribute and to a great extent to the retention of inositol phosphates. The response of WT and SL-depleted plants to the absence of P should be thus modified in the presence of sparingly-available P forms, through the activation of mechanisms that are more functional to inaccessible P scavenging, as observed by Edayilam and coworkers (2018) in *A. virginicus* or in *Lolium perenne* by Martin and coworkers (2004). For instance, high amounts of either organic acid anions or aromatic compounds in the root exudates may increase P acquisition efficiency in plants through acidification, chelation, and ligand exchange reactions that can mobilize metal-bound P (Arai and Sparks, 2007; Jones, 1998). Phenols can also favour P release via reductive dissolution of Fe hydr(oxides). However, how SLs can control these responses in the presence of sparingly-available P forms, especially organic, remains largely unknown.

In this chapter, we aimed at **evaluating the ability of WT and SL-depleted tomato plants grown under variable P availability conditions to mine P allowing for nutrient uptake and utilization.** A hydroponic experiment analogous to the one described in Chapter 3 was performed, but in this case P was provided as soluble inorganic phosphate, soluble *myo*-inositol hexaphosphate (*myo*InsP6) and as the coprecipitated form of these two P-containing compounds following Fe(II) oxidative precipitation. At the end of the experiment, we measured the plant biomass, P, N, C and Fe content, and root enzymatic activity was assayed. Root exudates were characterized for DOC content and degree of aromaticity, and proton and organic acid anion exudation. We hypothesized that **soluble organic and mineral forms of P will alter the root exudates profile of tomato plants depending on SL production, and**

that root exudates will be more acidic and abundant in organic acid anions and phenolic compounds in the presence of scarcely-available P. In addition, we hypothesised a **higher activity of Pi-solubilizing enzymes in the roots of plants exposed to sparingly-available P forms.**

5.2 Materials and methods

5.2.1 *Plant material*

The plant material used in this study was the same as the one described in Chapter 2 (section 2.2.1.).

5.2.2 *Plant growth conditions*

WT and SL-depleted tomato seeds were germinated and transferred to plastic pots filled with silica sand as described in Chapter 3. Plants were allowed to grow for 45 days, inside a growth chamber with a 16/8 hours light/dark cycle, air temperature of 25°C and relative humidity ≥70%, with a light intensity of 100 µmol $m^{-2}s^{-1}$. The nutrient solution was the same as described in section 3.2.2. It was renewed every day and the initial pH was adjusted to 6.0.

5.2.3 *Phosphorus nutritional conditions and collection of root exudates*

After 45 days of growth in sand, plants were transplanted to 250 mL flasks containing 200 mL of aerated nutrient solution. After two days of acclimation in the hydroponic growth systems with the complete nutrient solution, roots were gently rinsed with deionized water to remove traces of P. After that, four plants per genotype were kept for 15 days in a P-free (–P, 0 µM KH_2PO_4) nutrient solution, in the complete nutrient solution (+P, 80 µM KH_2PO_4) or in a nutrient solution with the organic P form inositol hexaphosphate (*myo*InsP6), at a final P concentration of 80 µM. In addition, 4 plants per genotype were supplied with a sparingly-available source of P in the form of a P-Fe coprecipitate, both with Pi and *myo*InsP6, synthesised as described in Chapter 4 at the initial $(P/Fe)_0$ ratio of 0.5. A resume of the properties of the two coprecipitates is reported in Table 5.1. The amount of coprecipitated system was dosed in order to obtain a final concentration of 80 µM P in the 250 mL flasks. These two treatments, which will be referred to as COP-Pi and COP-*myo*InsP6, received a nutrient solution without

P, and in all treatments (except +P) KCl replaced KH_2PO_4 to provide plants with the same amount of K. Solutions were constantly aerated along the experiment, and the nutrient solution was renewed every day in order to restore the initial volume. After 15 days, root exudates were collected and filtered using 0.22 µm nylon membrane filters and stored at –20°C for further analyses. Plants were harvested, divided into shoots and roots, and the fresh biomass was recorded. Root subsamples were frozen with liquid N_2 and stored at –80°C for enzymatic analysis, while the remaining roots and shoots were dried at +40°C, ground separately in a mortar, passed through a 0.5 mm mesh sieve and used for elemental analyses.

Table 5.1: Specific surface area (SSA), total mesopore volume, ζ potential and element composition of the Pi- and *myo*InsP6-coprecipitated systems at initial $(P/Fe)_0$ ratio = 0.5.

Sample	Initial P/Fe	SSA ($m^2\ g^{-1}$)	Mesopore volume ($mm^3\ g^{-1}$)	ζ potential (mV)	Chemical P/Fe ratio	XPS P/Fe ratio
COP-Pi	0.5	194	850	2	0.47	1.15
COP-*myo*InsP6	0.5	193	882	–38	0.48	0.92

5.2.4 *Plant analysis*

5.2.4.1 *Elemental analysis*

Concentration of total P in plant tissues was determined colorimetrically after sulfuric-perchloric digestion, as described in section 3.2.4.1. P-acquisition efficiency (PAE) values were calculated as the ratio of P accumulated in tissues to P exogenously supplied during both plant growth in sand and the hydroponic experiment (Neto *et al*., 2016). Iron concentration of roots was measured by atomic absorption spectrometry (PerkinElmer AAnalyst 1400, Norwalk, CT, USA) after acidic dissolution. Total C and N contents were determined by dry combustion (UNICUBE, Elementar Analysensysteme GmbH, Langensenbold, Germany).

5.2.4.2 *Exudates analysis and enzyme activity*

Root exudates were analyzed for DOC, protons, total P, Fe and organic acid anions content, as described in section 3.2.4.4. Iron concentration of the exudates was measured by atomic absorption spectrometry (PerkinElmer

AAnalyst 1400, Norwalk, CT, USA). In addition, UV absorption at λ = 254 nm was measured (Helios Gamma Spectrophotometer, Thermo Electron, Waltham, MA). The SUVA values, calculated by normalizing measured absorbance values to the concentration of DOC, were used as an estimate for the aromatic content of exudates samples (Weishaar *et al*., 2003). Phosphatase and phytase activity were determined as described in section 3.2.4.3.

5.2.5 *Statistics*

For all determinations, the analysis of variance (one-way ANOVA) was performed using the SPSS software version 26.0 (SPSS, Chicago, IL, USA), and was followed by pair-wise post-hoc analyses (Student-Newman-Keuls test) to determine which means differed significantly at $p < 0.05$ (± SE). In addition, to evaluate the effect of plant genotype, P treatment and the combination of the two on the measured parameters, we used a linear mixed-effect ANOVA model performed with the statistical programming language R (R Core Team, 2020). Figures were created using SigmaPlot ver. 12.5 software (Systat, San Jose, CA, USA), with means presented with standard errors.

5.3 Results

5.3.1 *Plant growth parameters and elemental composition*

Under all P nutritional conditions, plants phenotype was comparable to that observed in Chapter 3, with SL-depleted plants displaying increased shoot branching in comparison to WT plants (Fig. 5.1).

Maximal dry root biomass was displayed by both genotypes under +P conditions, with comparable values (Table 5.2). Similarly, under –P, the root biomass did not differ between genotypes and was lower than the +P case. The lowest root biomass values were associated with plants grown with coprecipitates, even though roots of SL-depleted plants were generally more developed compared to the WT, especially when plants received COP-Pi (Table 5.2). Root biomass was strongly dependent on the P treatment ($p < 0.001$), plant genotype ($p < 0.01$) and the combination of the two ($p < 0.05$). The highest shoot biomass values were those of SL-depleted plants under +P and *myo*InsP6 conditions, which produced

more shoot biomass than WT plants under the same growing conditions (Table 5.2). Under –P, the shoot biomass of SL-depleted plants was only slightly higher than that of the WT (Table 5.2). For both genotypes, the lowest shoot biomass accumulation was observed under –P or in the presence of COP-*myo*InsP6 (Table 5.2). The shoot biomass was strongly influenced by the P treatment ($p < 0.001$), plant genotype ($p < 0.001$) and the combination of the two parameters ($p < 0.001$).

Figure 5.1: Representative examples of wild-type (WT) and SL-depleted (SL–) plants. Plants were grown in quartz sand for 45 days with a nutrient solution containing 80 µM Pi then transferred to hydroponic culture and subjected to different P treatments for 15 days.

The R/S ratios of SL-depleted plants were lower than the corresponding WT genotype when P was present in the nutrient solution either as Pi or *myo*InsP6, given the higher shoot biomass accumulation (Table 5.2). For both genotypes, the R/S ratio slightly increased under –P compared to +P and *myo*InsP6 conditions, even if the highest R/S value was that of WT plants (Table 5.2). The R/S ratio of WT plants was sensibly lower in the presence of individual coprecipitates than when these compounds were provided in the nutrient solution, while the opposite was observed for SL-depleted plants, whose R/S

ratios slightly increased if compared to +P and *myo*InsP6 conditions (Table 5.2).

Table 5.2: Effect of P treatments on dry matter production and root/shoot ratio (R/S) of wild-type (WT) and SL-depleted (SL–) tomato plants after 15 days of hydroponic culture. Abbreviations: DW, dry weight. Each value represents the mean of four replicates (± SE). Different letters indicate significant differences between treatments ($p < 0.05$).

	Root DW (g)	Shoot DW (g)	R/S
WT +P	0.76 ± 0.01 ^{a}	0.54 ± 0.01 ^{b}	1.28 ± 0.12 ^{ab}
WT +*myo*InsP6	0.54 ± 0.02 ^{abc}	0.40 ± 0.02 ^{cd}	1.34 ± 0.05 ^{ab}
WT +COP-Pi	0.39 ± 0.03 ^{bcd}	0.45 ± 0.01 ^{bcd}	0.92 ± 0.04 ^{bc}
WT +COP-*myo*InsP6	0.24 ± 0.01 ^{d}	0.35 ± 0.04 ^{d}	0.75 ± 0.05 ^{c}
WT –P	0.55 ± 0.07 ^{abc}	0.38 ± 0.01 ^{cd}	1.44 ± 0.12 ^{a}
SL– +P	0.73 ± 0.09 ^{a}	0.73 ± 0.06 ^{a}	1.00 ± 0.09 ^{bc}
SL– +*myo*InsP6	0.63 ± 0.03 ^{ab}	0.71 ± 0.03 ^{a}	0.84 ± 0.04 ^{bc}
SL– +COP-Pi	0.62 ± 0.07 ^{ab}	0.54 ± 0.04 ^{b}	1.07 ± 0.04 ^{abc}
SL– +COP-*myo*InsP6	0.37 ± 0.06 ^{cd}	0.38 ± 0.02 ^{cd}	0.95 ± 0.13 ^{abc}
SL– –P	0.52 ± 0.12 ^{abc}	0.49 ± 0.02 ^{bc}	1.03 ± 0.10 ^{abc}

Also in this case, both P treatment ($p < 0.01$) and the plant genotype ($p < 0.05$), as well as the combination of the two ($p < 0.001$), concurred to influence this parameter.

Phosphorus content in roots and shoots is reported in Fig. 5.2, while total P content per plant is reported in Fig. 5.3a. The highest P amount in tissues was measured in +P SL-depleted plants (Fig. 5.3a), in both roots and shoots (Fig. 5.2). The total P content of +P WT plants was comparable to that of both genotypes treated with *myo*InsP6, but the shoot P content of *myo*InsP6 SL-depleted plants was higher than the WT (Fig. 5.2). In general, the shoot P content was higher (or slightly higher) in the shoots of SL-depleted plants, in line with the greater shoot biomass production, while it was comparable in the roots of the two genotypes (Fig. 5.2). As a result, when comparing the same P treatment, the total P content was higher in SL-depleted than in WT plants (Fig. 5.3a). For both genotypes, the lowest accumulation of P was observed in the presence of COP-*myo*InsP6, with a slightly higher accumulation in SL-depleted plants, again attributable to the different P content at the shoot level (Fig. 5.2 and 5.3a). Root P content was influenced mainly by the P treatment ($p < 0.001$) and to a lesser

extent by the plant genotype ($p < 0.05$), which conversely played a more significant role in the accumulation of P in the shoots ($p < 0.001$), along with the combination of the two parameters ($p < 0.001$). The higher P accumulation by SL-depleted plants, notwithstanding the same amount of provided P, led to generally higher P-acquisition efficiency (PAE) values than the WT (Fig. 5.3b). Maximal PAE value was referred to +P SL-depleted plants, which was significantly higher when compared to the WT. Also with the two coprecipitates and under –P conditions, SL-depleted plants displayed higher PAE if compared to the WT, while it was only slightly higher with readily-available *myo*InsP6 (Fig. 5.3b). However, the PAE of plants grown in the presence of the two coprecipitates was the lowest among all P treatments (Fig. 5.3b). As observed in Chapter 3, PAE of both WT and SL-depleted plants decreased from +P to –P conditions, even if in this experiment we only observed a slightly decreasing trend, without statistical differences (Fig. 5.3b).

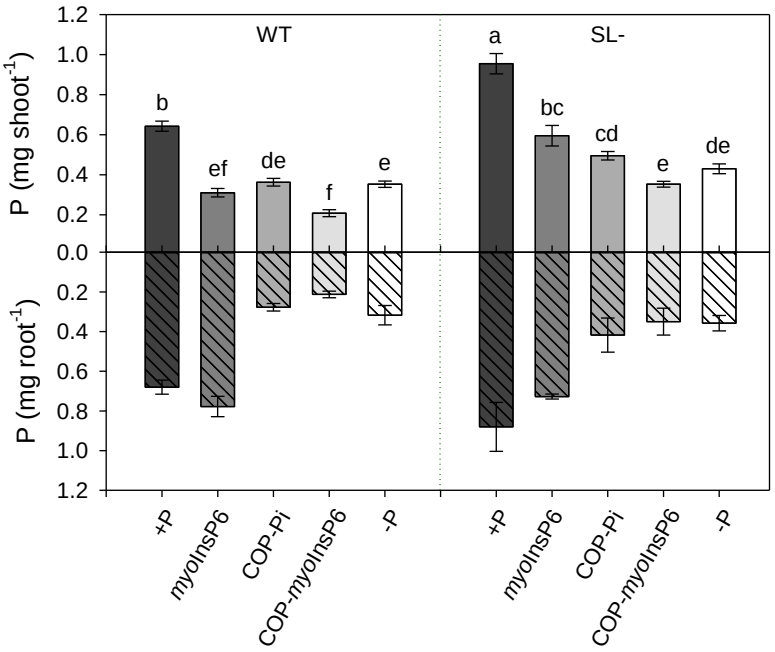

Figure 5.2: Root and shoot P content of wild-type (WT) and SL-depleted (SL–) tomato plants after 15 days of hydroponic culture with different P forms (+P, *myo*InsP6, COP-Pi, COP-*myo*InsP6) or without P (–P). Each value represents the mean of four replicates (± SE). Different letters above bars indicate significant differences between treatments ($p < 0.05$).

PAE values were more importantly influenced by the plant genotype ($p < 0.001$) than by the P treatment, which however influenced this parameter ($p < 0.05$).

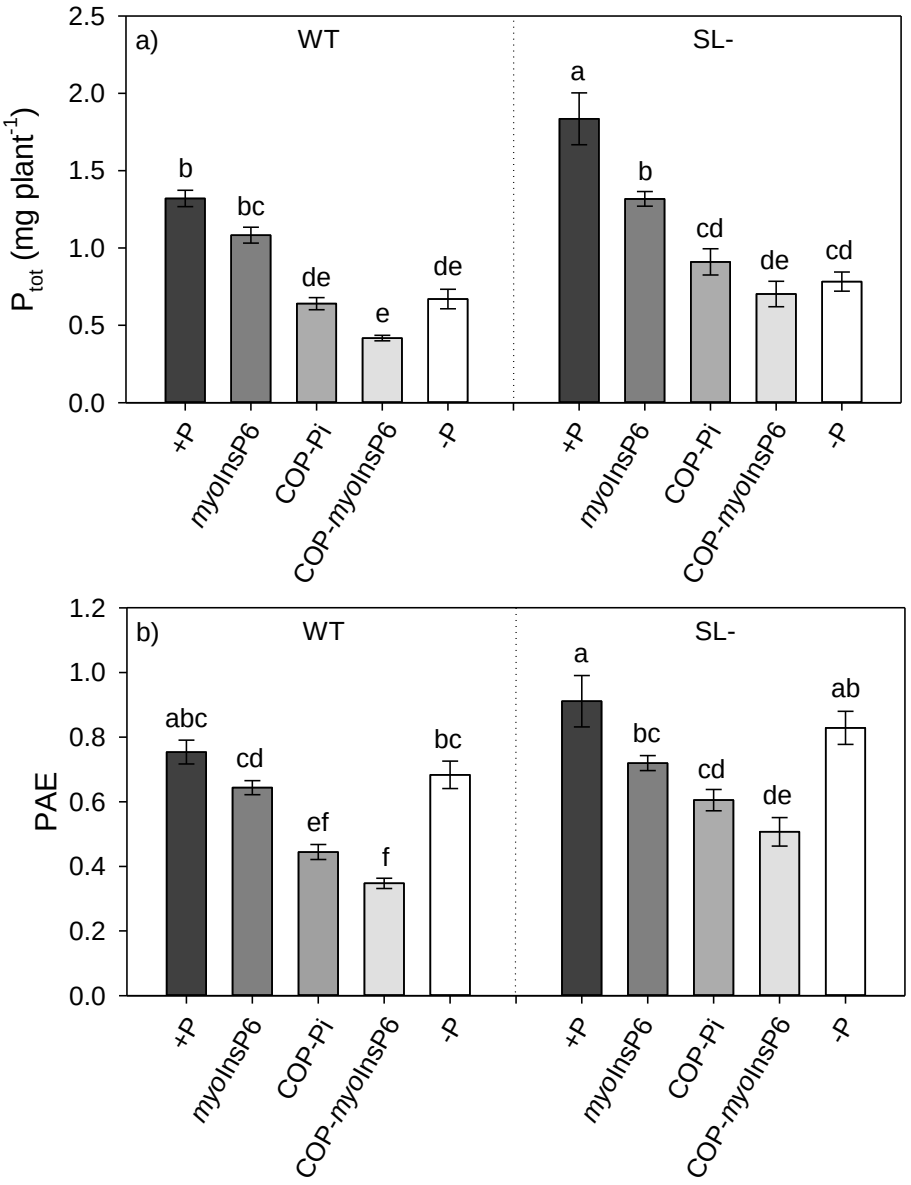

Figure 5.3: a) Total plant P content and b) P-acquisition efficiency (PAE) of wild-type (WT) and SL-depleted (SL–) tomato plants after 15 days of hydroponic culture with different P forms (+P, *myo*InsP6, COP-Pi, COP-*myo*InsP6) or without P (–P). Each value represents the mean of four replicates (± SE). Different letters above bars indicate significant differences between treatments ($p < 0.05$).

Plants C, N and Fe content are reported in Table 5.3. Carbon content of the two genotypes ranged between ~ 0.2 and 0.5 g of C plant^{-1}. In general, SL-depleted plants displayed higher C contents than the WT, especially with *myo*InsP6 and COP-Pi (Table 5.3).

Table 5.3: Carbon (C) and nitrogen (N) content, N/P ratios and root iron (Fe_{root}) content in wild-type (WT) and SL-depleted (SL–) tomato plants after 15 days of hydroponic culture with different P forms (+P, *myo*InsP6, COP-Pi, COP-*myo*InsP6) or without P (–P). Each value represents the mean of four replicates (± SE). Different letters indicate significant differences between treatments ($p < 0.05$).

	C (g plant^{-1})	N (g plant^{-1})	N/P ratio	Fe_{root} (mg/g)
WT +P	0.48±0.03 ^{ab}	0.028±0.003 ^{bcd}	21.3±0.7 ^{d}	0.72±0.03 ^{d}
WT +*myo*InsP6	0.35±0.01 ^{cd}	0.033±0.001 ^{bc}	29.4±0.4 ^{c}	0.82±0.02 ^{cd}
WT +COP-Pi	0.32±0.01 ^{d}	0.025±0.002 ^{bcd}	39.9±0.9 ^{ab}	1.10±0.02 ^{a}
WT +COP-*myo*InsP6	0.19±0.01 ^{e}	0.022±0.002 ^{d}	43.8±0.7 ^{a}	1.11±0.05 ^{a}
WT –P	0.36±0.02 ^{cd}	0.028±0.003 ^{bcd}	38.3±0.9 ^{ab}	1.02±0.06 ^{ab}
SL– +P	0.57±0.06 ^{a}	0.035±0.003 ^{b}	18.5±0.9 ^{d}	0.88±0.04 ^{c}
SL– +*myo*InsP6	0.51±0.01 ^{ab}	0.045±0.003 ^{a}	28.5±0.9 ^{c}	0.91±0.02 ^{bc}
SL– +COP-Pi	0.46±0.04 ^{abc}	0.035±0.003 ^{b}	33.6±0.8 ^{ab}	1.11±0.05 ^{a}
SL– +COP-*myo*InsP6	0.26±0.03 ^{de}	0.025±0.003 ^{cd}	37.0±0.5 ^{b}	1.11±0.04 ^{a}
SL– –P	0.43±0.03 ^{bc}	0.030±0.004 ^{bc}	33.3±0.8 ^{b}	1.04±0.01 ^{ab}

For both genotypes, the lowest value was obtained with COP-*myo*InsP6, for C and N as well. N values widely differed among treatments, with SL-mutants generally accumulating more N than WT plants, as already observed in Chapter 3. In both genotypes, N content was higher when *myo*InsP6 was provided in the nutrient solution compared to Pi, while it was comparable under +P and –P conditions (Table 5.3). As for the not readily-available P forms, N content was higher with COP-Pi than COP-*myo*InsP6 in both genotypes. N/P ratios showed a clear accumulation of N under P-limited conditions, i.e., when Pi and *myo*InsP6 were provided as coprecipitate or without P (–P conditions). Both C and N content in plants were significantly influenced by the P treatment ($p < 0.001$) and the plant genotype ($p < 0.001$), and not by the combined effect of the two.

The highest Fe content in root tissues was that of plants provided with either

COP-Pi or COP-*myo*InsP6 (~ 1.1 mg g^{-1}), without statistical differences between genotypes (Table 5.3). Intermediate values were obtained under –P conditions or in the presence of soluble *myo*InsP6, while the lowest Fe contents were those of +P plants, with WT plants displaying significantly lower values than SL-depleted plants (Table 5.3). Iron accumulation in roots was significantly influenced by the P treatment ($p < 0.001$) and less by the plant genotype ($p < 0.05$), whereas, as for C and N, it was not affected by the combined effect of the P treatment and plant genotype.

5.3.2 *Root enzymatic activity*

Phosphatase activity was the highest in WT and SL-depleted plants in the presence of COP-*myo*InsP6, immediately followed by plants provided with COP-Pi, without statistical differences between genotypes (Fig. 5.4a). The provision of P in the form of soluble *myo*InsP6 salt increased the activity of phosphatases with respect to the +P treatment, with a slightly higher activity in SL-depleted than WT plants (Fig. 5.4a). Phytase activity in P-starved plants and plants provided with sparingly-available P forms was higher than in soluble-P-provided plants, except for the case of plants treated with COP-*myo*InsP6, which showed comparable values (Fig. 5.4b). Also in this case, the highest activity was observed in the presence of COP-*myo*InsP6, while values observed in the presence of soluble *myo*InsP6 and COP-Pi were intermediate between –P and COP-*myo*InsP6 values (Fig. 5.4b). Both phosphatase and phytase activity were significantly influenced by the P treatment ($p < 0.0001$) and, to a lesser extent, by the plant genotype ($p < 0.05$).

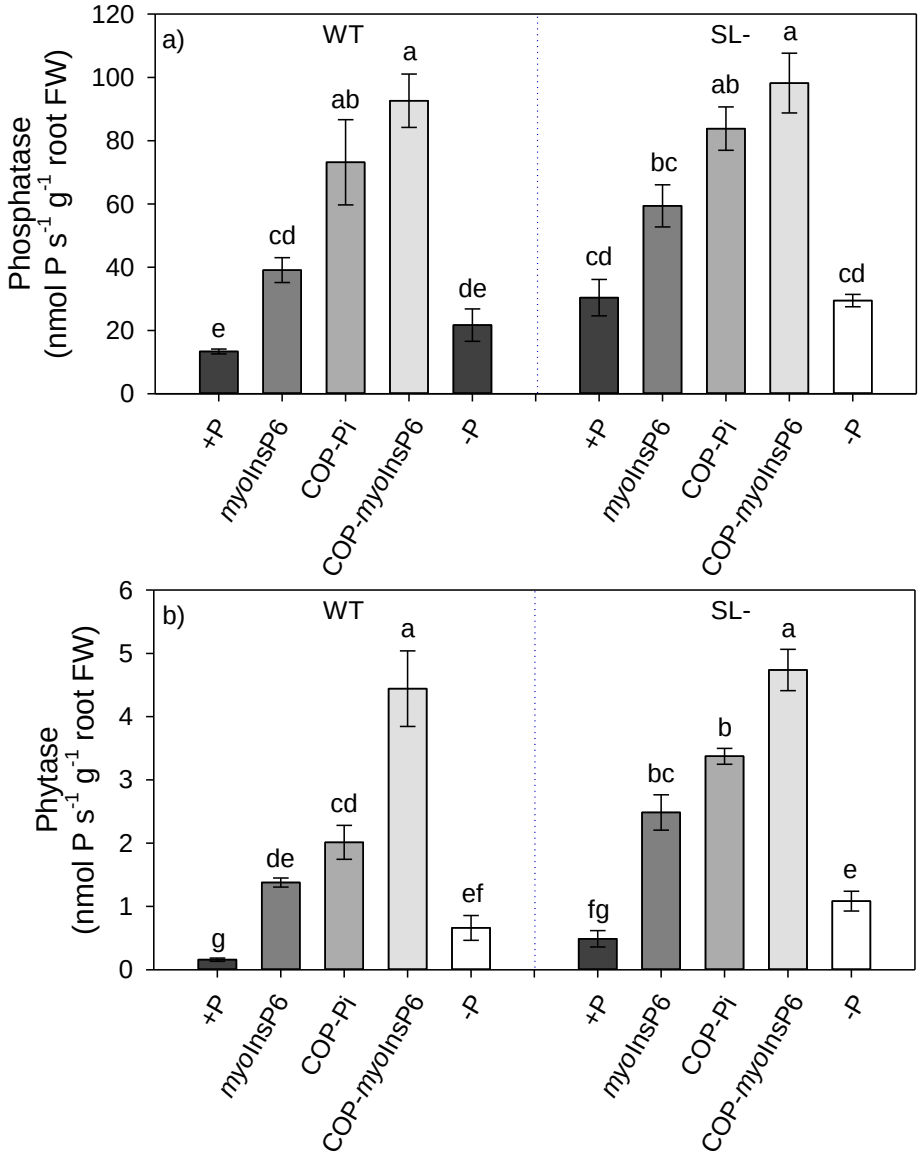

Figure 5.4: a) Phosphatase and b) phytase activity in roots of wild-type (WT) and SL-depleted (SL–) tomato plants after 13 days of hydroponic culture with different P forms (+P, *myo*InsP6, COP-Pi, COP-*myo*InsP6) or without P (–P). Each value represents the mean of four replicates (± SE). Different letters above bars indicate significant differences between treatments ($p < 0.05$).

5.3.3 *Exudates analysis*

At the end of the 15 days of experiment, no P or Fe were detected in the exudates of both WT and SL-depleted plants under any P treatment. However, part of the coprecipitate was still present in the suspensions of plants treated with COP-Pi and COP-*myo*InsP6.

5.3.3.1 *Dissolved organic C exudation*

The amount of exuded C at the end of two-week period in the nutrient solution ranged between 0.63 and 1.72 mg C g^{-1} plant (Fig. 5.5). Higher values of C exudation were generally displayed by WT than SL-depleted plants. The presence of COP-*myo*InsP6 triggered the exudation of C by both WT and SL-depleted plants, the former exuding slightly higher amounts. If compared to +P, exudation under –P increased in both WT and SL-depleted plants, but the difference was statistically significant only for SL-depleted plants. When P was provided as *myo*InsP6 or COP-Pi, C exudation was comparable in SL-depleted and WT plants. Among the treatments and genotypes, the lowest exudation was revealed in SL-depleted plants under either +P conditions or in the presence of COP-Pi. The high C exudation levels by plants grown with COP-*myo*InsP6 were also accompanied by high SUVA values (Fig. 5.5), of 0.82 and 0.94 L mg^{-1} m^{-1} for WT and SL-depleted plants, respectively. High SUVA values were observed also when P was provided as soluble *myo*InsP6 (0.82 L mg^{-1} m^{-1} for WT plants and 0.83 L mg^{-1} m^{-1} for SL-depleted plants), without statistical differences between the two genotypes. The SUVA levels were the lowest in root exudates of SL-depleted plants with COP-Pi (0.52 L mg^{-1} m^{-1}) and under –P conditions (0.53 L mg^{-1} m^{-1}), and generally intermediate in the other cases. Finally, the statistical analysis revealed that C exudation was significantly influenced by both P treatment ($p < 0.001$) and plant genotype ($p < 0.001$), while the aromaticity of the exuded compounds was only affected by the P treatment ($p < 0.001$).

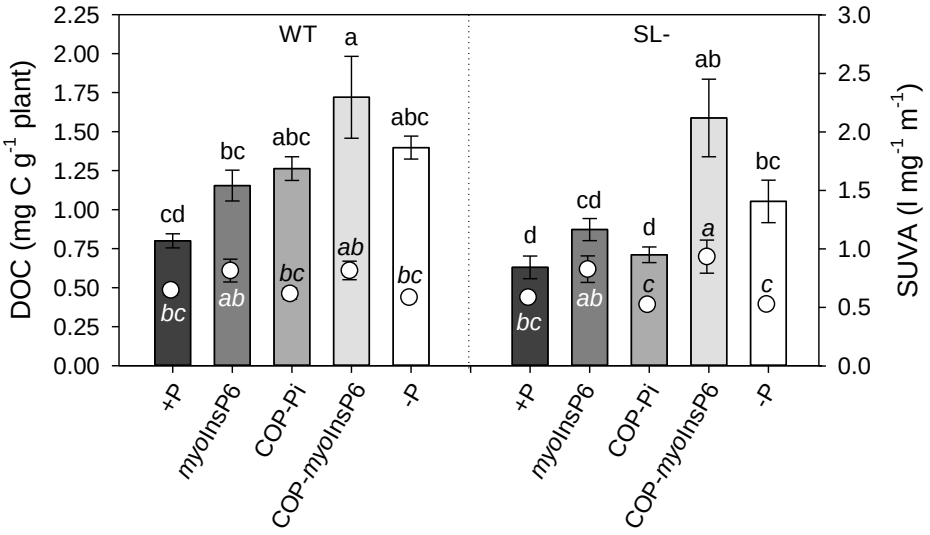

Figure 5.5: Dissolved organic C (DOC, bars) content and respective SUVA indexes (white circles) in the exudates of wild-type (WT) and SL-depleted (SL–) tomato plants after 15 days of hydroponic culture with different P forms (+P, *myo*InsP6, COP-Pi, COP-*myo*InsP6) or without P (–P). Each value represents the mean of four replicates (± SE). Different letters above bars indicate significant differences between treatments ($p < 0.05$).

5.3.3.2 *Proton exudation*

Proton release by WT and SL-depleted plants under different P conditions was significantly dependent on the P treatment only ($p < 0.001$). The highest amount of exuded protons was the one observed in the presence of *myo*InsP6, reaching values as high as 120 mmol H^+ g^{-1} root in the case of WT plants treated with *myo*InsP6 (Fig. 5.6). On the contrary, the lowest proton release was observed under +P, COP-Pi and –P conditions. Higher amounts of protons were instead exuded by both genotypes in the presence of COP-*myo*InsP6, even if without statistical differences (Fig. 5.6).

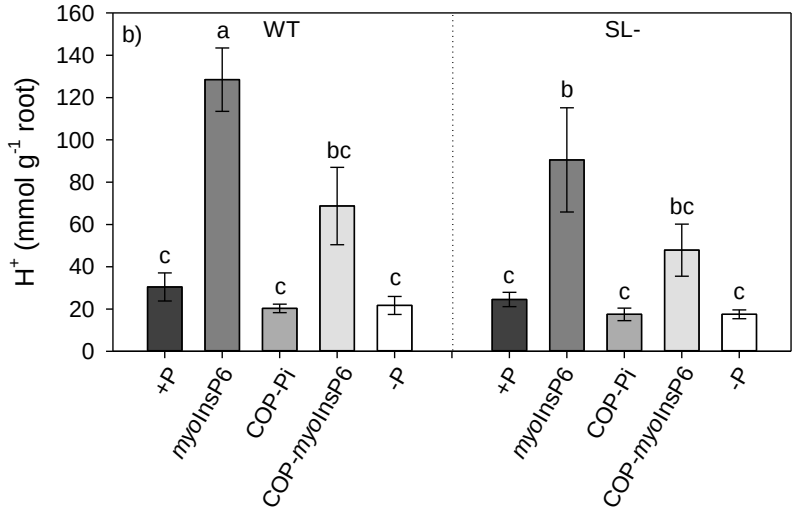

Figure 5.6: H^+ content of exudates of wild-type (WT) and SL-depleted (SL–) tomato plants after 15 days of hydroponic culture with different P forms (+P, *myo*InsP6, COP-Pi, COP-*myo*InsP6) or without P (–P). Each value represents the mean of four replicates (± SE). Different letters above bars indicate significant differences between treatments ($p < 0.05$).

5.3.3.3 *Organic acid anion exudation*

Quantitative analysis of organic anions revealed variable amounts of oxalic, tartaric, citric, malic and succinic anions, while other were only detectable in traces. As observed in Chapter 3, oxalate was the organic anion that more contributed to organic C accumulation in the exudates. In both WT and SL-depleted plants, its concentration increased under –P conditions (Fig. 5.7a). With COP-Pi and COP-*myo*InsP6, its exudation slightly increased in WT plants if compared to the relative soluble form, while decreased in SL-depleted plants. On the contrary, succinate exudation was not triggered by the presence of COP-Pi, while it slightly increased with COP-*myo*InsP6 in both genotypes and under –P conditions in WT plants (Fig. 5.7b). The highest amount of tartrate and malate were quantified in the exudates of WT plants under +P conditions (Fig. 5.7c,e). Tartrate exudation was induced by P-deficiency and low P bioavailability in SL-depleted plants (Fig. 5.7c), while malate concentration in the exudates of the same genotype increased with *myo*InsP6 (Fig. 5.7e). In the remaining cases, no tartrate or malate were detected in the exudates.

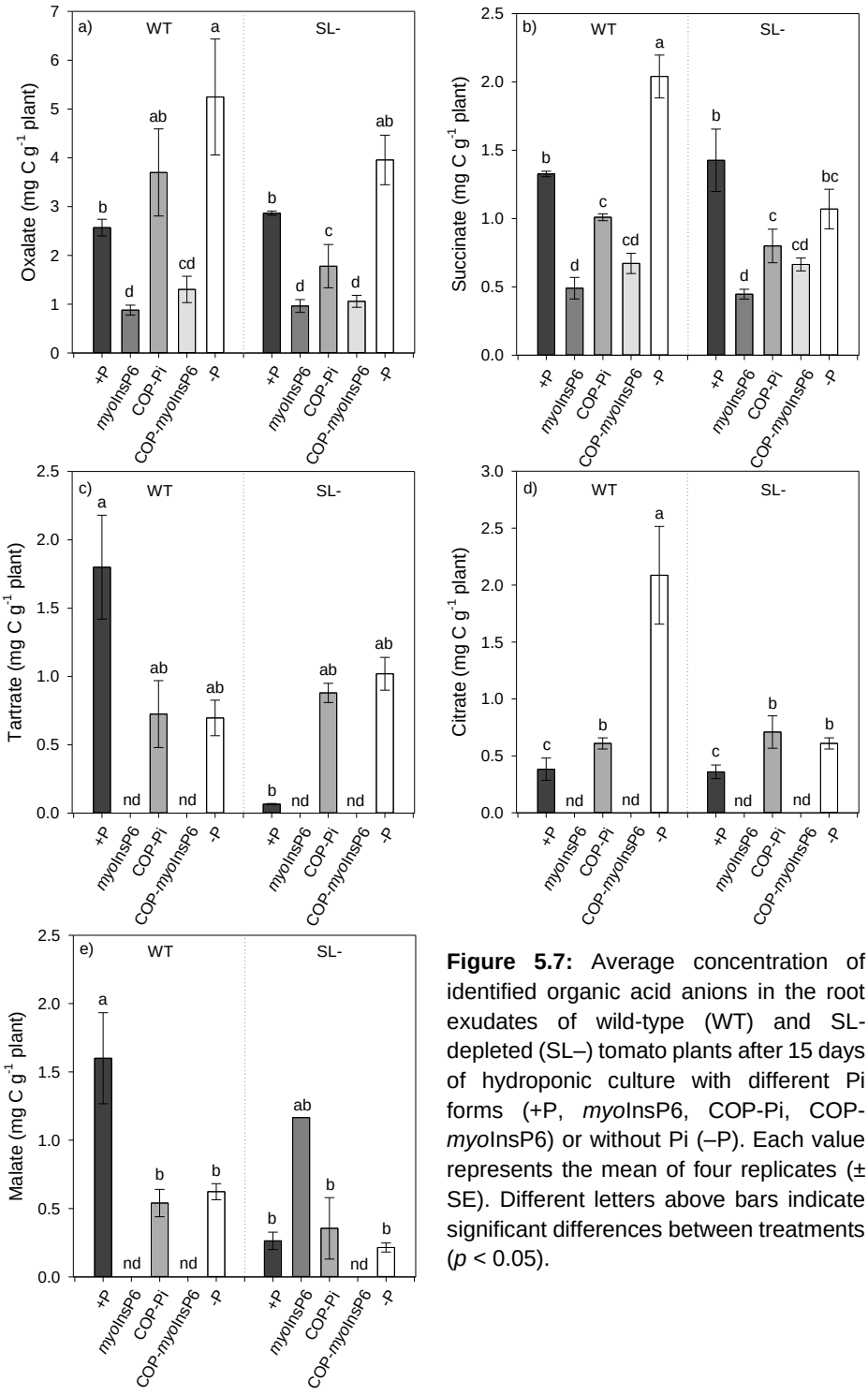

Figure 5.7: Average concentration of identified organic acid anions in the root exudates of wild-type (WT) and SL-depleted (SL–) tomato plants after 15 days of hydroponic culture with different Pi forms (+P, *myo*InsP6, COP-Pi, COP-*myo*InsP6) or without Pi (–P). Each value represents the mean of four replicates (± SE). Different letters above bars indicate significant differences between treatments ($p < 0.05$).

Finally, citrate exudation by both genotypes significantly increased with COP-Pi and –P, reaching maximum values in WT plants, while it was not detected in the presence of *myo*InsP6, either soluble or coprecipitated (Fig. 5.7d).

5.4 Discussion

Both tomato genotypes were able to use P from *myo*InsP6 when it was provided as soluble salt. However, such a capacity was strongly reduced when *myo*InsP6 was coprecipitated with Fe, with lower P acquisition than from COP-Pi. These results are in line with Findenegg and Nelemans (1993), who found that *Zea mays* plants grown in quartz sand could use 40 mM *myo*InsP6 as a source of P for nutrition, but did not grow when *myo*InsP6 was added to a P-retaining soil. Similarly, *myo*InsP6 was equivalent to Pi as a P source for *Lupinus* spp. in sand, but was a poor substrate in soil (Adams and Pate, 1992), and Martin and coworkers (2004) observed a limited availability of *myo*InsP6 to *Lolium perenne* L. when adsorbed on goethite. However, not all plants species are able to use *myo*InsP6 as a source of P. Hayes and coworkers (2000), for instance, observed that six pasture species could obtain little P from soluble *myo*InsP6 when grown in sterile media, even when it was supplied at high concentration. Differences among species could be due to a diverse contribution of root phytase activity to PSRs. In fact, we observed a high capacity of tomato plants, especially SL-depleted, to produce a significantly higher amount of phytases in the presence of *myo*InsP6 than under +P conditions, which can easily explain the high P acquisition from soluble *myo*InsP6. However, despite the even higher phytase production by WT and SL-depleted plants with COP-*myo*InsP6, both genotypes were scarcely able to use *myo*InsP6 if coprecipitated with Fe. Phytase activity was indeed reported to be inhibited when *myo*InsP6 is retained by soil surfaces (George *et al.,* 2007). Giaveno and coworkers (2010) also pointed out that phytases where not able to hydrolyze the organic P compound when it was adsorbed on various iron oxides. We can further infer that also Fe(II) oxidative coprecipitation could hamper *myo*InsP6 hydrolysis by phytases and can limit P acquisition by plants. Irrespective of P forms, SL-depleted plants were able to accumulate a greater shoot biomass and more P than the corresponding WT,

confirming the phenotypic shoot modifications observed in Chapter 3 (Gomez-Roldan *et al*., 2008; Umehara *et al*., 2008). The higher P uptake by SL-depleted plants following *myo*InsP6 supply could be, together with the higher activity of Pi-solubilizing enzymes, the result of an increased expression of high-affinity Pi transporters, and exudation of organic acid anions identified in Chapter 3, which seem to be constitutive traits of SL-depleted plants due to a possibly altered perception of P in the external medium. For these reasons, SL-depleted plants appeared to be slightly more effective at accessing sparingly soluble P while WT plants were remarkably poor at retrieving P from either COP-Pi or COP-*myo*InsP6.

The sparingly available forms of P did not affect the relative allocation of dry matter between roots and shoots of both genotypes, resulting in R/S ratios even lower than those observed under +P conditions. It is known that plants allocate more C to the root system in P deficient soils, resulting in increased R/S ratio and greater exploration of the surface soil, thereby enhancing the acquisition of less-available P (Rao *et al*., 2016; Vance *et al.*, 2003). However, as observed by Edayilam and coworkers (2018) in a similar experiment in which *A. Virginicus* plants were grown in the presence of $FePO_4$ or $Ca_3(PO_4)_2$, plants could rely more on physiological modifications for P foraging rather than on root morphology alterations. Besides, other plants experiencing P deficiency, as *Lupinus albus, Lupinus cosentinii* and *Cicer arietinum,* proved to depend on both mechanisms, enhancing P acquisition through root exudation following the formation of cluster-roots (Pearse *et al*., 2007).

In the present experiment, all treatments provoked a pH decrease of the solution if compared to the initial pH of 6.0. The amount of protons in root exudates significantly negatively correlated with plant biomass ($\rho = -0.621$, $p < 0.05$) and P content in the plant ($\rho = -0.668$, $p < 0.05$), indicating that high levels of protons in the exudates were certainly related to a major P uptake. The presence of *myo*InsP6 triggered a sharp increase of proton release when it was provided in the nutrient solution and a moderate increase if present as coprecipitate in both genotypes, indicating that the prompt response to this particular P form was

independent from SL production. Both genotypes could in fact increase the release of protons to favour the hydrolysis of *myo*InsP6 by phytases, whose optimal pH is around 5 (Giaveno *et al*. 2010). In addition, the hydrolytic reaction can produce protons contributing to the solution acidification and justifying this high acidity of the exudates.

At the provided concentration of *myo*InsP6, plant growth was substantially the same as under +P conditions in the case of SL-depleted plants, while it was lower for WT plants, in spite of the greater quantity of exuded protons and DOC. This, in line with higher biomass accumulation and P uptake by SL-depleted plants, could be a further indication of the regulation exerted by SLs on P uptake when the concentration of this nutrient is below optimal levels.

Interestingly, we observed a net decrease of biomass production and P accumulation with *myo*InsP6 coprecipitated with Fe. The presence of COP-*myo*InsP6 triggered an important increase in proton exudation that could have caused a remarkable oxide dissolution, increasing both P and Fe concentration in the solution and possibly explaining the high Fe concentration in the root of WT and SL-depleted plants treated with COP-*myo*InsP6. The increased Fe uptake could also be a consequence of P starvation and, given the negative correlation of root Fe concentration with root biomass ($\rho = -0.662$, $p < 0.05$), the elevated uptake of Fe could have impaired root and general plant growth. Accumulation of relatively high levels of Fe in the roots of P-deficient plants has in fact led to the idea that root growth inhibition may be caused by Fe toxicity (Rouached *et al.,* 2010; Ward *et al*., 2008). Müller and coworkers (2015) showed in fact that overaccumulation of Fe^{3+} in root tips plants subjected to P deficiency generated a high level of reactive oxygen species (ROS), resulting in an increased deposition of callose in cell walls and plasmodesmata. The enhanced callose deposition, likely triggered by redox signalling started by the ferroxidase *LPR1* (LOW PHOSPHATE ROOT1), interfered with the intercellular movement of the SHORT ROOT protein, impairing root growth. The accumulation of Fe in the roots of COP-*myo*InsP6-treated, as well as COP-Pi-treated plants, could therefore be a possible cause of the growth arrest that we observed, reflected by biomass

accumulation and P uptake values even lower than those observed in the absence of P. *Myo*-inositol hexaphosphate (either in the solution or as coprecipitate) was also associated to a high N uptake, irrespective of the production of SLs. We hypothesize that the higher N accumulation, together with the negative correlation between P and N concentration in plants ($\rho = -0.821$, $p < 0.001$) and in line with the results reported in Chapter 3, could be related to the larger synthesis of exoenzymes for P mineralization catalysis (Spohn, 2016). In fact, although plant N concentration usually decreases with increasing P limitation, possibly due to decreased levels of leaf cytokinin (de Groot *et al.*, 2003), several studies showed that N addition to low P treated plants increased phosphatase activity, which indicated that plants used N to mobilize and acquire P from organic sources and increase internal recycling of P (Heuck *et al.,* 2018; Schleuss *et al*., 2020; Widdig *et al.,* 2019).

Notably, when P was provided as COP-Pi, the amount of protons exuded per gram of root did not differ from the amount exuded under +P and –P conditions, indicating that either plants do not perceive the presence of Pi when it is coprecipitated with Fe, or that proton extrusion is not the principal strategy they activate to retrieve low accessible P. In fact, the amount of C exuded with COP-Pi, at least for WT plants, was higher than that observed under +P conditions, and was reflected by a higher exudation of some organic acid anions, while SL-depleted plants only slightly increased the exudation of C with COP-Pi. Therefore, the slightly higher capability of SL-depleted plants to uptake P was probably related to the activity of Pi-solubilizing enzymes, that was intermediate between those observed with *myo*InsP6 and COP-*myo*InsP6. In the present experiment, SL-depleted plants confirmed the trend observed in Chapter 3 and exuded the lowest amount of C under +P conditions, and higher ones and comparable to those of WT plants under –P. The profile of organic anion exudation confirmed that the majority of C consisted of oxalate, while other as succinate, tartrate, citrate and malate contributed to C exudation to a lesser extent. The different amounts of organic acids with respect to what observed in Chapter 3 could be due to the effect of the diverse P form used in this experiment, ad observed by

Lambers and coworkers (2002). Organic acid anion exudation was, however, triggered by the absence of Pi rather than the presence of a sparingly-available P form. The presence of *myo*InsP6 led to higher level of C exudation if compared to Pi, especially by SL-depleted plants, even if C amount was almost always lower than that exuded by WT plants. According to the SUVA index, the C-bearing compounds were more aromatic, so they possibly included molecules as polyphenols that could release P by dissolving the oxide to which it is bound (Juszczuk *et al*., 2004). Even if WT plants exuded comparable amounts of C and with the same aromaticity levels in the presence of both Pi and *myo*InsP6, the highest amount of C exuded was in the presence of COP-*myo*InsP6, which could have led to a higher dissolution of the coprecipitate, together with the activity of Pi-solubilizing enzymes.

In general, the two genotypes activated different responses to bypass P shortage or low P bioavailability, although this did not turn in an efficient use of the P present in coprecipitates. Despite the rather acidic pH and the elevated amount of DOC exuded and enzymes produced in roots, plants were not able to acquire P from coprecipitates, resulting in biomass parameters that were substantially comparable to those obtained under –P conditions. One possible reason is that these two strategies negatively affected each other. Proton release into poorly buffered nutrient solution could lower the pH, shifting the carboxylic acid/carboxylate ratio towards the acid form, and therefore reducing their efficiency in displacing P from the coprecipitate or dissolving the oxide, at least in the case of COP-*myo*InsP6 (Pearse *et al*., 2007). In addition, Zhao and coworkers (2014) observed that the maximum P-extracting capability from calcareous soil by four plant species (two woody Moraceae plants and two herbaceous cruciferous plants) was observed after 40 days of treatment, in concomitance with the maximum C losses. Also, Edayilam and coworkers (2018) observed differences in P uptake from low available forms of P ($Ca_3(PO_4)_2$ and $FePO_4$) after 16 weeks of growth. We can thus infer that in two weeks of treatment with coprecipitates plants just perceived a different form of P and started activating favourable mechanisms to scavenge the nutrient.

It is also implied that the properties of the sparingly-available P sources play a pivotal role in determining the extent of P absorption by plants. The coprecipitates used in this experiment presented similar mesopore volume but rather different surface charge (+2 mV COP-Pi *vs.* -38 mV COP-*myo*InsP6). The elevated and negative surface charge of COP-*myo*InsP6 could have prevented organic acid anions to approach the coprecipitate surface due to electrostatic repulsion, resulting in decreased efficiency of ligand-exchange/dissolution mechanisms. Conversely, COP-Pi surface was positively charged and more enriched in P (Table 5.1) than COP-*myo*InsP6, allowing organic acids to compete with P for retention sites.

CHAPTER 6

General discussion and conclusions

6.1 Tomato morphological and physiological adaptations to P stress are under SL control

In this thesis, I investigated the tight interconnection between P and tomato plant growth and development as influenced by SLs, a recently discovered class of plant hormones. First, I studied the impact of reduced SL biosynthesis on root architecture modifications in response to P starvation (Chapter 2). My results highlight a fine modulation of plant responses exerted by small variations of P concentration in the external medium and timing of P-stress imposition. I indeed observed that, depending on whether plants were grown under totally P-deprived conditions or in suboptimal P levels, SLs significantly affected those root traits that all allow for enhanced soil exploration by the roots, namely root volume and diameter, primary and total root length, and lateral root number (Fig. 6.1).

Complete P deprivation (0 µM Pi) since germination impaired typical P stress responses and resulted in reduced plant growth in both WT and SL-depleted plants. The analysis of root P-solubilizing enzymes highlighted how their activity was enhanced under P deprivation in both genotypes and was significantly higher in SL-depleted plants, possibly justifying the missing onset of the expected architectural PSRs. A period of sub-optimal P supply (10 µM Pi) instead induced P-stress responses in WT plants if compared to normal P conditions (80 µM Pi), while some features of these responses were attenuated in SL-depleted plants. Finally, when P stress was imposed after an initial acclimation period, these trait modifications were emphasized in WT plants, while significantly repressed in SL-deficient plants, similar to plants held under continuous P shortage. These results confirm the importance of SLs for optimal plant development and adaptation to P stress also in tomato, after being extensively investigated in other crop species. The cause of the impaired root response by SL-depleted plants may be found at

the microscopic level, as SL-depleted plants displayed clear root alterations in terms of cell differentiation and tissue specification already under +P conditions. Apart from the well-known roles of SLs in plant development (e.g., shoot branching inhibition and initiation of leaf senescence), and consistently with root

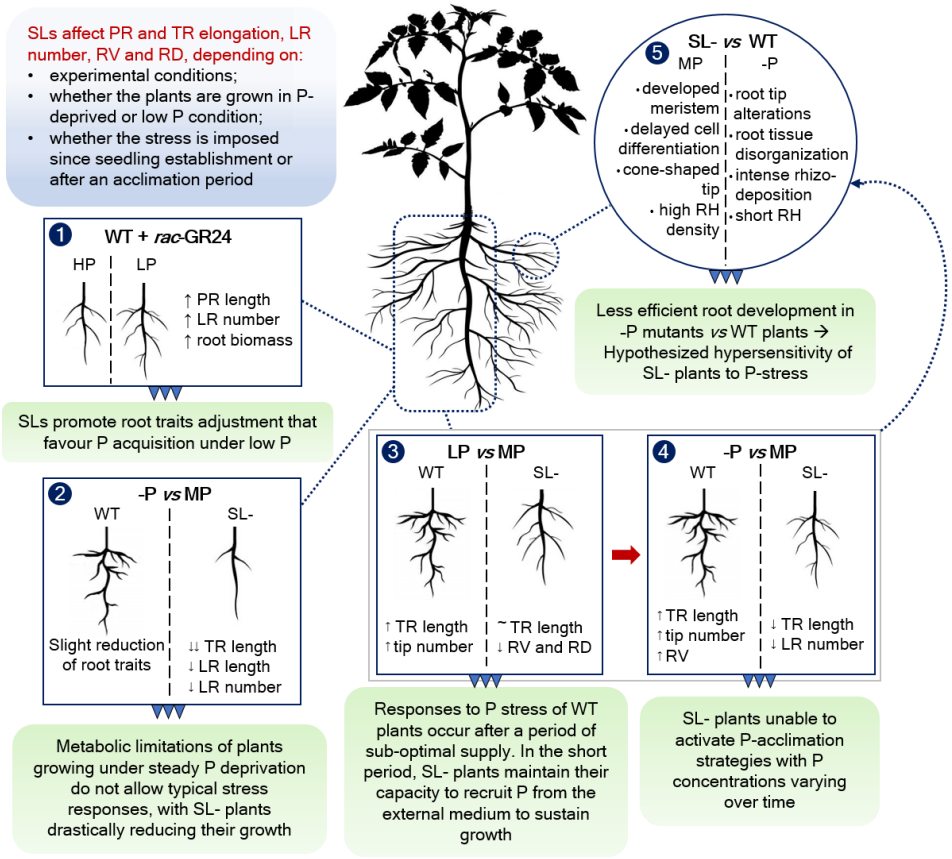

Figure 6.1: Conclusive conceptual summary of Chapter 2. 1) SL analogue (*rac*-GR24) application to wild-type (WT) tomato plants under low P promoted root morphological modification to favour P acquisition; 2) the continuous growth under P stress (–P) limited root capacity to respond to P stress, especially in the SL-depleted (SL–) plants; 3) under suboptimal P supply (LP), a detectable role of SL in improving plants responses to P stress was highlighted: SL– plants showed an attenuated capacity to respond to LP, for some specific features; 4) imposition of severe stress (no P, –P in the scheme) after acclimation on LP revealed the inability of SL– plants to respond to P stress in the long term, possibly because of 5) root development impairment caused by the anatomical modifications observed at the microscopic scale. Abbreviations: PR, primary root; TR, total root; LR, lateral root; RV, root volume; RD, root diameter; RH, root hair.

architectural and cellular modifications observed at both P levels (Chapter 2), reduced SL biosynthesis caused a higher P demand under normal growing conditions (+P, 80 µM Pi), as highlighted by the hydroponic experiment conducted in Chapter 3. High-affinity Pi transporters were significantly up-regulated in the roots of SL-depleted plants already under +P conditions, as well as the Pi-solubilizing enzymes phosphatases and phytases, resulting in higher P uptake and accumulation in tissues, especially shoots (Fig. 6.2). Under –P conditions, however, the onset of these same responses was not as intense as conceivable from the higher P necessity displayed by SL-depleted plants under +P. The reduced SL production could therefore be responsible for both the disorganized response to normal P conditions, which were perceived as optimal for growth by WT plants but induced some PSRs in SL-depleted plants, and for the lack of responses to P stress by this same genotype, possibly because of an altered P perception caused by the morphological disorganization at the root tip. Nevertheless, a total insensitivity of SL-depleted plants to external P status should be ruled out, given the activation of other physiological modifications belonging to the set of PSRs. In fact, WT plants seemed to rely more on root architectural modifications and proton extrusion to cope with P-deficiency rather than on C exudation, whose amount in the exudates did not change quantitatively under –P conditions but was released more rapidly. On the contrary, P-stressed SL-depleted plants exuded significantly higher amounts of organic C (mainly oxalic acid anions) than under +P conditions, and activated the response of rhizosphere acidification only after several days since the beginning of P stress, possibly due to a negative feedback of P concentration in the shoots. These results imply an important temporal aspect in the response of plants to P stress, which appears to be under the regulative control of SLs and that had never been highlighted so far. Strigolactones in fact favoured a fast and equilibrated plant response to progressive P reduction, allowing the maintenance of an adequate physiological equilibrium at P concentrations as low as 80 µM.

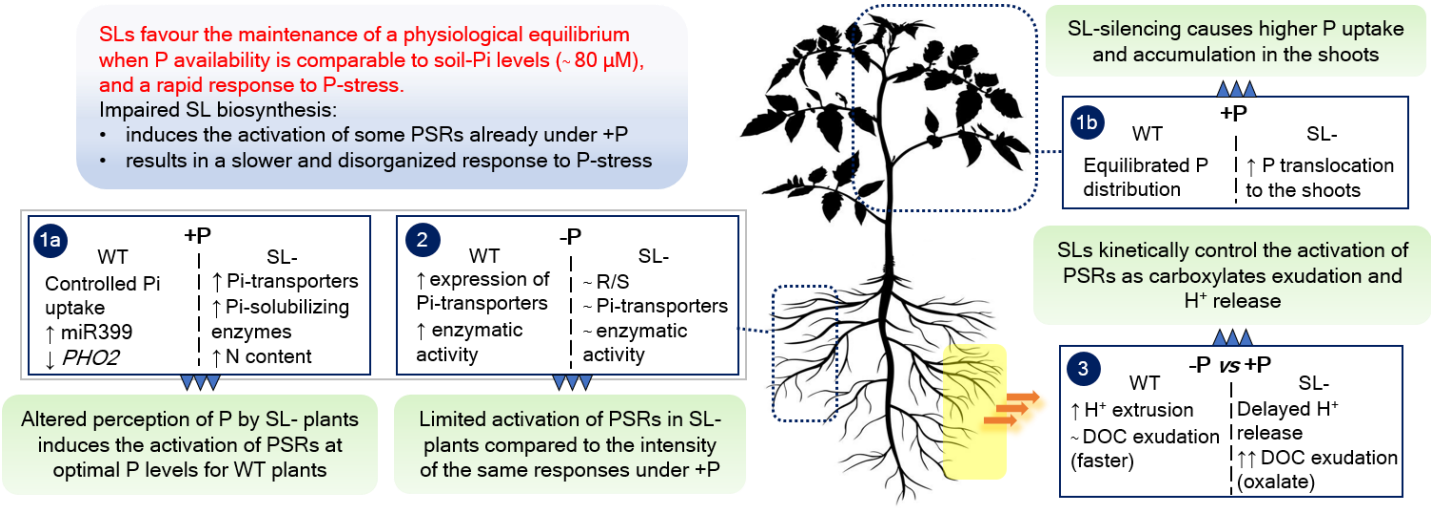

Figure 6.2: Conclusive conceptual summary of Chapter 3. 1a) SL-silencing caused a significant up-regulation of high-affinity Pi transporters and Pi-solubilizing enzymes under +P conditions (80 µM Pi), possibly indicating an altered perception of external P; 1b) this resulted in higher P consumption from the nutrient solution and accumulation in the shoots of SL-depleted plants (SL–). 2) Under P starvation (–P), however, the onset of these same P starvation responses (PSRs) was not proportioned to the higher P demand displayed under +P, with comparable Pi transporters expression, R/S ratio and enzymatic activity to P-starved WT plants. 3) Finally, SLs exerted a temporal regulation on tomato plants responses to P stress, promptly activating organic acid anion exudation while delaying proton (H^+) extrusion by SL– plants. Abbreviations: DOC, dissolved organic C.

With lower P concentrations or under –P conditions, plants producing SLs started activating some of the well-known PSRs. Conversely, reduced SL biosynthesis caused a delayed and disorganized response with a larger consumption of P.

6.2 Oxidative Fe + P coprecipitation contributes to inorganic and organic P retention in soil and limits P availability to tomato plants

During the setup of the experiments reported in Part I, ample effort was devoted to the adoption of the P growing conditions that best resembled soil-P levels and that, at the same time, sustained the optimal growth of tomato plants preventing, however, an excessive P accumulation in tissues, a possible cause of delayed PSRs. Nevertheless, at least two other aspects that influence P availability in soil and could therefore affect plants morphological and physiological adaptations should be taken into consideration. First, a large percentage of soil P can occur as organic molecules that, although representing an important source of P for plants, require mineralization to Pi before acquisition, implying the production of enzymes as phytases and phosphatases. Secondly, many soil abiotic processes contribute to the retention and accumulation of P in the solid phase, resulting in a low availability of P in the soil solution. Although the processes of surface adsorption and precipitation have been widely investigated, little is known about the coprecipitation of inorganic and organic P following the oxidative precipitation of Fe (hydr)oxides. For this reason, in Chapter 4 I deeply investigated how coprecipitation of Pi and *myo*InsP6 with Fe can affect P dynamics and properties of the precipitated material, compared to adsorption, when conditions shift from anaerobic to aerobic. The results of kinetics evidenced a much higher P retention offered by coprecipitation with respect to adsorption for both the P compounds studied, particularly at high initial $(P/Fe)_0$ ratios (Fig. 6.3). In particular, Fe(II) oxidative precipitation in the presence of low Pi concentrations was slowed down with respect to P-free ferrihydrite precipitation, probably due to the interference and poisoning of the anion with the (hydr)oxide crystallization nuclei, leading to the formation of small nanometric particles. At greater Pi concentrations, particles were more aggregated, with a lower surface area and increased porosity, likely

due to the simultaneous salt precipitation and (hydr)oxide formation, which could represent a further obstacle for P interception by plants.

Conversely to Pi, the presence of *myo*InsP6 accelerated Fe(II) oxidation and precipitation through the rapid formation of more easily oxidizable Fe-*myo*InsP6 complexes, as evidenced by the immediate disappearance of P from the solution. The presence of multiple phosphate groups on the same molecule could favour the growth of Fe oxides in more directions, leading to a greater extent of inclusion within the systems with respect to Pi coprecipitates. Nevertheless, as for Pi, the adsorption on the forming surface seemed to dominate over the precipitation of the salt at low *myo*InsP6 concentrations, and remained a relevant mechanism even at high *myo*InsP6 concentration.

Coprecipitation of soluble organic P compounds as *myo*InsP6 during Fe(II) oxidation is therefore a much more complex process than adsorption, occurring through several mechanisms and with different kinetics depending mostly on P species and $(P/Fe)_0$ ratio. The type and initial concentration of P may indeed lead to the formation of Fe(III)-coprecipitates with different surface properties which can in turn affect their reactivity at the solid/solution interface and modulate the plants response in order to achieve the best scavenging efficiency. The larger P retention and the different morphological and mineralogical features of coprecipitates obtained with *myo*InsP6 compared to Pi may further increase its stabilization and selective accumulation in soil while reducing P bioavailability and accessibility to plants.

Indeed, when P was provided to tomato plants as the coprecipitated form of *myo*InsP6 (Chapter 5), both genotypes were scarcely able to use it, possibly due to the inhibition of phytases already reported for *myo*InsP6 adsorbed on the surface of various Fe oxides, even if their activity was greatly stimulated (Fig. 6.3). A similar but less pronounced inability to take up P was observed in the presence of COP-Pi, whose surface properties possibly facilitated the interception of P by plants. On the contrary, both genotypes were able to acquire P from *myo*InsP6 when it was provided as a soluble salt, and SL-depleted plants again exhibited unregulated P acquisition capacity under all P treatments,

confirming the central role of SL in P acquisition regardless of P form. However, the comparable decrease of the solution pH by the two genotypes in the presence of soluble *myo*InsP6 led us to the conclusion that the type of provided P can prevail over SL control in the establishment of this specific PSR, even if this comparable behaviour could be the result of very different kinetics of PSR activations, as observed for proton extrusion in Chapter 3.

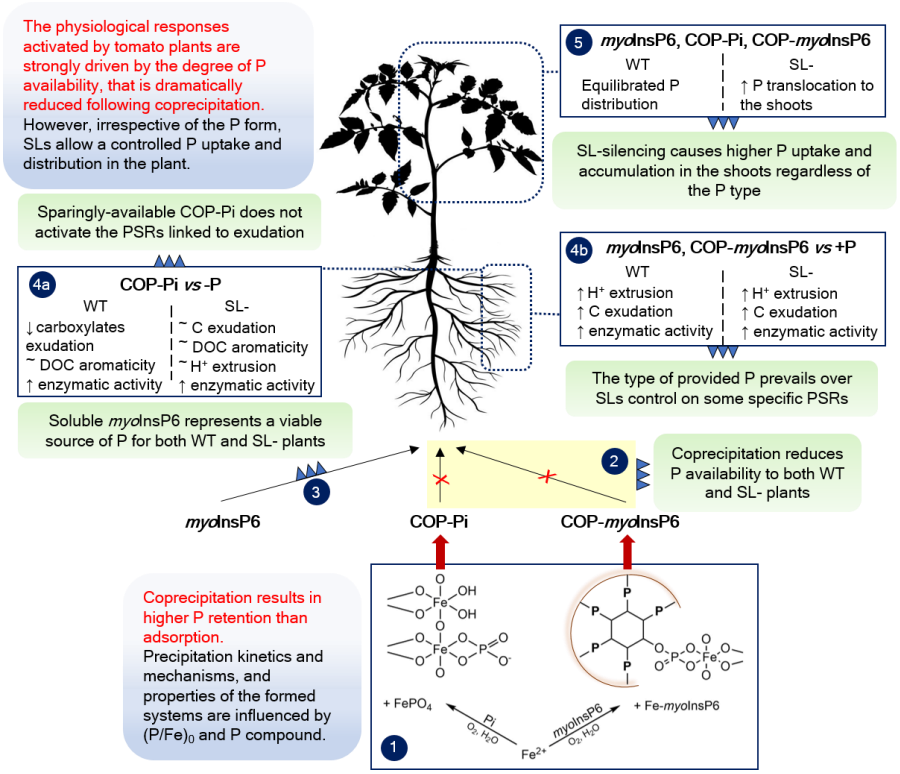

Figure 6.3: Conclusive conceptual summary of Chapters 4 and 5. 1) P retention by coprecipitation was generally greater if compared to adsorption. The type of P compound and the initial P to Fe ratio [$(P/Fe)_0$] strongly influenced the process kinetics and properties of the formed systems. The main mechanisms involved were precipitation, adsorption and occlusion within the forming particles. 2) Both WT and SL-depleted (SL–) plants were not able to retrieve P from coprecipitates, while 3) they could use P from soluble *myo*-inositol hexaphosphate (*myo*InsP6). 4a) Organic acid anion exudation was triggered by P deficiency rather than the presence of COP-Pi, possibly because a delayed activation of plants response to sparingly-available P. 4b) Both *myo*InsP6 forms induced similar response in the two genotypes, indicating a prevailing influence of the P form over SL control. 5) However, under either P condition, P uptake and accumulation was higher in SL– plants, highlighting their central role in guaranteeing an optimal P management. Abbreviations: DOC, dissolved organic C. Brown line: Fe oxide surface.

With reference to process kinetics, another significant outcome concerns organic acid anion exudation, which was quantitatively higher in WT than in SL-depleted plants and was triggered by the absence of P rather that the presence of the sparingly-available COP-Pi. This could be due to the short duration of the hydroponic treatment, that probably was not sufficient for tomato plants to perceive the P form and activate the appropriate responses, regardless of the control of SL over PSRs. However, C-bearing compounds exuded in the presence of both soluble or coprecipitated *myo*InsP6 were more aromatic, possibly including organic molecules as polyphenols that could release P by dissolving the oxide to which it is bound.

6.3 General conclusions, environmental significance and future perspectives

The outcomes of the second part of the thesis complement the results obtained in Part I and point out important conclusions related to quantitative and kinetic aspects. The biotic processes exerted by plants in response to P shortage and the abiotic reactions of P repartition between the solid and liquid phase are strongly driven by P quantity. Both these processes occur with diverse kinetics and in soil can extensively influence each other, being also regulated by SLs. The rapid subtraction of *myo*InsP6 from the soil solution following coprecipitation could in fact be dealt with by WT plants, that have proven to rapidly respond to P status, unlike SL-depleted plants. However, this indirect kinetic control of SLs may be lacking when sparingly-available P systems are formed, as it seems that more than 15 days are necessary for tomato plants to adopt effective scavenging strategies.

These results have important agricultural implications since they draw attention to the central role of SLs in controlling not only the capability of tomato plants to respond to P stress, both at the morphological and physiological level, but also in guaranteeing an optimal P management through the regulation of physiological processes when the nutrient availability meets the P demand by plants. In addition, results obtained with SL-depleted plants highlight how the reduced biosynthesis of these plant hormones triggers a cascade of physiological

modifications, as the constitutive up-regulation of Pi transporter that certainly requires a high C cost, or the enhanced activity of Pi-solubilizing enzymes that indirectly influences N acquisition. The apparently well-orchestrated physiological modifications of SL-depleted plants however eventually result in disordered response to P deprivation, together with an inefficient internal P utilization.

Such results could allow the selection of tomato genotypes with enhanced P-use efficiency able to better adapt to low P environments, also in consideration of the rapid exhaustion of P resources and the issues linked to P-fertilizers inefficacy.

On the other hand, the investigation on P retention processes provide evidence of how coprecipitation, apart from being a complex process that involves several mechanisms depending on the P species and initial P/Fe ratio, can further contribute to the stabilization and selective accumulation of *myo*InsP6 in soil with respect to Pi and other organic P forms that may display lower affinity for Fe.

Future researches should be addressed to: i) investigate the efficiency of the organic acid anions identified in the root exudates of tomato plants in releasing P from the obtained adsorbed and coprecipitated Fe-P systems, compared to the reductive dissolution exerted by aromatic compounds as polyphenols, to connect physiological and soil processes in the frame of the plant-rhizosphere continuum; ii) evaluate the long-term efficacy of plants to scavenge scarcely-available P, extending the duration of the hydroponic experiment and allowing the identification of a possibly delayed activation of the physiological strategies to uptake P; iii) further investigate the modulation by SLs of plant responses as a function of P levels, employing soils with different available P levels.

REFERENCES

Abel, S., Ticconi, C.A., Delatorre, C.A. (2002). Phosphate sensing in higher plants. *Physiol. Plant.* **115**, 1–8.

Abel, S. (2011). Phosphate sensing in root development. *Curr. Opin. Plant Biol.* **14**, 303–309.

Adams, M.A., Pate, J.S. (1992). Availability of organic and inorganic forms of phosphorus to lupins (*Lupinus* spp.). *Plant Soil* **145**, 107–113.

Akiyama, K., Matsuzaki, K., Hayashi, H. (2005). Plant sesquiterpenes induce hyphal branching in arbuscular mycorrhizal fungi. *Nature* **435**, 824–827.

Akiyama, K., Hayashi, H. (2006). Strigolactones: chemical signals for fungal symbionts and parasitic weeds in plant roots. *Ann. Bot.* **97** (6), 925–931.

Akiyama, K., Ogasawara, S., Ito, S., Hayashi, H. (2010). Structural requirements of strigolactones for hyphal branching in AM fungi. *Plant Cell Physiol*. **51**, 1104–1117.

Al-Babili, S., Bouwmeester, H.J. (2015). Strigolactones, a novel carotenoid-derived plant hormone. *Annu. Rev. Plant Biol.* **66**, 161–186.

Alder, A., Jamil, M., Marzorati, M., Bruno, M., Vermathen, M., Bigler, P., Ghisla, S., Bouwmeester, H., Beyer, P., Al-Babili, S. (2012). The path from beta-carotene to carlactone, a strigolactone-like plant hormone. *Science* **335**, 1348–1351.

Alothman, Z.A. (2012). A review: fundamental aspects of silicate mesoporous materials. *Materials* **5**, 2874–2902.

Anderson, G. (1980). Assessing organic phosphorus in soil. In: Khasawneh, F.E., Sample, E.C., Kamprath, E.J. (Eds.), The role of phosphorus in agriculture, American Society of Agronomy, Madison, WI, USA, pp. 411–431.

Arai, Y., Sparks, D.L. (2001). ATR-FTIR spectroscopic investigation on phosphate adsorption mechanisms at the ferrihydrite-water interface. *J. Colloid Interface Sci.* **214** (2), 317–326.

Arai, Y., Sparks, D.L. (2007). Phosphate reaction dynamics in soils and soil components: A multiscale approach. *Adv. Agron.* **94**, 135−179.

Arite, T., Kameoka, H., Kyozuka, J. (2012). Strigolactone positively controls crown root elongation in rice. *J. Plant Growth Regul*. **31**, 165–172.

Asmar, F., Gahoonia, T.S., Nielsen, N.E. (1995). Barley genotypes differ in activity of soluble extracellular phosphatase and depletion of organic phosphorus in the rhizosphere soil. *Plant Soil* **172**, 117–122.

Aung, K., Lin, S.I., Wu, C.C., Huang, Y.T., Su, C.L., Chiou, T.J. (2006). *pho2*, a phosphate overaccumulator, is caused by a nonsense mutation in a microRNA399 target gene. *Plant Physiol*. **141**, 1000–1011.

Aziz, T., Sabir, M., Farooq, M., Maqsood, M.A., Ahmad, H.R., Warraich, E.A. (2014). Phosphorus deficiency in plants: Responses, adaptive mechanisms, and signaling. In: Hakeem, K.R., Rehman, R.U.I., Tahir, I. (Eds.), Plant Signaling: Understanding the Molecular Crosstalk. Springer India: New Dehli, India, pp. 133–148.

Baldwin, J.C., Athikkattuvalasu, S.K., Raghothama, K.G. (2001). *LEPS2*, a phosphorus starvation-induced novel acid phosphatase from tomato. *Plant Physiol.* **125**, 728–737.

Barbier, F.F., Dun, E.A., Kerr, S.C., Chabikwa, T.G., Beveridge, C.A. (2019). An update on the signals controlling shoot branching. *Trends Plant Sci*. **24** (3), 220–236.

Bari, R., Datt Pant, B., Stitt, M., Scheible, W.R. (2006). PHO2, microRNA399, and PHR1 define a phosphate-signaling pathway in plants. *Plant Physiol.* **141**, 988–999.

Barrett, E.P., Joyner, L.G., Halenda, P.P. (1951). The determination of pore volume and area distribution in porous substances. I. Computations from nitrogen isotherms. *J. Am. Chem. Soc.* **73** (1), 373–380.

Barrientos, L.G., Murthy, P.N.N. (1996). Conformational studies of *myo*-inositol phosphates. *Carbohydr. Res*. **296**, 39–54.
Besford, R. (1979). Uptake and distribution of phosphorus in tomato plants. *Plant Soil* **51**, 331–340.
Bieleski, R.L. (1973). Phosphate pools, phosphate transport, and phosphate availability. *Annu. Rev. Plant Physiol.* **24**, 225–252.
Bonghi, C., Casadoro, G., Ramina, A., Rascio, N. (1993). Abscission in leaf and fruit explants of *Prunus persica* (L.) Batsch. *New Phytol.* **123**, 555–565.
Bozzo, G.G., Dunn, E.L., Plaxton, W.C. (2005). Differential synthesis of phosphate–Starvation inducible purple acid phosphatase isozymes in tomato (*Lycopersicon esculentum*) suspension cells and seedlings. *Plant Cell Environ*. **29**, 303–313.
Bradow, J.M., Connick Jr., W.J., Pepperman, A.B., Wartelle, L.H. (1990). Germination stimulation in wild oats (*Avena fatua* L.) by synthetic strigol analogs and gibberellic acid. *J. Plant Growth Regul.* **9**, 35–41.
Brewer, P.B., Koltai, H., Beveridge, C.A. (2013). Diverse roles of strigolactones in plant development. *Mol. Plant* **6** (1), 18–28.
Brewer, P.B., Dun, E.A., Gui, R., Mason, M.G., Beveridge, C.A. (2015). Strigolactone inhibition of branching independent of polar auxin transport. *Plant Physiol*. **168**, 1820–1829.
Brinch-Pedersen, H., Sorenson, L.D., Holm, P.B. (2002). Engineering crop plants: getting a handle on phosphate. *Trends Plant Sci.* **7**, 118–125.
Brunauer, S., Emmett, P.H., Teller, E. (1938). Adsorption of gases in multimolecular layers. *J. Am. Chem. Soc*. **60** (2), 309–319.
Bürger, M., Chory, J. (2019). The many models of strigolactone signalling. *Trends Plant Sci*. **25** (4), 395–405.
Butler, L.G. (1995). Chemical communication between the parasitic weed Striga and its crop host. In Inderjit, K.M.M., Dakshini, F.A. (Eds.), Allelopathy: organisms, processes, and application, Einhellig ACS Symp. Ser. 582. Washington, DC: Am. Chem. Soc, pp. 158–68.
Cardinale, F., Korwin Krukowski, P., Schubert, A., Visentin, I. (2018). Strigolactones: Mediators of osmotic stress responses with a potential for agrochemical manipulation of crop resilience. *J. Exp. Bot.* **69**, 2291–2303.
Ćavar, S., Zwanenburg, B., Tarkowski, P. (2015). Strigolactones: occurrence, structure, and biological activity in the rhizosphere. *Phytochem. Rev.* **14**, 691–711.
Celi, L., Lamacchia, S., Ajmone-Marsan, F., Barberis, E. (1999). Interaction of inositol hexaphosphate on clays: adsorption and charging phenomena. *Soil Sci.* **164** (8), 574–585.
Celi, L., Lamacchia, S., Barberis, E. (2000). Interaction of inositol phosphate with calcite. *Nutr. Cycling Agroecosyst.* **57***,* 271–277.
Celi, L., Presta, M., Ajmone-Marsan, F., Barberis, E. (2001). Effects of pH and electrolytes on inositol hexaphosphate interaction with goethite. *Soil Sci. Soc. Am. J.* **65** (3), 753–760.
Celi, L., De Luca, G., Barberis, E. (2003). Effects of interaction of organic and inorganic P with ferrihydrite and kaolinite-iron oxide systems on iron release. *Soil Sci*. *168* (7), 479–488.
Celi, L., Barberis, E. (2004). Abiotic stabilization of organic phosphorus in the environment. In: Turner, B.L., Frossard, E., Baldwin, D.S. (Eds.), Organic Phosphorus in the Environment. CABI Publishing, Wallingford, UK, pp. 113–132.
Celi, L., Prati, M., Magnacca, G., Santoro, V., Martin, M. (2020). Role of crystalline iron oxides on stabilization of inositol phosphates in soil. *Geoderma* **374**, 114442.

Charnikhova, T.V., Gaus, K., Lumbroso, A., Sanders, M., Vincken, J.P., De Mesmaeker, A., Ruyter-Spira, C.P., Screpanti, C., Bouwmeester, H.J. (2017). Zealactones. Novel natural strigolactones from maize. *Phytochemistry* **137**, 123–131.

Chatellier, X., West, M.M., Rose, J., Fortin, D., Leppard, G.G., Ferris, F.G. (2004). Characterization of iron-oxides formed by oxidation of ferrous ions in the presence of various bacterial species and inorganic ligands. *Geomicrobiol. J.* **21** (2), 99–112.

Chatellier, X., Grybos, M., Abdelmoula, M., Kemner, K.M., Leppard, G.G., Mustin, C., West, M.M., Paktunc, D. (2013). Immobilization of P by oxidation of Fe(II) ions leading to nanoparticle formation and aggregation. *Appl. Geochem.* **35**, 325–339.

Chen, C., Dynes, J.J., Wang, J., Sparks, D.L. (2014). Properties of Fe-organic matter associations via coprecipitation versus adsorption. *Environ. Sci. Technol.* **48** (23), 13751–13759.

Chen, A., Chen, X., Wang, H., Liao, D., Gu, M., Qu, H., Sun, S., Xu, G. (2014a). Genome-wide investigation and expression analysis suggest diverse roles and genetic redundancy of Pht1 family genes in response to Pi deficiency in tomato. *BMC Plant Biol.* **14**, 61.

Chien, P.S., Chiang, C.P., Leong, S.J., Chiou, T.J. (2018). Sensing and signaling of phosphate starvation: from local to long distance. *Plant Cell Physiol.* **59** (9), 1714–1722.

Chiou, T.J., Aung, K., Lin, S.I., Wu, C.C., Chiang, S.F., Su, C.L. (2006). Regulation of phosphate homeostasis by microRNA in *Arabidopsis*. *Plant Cell* **18**, 412–421.

Chiou, T.J., Lin, S.I. (2011). Signaling network in sensing phosphate availability in plants. *Annu. Rev. Plant Biol.* **62**, 185–206.

Condron, L.M., Turner, B.L., Cade-Menun, B.J. (2005). Chemistry and dynamics of soil organic phosphorus. In: Sims, J.T., Sharpley, A.N. (Eds.), Phosphorus: agriculture and the environment. American Society of Agronomy, Crop Science Society of America, Soil Science Society of America, Inc., Madison, WI, pp 87–121.

Cook, C.E., Whichard, L.P., Turner, B., Wall, M.E., Egley, G.H. (1966). Germination of witchweed (Striga lutea Lour.): isolation and properties of a potent stimulant, *Science* **154**, 1189–1190.

Corbridge, D.E.C. (1985). Phosphorus: an outline of its chemistry, biochemistry and technology. Elsevier, Amsterdam, pp. 761.

Cordell, D., Drangert, J.O., White, S. (2009). The story of phosphorus: global food security and food for thought. *Glob. Environ. Change.* **19**, 292–305.

Costello, A.J.R., Glonek, T., Myers, T.C. (1976). ^{31}P nuclear magnetic resonance: pH titrations of *myo*-inositol hexaphosphate. *Carbohydr. Res.* **46** (2), 159–171.

Czarnecki, O., Yang, J., Weston, D.J., Tuskan, G.A., Chen, J.G. (2013). A dual role of strigolactones in phosphate acquisition and utilization in plants. *Int. J. Mol. Sci.* **14**, 7681–7701.

de Groot, C.C., Marcelis, L.F.M., van den Boogaard, R., Lambers, H. (2001). Growth and dry-mass partitioning in tomato as affected by phosphorus nutrition and light. *Plant Cell Environ.* **24**, 1309–1317.

de Groot, C.C., Marcelis, L.F.M., van den Boogaard, R., Kaiser, W.M., Lambers, H. (2003). Interaction of nitrogen and phosphorus nutrition in determining growth. *Plant Soil* **248**, 257–268.

de Souza Campos, P.M., Cornejo, P., Rial, C., Borie, F., Varela, R.M., Seguel, A., López-Ráez, J.A. (2019). Phosphate acquisition efficiency in wheat is related to root:shoot ratio, strigolactone levels, and PHO2 regulation. *J. Exp. Bot.* **70** (20), 5631–5642.

Decker, E.L., Alder, A., Hunn, S., Ferguson, J., Lehtonen, M.T., Scheler, B., Kerres, K.L., Wiedemann, G., Safavi-Rizi, V., Nordzieke, S., Balakrishna, A., Baz, L., Avalos, J., Valkonen, J.P.T., Reski, R., Al-Babili, S. (2017). Strigolactone biosynthesis is evolutionarily conserved, regulated by phosphate starvation and contributes to

resistance against phytopathogenic fungi in a moss, *Physcomitrella patens. New Phytol.* **216**, 455–468.
Ding, Y., Feng, R., Wang, R., Guo, J., Zheng, X. (2014). A dual effect of Se on Cd toxicity: Evidence from plant growth, root morphology and responses of the antioxidative systems of paddy rice. *Plant Soil* **375**, 289–301.
Dixon, M., Simonne, E., Obreza, T., Liu, G. (2020). Crop response to low phosphorus bioavailability with a focus on tomato. *Agronomy* **10** (5), 617.
Drew, M.C., Saker, L.R., Barber, S.A., Jenkins, W. (1984). Changes in the kinetics of phosphate and potassium absorption in nutrient-deficient barley roots measured by a solution-depletion technique. *Planta* **160**, 490–499.
Duby, G., Boutry, M. (2009). The plasma membrane proton pump ATPase: A highly regulated P-type ATPase with multiple physiological roles. *Pflug. Arch. Eur. J. Physiol.* **457**, 645–655.
Edayilam, N., Montgomery, D., Ferguson, B., Maroli, A.S., Martinez, N., Powell, B.A., Tharayil, N. (2018). Phosphorus stress-induced changes in plant root exudation could potentially facilitate Uranium mobilization from stable mineral forms. *Environ. Sci. Technol.* **52**, 7652–7662.
Elzinga, E.J., Sparks, D.L. (2007). Phosphate adsorption onto hematite: an in-situ ATR-FTIR investigation of the effects of pH and loading level on the mode of phosphate surface complexation. *J. Colloid Interface Sci.* **308** (1), 53–70.
Epstein, E. (1994). The anomaly of silicon in plant biology. *Proc. Natl. Acad. Sci. USA* **91**, 11–17.
Eusterhues, K., Wagner, F.E., Hausler, W., Hanzlik, M., Knicker, H., Totsche, K.U., Kogel-Knabner, I., Schwertmann, U. (2008). Characterization of ferrihydrite-soil organic matter coprecipitates by X-ray diffraction and Mossbauer spectroscopy. *Environ. Sci. Technol.* **42** (21), 7891–7897.
Findenegg, G.R., Nelemans, J.A. (1993). The effect of phytase on the availability of P from myo-inositol hexaphosphate (phytate) for maize roots. *Plant Soil* **154**, 189–196.
Flematti, G.R., Scaffidi, A., Waters, M.T., Smith, S.M. (2016). Stereospecificity in strigolactone biosynthesis and perception. *Planta* **243**, 1361–1373.
Floková, K., Shimels, M., Andreo Jimenez, B., Bardaro, N., Strnad, M., Novák, O., Bouwmeester, H.J. (2020). An improved strategy to analyse strigolactones in complex sample matrices using UHPLC–MS/MS. *Plant Methods* **16**, 125.
Foehse, D., Jungk, A. (1983). Influence of phosphate and nitrate supply on root hair formation of rape, spinach and tomato plants. *Plant Soil* **74**, 359–368.
Freed, C., Adepoju, O., Gillaspy, G. (2020). Can inositol pyrophosphates inform strategies for developing low phytate crops? *Plants* **9** (1), 115.
Frossard, E., Condron, L.M., Oberson, A., Sinaj, S., Fardeau, J.C. (2000). Processes governing phosphorus availability in temperate soils. *J. Environ. Qual.* **29**, 12–53.
Furihata, T., Suzuki, M., Sakurai, H. (1992). Kinetic characterization of two phosphate uptake systems with different affinities in suspension-cultured *Catharanthus roseus* protoplasts. *Plant Cell Physiol*. **33**, 1151–1157.
Gamir, J., Torres-Vera, R., Rial, C., Berrio, E., de Souza Campos, P.M., Varela, R.M., Macías, F.A., Pozo, M.J., Flors, V., López-Ráez, J.A. (2020). Exogenous strigolactones impact metabolic profiles and phosphate starvation signalling in roots. *Plant Cell Environ.* **43** (7), 1–14.
Garcia, M., Ascencio, J. (1992). Root morphology and acid phosphatase activity in tomato plants during development of and recovery from phosphorus stress. *J. Plant Nutr.* **15**, 2491–2503.
George, T.S., Simpson, R.J., Hadobas, P.A., Marshall, D.J., Richardson, A.E. (2007). Accumulation and phosphatase-lability of organic phosphorus in fertilised pasture soils. *Aust. J. Agric. Res.* **58** (1), 47–55.

George, T.S., Giles, C.D., Menezes-Blackburn, D., Condron, L.M., Gama-Rodrigues, A.C., Jaisi, D., Lang, F., Neal, A.L., Stutter, M.I., Almeida, D.S., Bol, R., Cabugao, K.G., Celi, L., Cotner, J.B., Feng, G., Goll, D.S., Hallama, M., Krueger, J., Plassard, C., Rosling, A., Darch, T., Fraser, T., Giesler, R., Richardson, A.E., Tamburini, F., Shand, C.A., Lumsdon, D.G., Zhang, H., Blackwell, M.S.A., Wearing, C., Mezeli, M.M., Almas, A.R., Audette, Y., Bertrand, I., Beyhaut, E., Boitt, G., Bradshaw, N., Brearley, C.A., Bruulsema, T.W., Ciais, P., Cozzolino, V., Duran, P.C., Mora, M.L., de Menezes, A.B., Dodd, R.J., Dunfield, K., Engl, C., Frazao, J.J., Garland, G., Gonzalez Jimenez, J.L., Graca, J., Granger, S.J., Harrison, A.F., Heuck, C., Hou, E.Q., Johnes, P.J., Kaiser, K., Kjar, H.A., Klumpp, E., Lamb, A.L., Macintosh, K.A., Mackay, E.B., McGrath, J., McIntyre, C., McLaren, T., Meszaros, E., Missong, A., Mooshammer, M., Negron, C.P., Nelson, L.A., Pfahler, V., Poblete-Grant, P., Randall, M., Seguel, A., Seth, K., Smith, A.C., Smits, M.M., Sobarzo, J.A., Spohn, M., Tawaraya, K., Tibbett, M., Voroney, P., Wallander, H., Wang, L., Wasaki, J., Haygarth, P.M. (2018). Organic phosphorus in the terrestrial environment: a perspective on the state of the art and future priorities. *Plant Soil* **427**, 191–208.

Gerke, J. (2015). The acquisition of phosphate by higher plants: Effect of carboxylate release by the roots. A critical review. *J. Plant Nutr. Soil Sci.* **178** (3), 351–364.

Giaveno, C., Celi, L., Richardson, A.E., Simpson, R.J., Barberis, E. (2010). Interaction of phytases with minerals and availability of substrate affect the hydrolysis of inositol phosphates. *Soil Biol. Biochem.* **42** (3), 491–498.

Gilbert, N. (2009). Environment: the disappearing nutrient. *Nature* **461**, 716–718.

Gomez-Roldan, V., Fermas, S., Brewer, P.B., Puech-Pagès, V., Dun, E.A., Pillot, J.P., Letisse, F., Matusova, R., Danoun, S., Portais, J.C., Bouwmeester, H.J., Bécard, G., Beveridge, C.A., Rameau, C., Rochange, S.F. (2008). Strigolactone inhibition of shoot branching. *Nature* **455**, 189–194.

Gorra, R., Webster, G., Martin, M., Celi, L., Mapelli, F., Weightman, A.J. (2012). Dynamic microbial community associated with iron-arsenic co-precipitation products from a groundwater storage system in Bangladesh. *Microb. Ecol.* **64** (1), 171–186.

Gregg, S.J., Sing, K.S.W. (1982). Adsorption, surface area and porosity. Academic Press, London.

Grosvernor, A.P., Kobe, B.A., Biesinger, M.C., McIntyre, N.S. (2004). Investigation of multiplet splitting of Fe 2p XPS spectra and bonding in iron compunds. *Surf. Interface Anal.* **36** (12), 1564–1574.

Grün, A., Buchner, P., Broadley, M.R., Hawkesford, M.J. (2017). Identification and expression profiling of Pht1 phosphate transporters in wheat in controlled environments and in the field. *Plant Biol.* **20**, 374–389.

Guan, X.H., Shang, C., Zhu, J., Chen, G.H. (2006). ATR-FTIR investigation on the complexation of *myo*-inositol hexaphosphate with aluminum hydroxide. *J. Colloid Interface Sci*. **293** (2), 296–302.

Gutjahr, C., Parniske, M. (2013). Cell and developmental biology of arbuscular mycorrhiza symbiosis. *Annu. Rev. Cell Dev. Biol.* **29**, 593–617.

Haran, S., Logendra, S., Seskar, M., Bratanova, M., Raskin, I. (2000). Characterization of Arabidopsis acid phosphatase promoter and regulation of acid phosphatase expression. *Plant Physiol.* **124**, 615–626.

Harrison, A.F. (1987). Soil organic Phosphorus - A review of world literature. CAB International, Wallingford, Oxon, UK, pp. 257.

Hayes, J.E., Richardson, A.E., Simpson, R.J. (1999). Phytase and acid phosphatase activities in extracts from roots of temperate pasture grass and legume seedlings. *Aust. J. Plant Physiol.* **26** (8), 801–809.

Hayes, J.E., Richardson, A.E., Simpson, R.J. (2000). The growth and phosphorus utilization of plants in sterile media when supplied with inositol hexaphosphate, glucose 1-phosphate or inorganic phosphate. *Plant Soil* **220**, 165–174.

Heuck, C., Smolka, G., Whalen, E.D., Frey, S., Gundersen, P., Moldan, F., Fernandez, I.J., Spohn, M. (2018). Effects of long-term nitrogen addition on phosphorus cycling in organic soil horizons of temperate forests. *Biogeochemistry* **141**, 167–181.

Hinsinger, P. (2001). Bioavailability of soil inorganic P in the rhizosphere as affected by root-induced chemical changes: A review. *Plant Soil* **237**, 173–195.

Hodge, A. (2004). The plastic plant: root responses to heterogeneous supplies of nutrients. *New Phytol.* **162**, 9–24.

Hoffland, E. (1992). Quantitative evaluation of the role of organic acid exudation in the mobilization of rock phosphate by rape. *Plant Soil* **140**, 279–289.

Holford, I.C.R. (1997). Soil phosphorus: Its measurement, and its uptake by plants. *Soil Res*. **35**, 227–240.

Janney, D.E., Cowley, J.M., Busek, P.R. (2000). Transmission electron microscopy of synthetic 2- and 6-line ferrihydrite. *Clay Clay Miner.* **48** (1), 111–119.

Jarosch, K.A., Doolette, A.L., Smernik, R.J., Tamburini, F., Frossard, E., Bünemann, E.K. (2015). Characterisation of soil organic phosphorus in NaOH-EDTA extracts: A comparison of ^{31}P NMR spectroscopy and enzyme addition assays. *Soil Biol. Biochem*. **91**, 298–309.

Jia, Y., Xu, L., Wang, X., Demopoulos, G.P. (2007). Infrared spectroscopic and X-ray diffraction characterization of the nature of adsorbed arsenate on ferrihydrite. *Geochim. Cosmochim. Acta* **71** (7), 1643–1654.

Jia, K.P., Baz, L., Al-Babili, S. (2018). From carotenoids to strigolactones. *J. Exp. Bot.* **69** (9), 2189–2204.

Jiang, X., Chen, W.L., Xu, C.X., Zhu, H.H., Yao, Q. (2015). Influences of arbuscular mycorrhizal fungus and phosphorus level on the lateral root formation of tomato seedlings. *J. Appl. Ecol.* **26**, 1186–1192.

Johnson, A.W., Gowada, G., Hassanali, A., Knox, J., Monaco, S., Razavi, Z., Rosebery, G. (1981). The preparation of synthetic analogues of strigol. *J. Chem. Soc., Perkin Trans.* **1***,* 1734–1743.

Johnson, J.F., Allan, D.L., Vance, C.P., Weiblen, G. (1996). Root carbon dioxide fixation by phosphorus deficient *Lupinus albus*. Contribution to organic acid exudation by proteoid roots. *Plant Physiol.* **112**, 19–30.

Johnson, B.B., Quill, E., Angove, M.J. (2012). An investigation of the mode of sorption of inositol hexaphosphate to goethite. *J. Colloid Interface Sci.* **367** (1), 436–442.

Jones, D., Darrah, P.R. (1995). Influx and efflux of organic acids across the soil-root interface of *Zea mays* L. and its implications in rhizosphere C flow. *Plant Soil* **173**, 103–109.

Jones, D.L. (1998). Organic acids in the rhizosphere−a critical review. *Plant Soil* **205** (1), 25−44.

Jones, A.M., Griffin, P.J., Waite, T.D. (2015). Ferrous iron oxidation by molecular oxygen under acidic conditions: the effect of citrate, EDTA and fluvic acid. *Geochim. Cosmochim. Acta* **160**, 117–131.

Juszczuk, I.M., Wiktorowska, A., Malusa, E., Rychter, A.M. (2004). Changes in the concentration of phenolic compounds and exudation induced by phosphate deficiency in bean plants (*Phaseolus vulgaris L.*). *Plant Soil* **267**, 41−49.

Kaegi, R., Voegelin, A., Folini, D., Hug, S.J. (2010). Effect of phosphate, silicate and Ca on the morphology, structure and elemental composition of Fe(III)-precipitates formed in aerated Fe(II) and As(III) containing water. *Geochim. Cosmochim. Acta* **74** (20), 5798–5816.

Kapulnik, Y., Delaux, P.M., Resnick, N., Mayzlish-Gati, E., Wininger, S., Bhattacharya, C., Séjalon-Delmas, N., Combier, J.P., Bécard, G., Belausov, E., Beeckman, T., Dor, E., Hershenhorn, J., Koltai, H. (2011). Strigolactones affect lateral root formation and root-hair elongation in *Arabidopsis*. *Planta* **233**, 209–216.

Kapulnik, Y., Resnick, N., Mayzlish-Gati, E., Kaplan, Y., Wininger, S., Hershenhorn, J., Koltai, H. (2011a). Strigolactones interact with ethylene and auxin in regulating root-hair elongation in Arabidopsis. *J. Exp. Bot.* **62**, 2915–2924.

Kashyap, S., Woehl, T.J., Liu, X., Mallapragada, S.K., Prozorov, T. (2014). Nucleation of iron oxide nanoparticles mediated by Mms6 protein in situ. *ACS Nano* **8** (9), 9097–9106.

Khan, H., Paull, J.G., Siddique, K., Stoddard, F. (2009). Faba bean breeding for drought-affected environments: a physiological and agronomic perspective. *Field Crops Res*. **115**, 279–286.

Kihara, T., Wada, T., Suzuki, Y., Hara, T., Koyama, H. (2003). Alteration of citrate metabolism in cluster roots of white lupin. *Plant Cell Physiol.* **44**, 901–908.

Kohlen, W., Charnikhova, T., Liu, Q., Bours, R., Domagalska, M.A., Beguerie, S., Verstappen, F., Leyser, O., Bouwmeester, H.J., Ruyter-Spira, C. (2011). Strigolactones are transported through the xylem and play a key role in shoot architectural response to phosphate deficiency in nonarbuscular mycorrhizal host Arabidopsis. *Plant Physiol*. **155**, 974–987.

Kohlen, W., Charnikhova, T., Lammers, M., Pollina, T., Tóth, P., Haider, I., Pozo, M.J., de Maagd, R.A., Ruyter-Spira, C., Bouwmeester, H.J. (2012). The tomato *CAROTENOID CLEAVAGE DIOXYGENASE 8* (*SlCCD8*) regulates rhizosphere signaling, plant architecture and affects reproductive development through strigolactone biosynthesis. *New Phytol.* **196**, 535–547.

Kohlen, W., Charnikhova, T., Bours, R., López-Ráez, J.A., Bouwmeester, H.J. (2013). Tomato strigolactones: A more detailed look. *Plant Signal. Behav*. **8**, 125–130.

Koltai, H., Lekkala, S.P., Bhattacharya, C., Mayzlish-Gati, E., Resnick, N., Wininger, S., Dor, E., Yoneyama, K., Hershenhorn, J., Joel, D.M., Kapulnik, Y. (2010). A tomato strigolactone-impaired mutant displays aberrant shoot morphology and plant interactions. *J. Exp. Bot.* **61**, 1739–1749.

Koltai, H., Dor, E., Hershenhorn, J., Joel, D.M., Weininger, S., Lekalla, S., Shealtiel, H., Bhattacharya, C., Eliahu, E., Resnick, N., Barg, R., Kapulnik, Y. (2010a). Strigolactones' effect on root growth and root-hair elongation may be mediated by auxin-efflux carriers. *J. Plant Growth Regul.* **29**, 129–136.

Koltai, H. (2011). Strigolactones are regulators of root development. *New Phytol.* **190**, 545–549.

Koltai, H. (2013). Strigolactones activate different hormonal pathways for regulation of root development in response to phosphate growth conditions. *Ann. Bot.* **112,** 409–415.

Lai, Y.M., Liang, X.F., Yang, S.Y., Wang, J.X., Cao, L.H., Dai, B. (2011). Raman and FTIR spectra of iron phosphate glasses containing cerium. *J. Mol. Struct.* **992** (1–3), 84–88.

Lambers, H., Juniper, D., Cawthray, G.R., Veneklaas, E.J., Martínez-Ferri, E. (2002). The pattern of carboxylate exudation in *Banksia grandis* (Proteaceae) is affected by the form of phosphate added to the soil. *Plant Soil* **238**, 111–122.

Lambers, H., Shane, M.W., Cramer, M.D., Pearse, S.J., Veneklaas, E.J. (2006). Root structure and functioning for efficient acquisition of phosphorus: Matching morphological and physiological traits. *Ann. Bot.* **98**, 693–713.

Li, L., Stanforth, R. (2000). Distinguishing adsorption and surface precipitation of phosphate on goethite (α -FeOOH). *J. Colloid Interface Sci.* **230** (1), 12–21.

Li, Y., Zhang, J., Zhang, X., Fan, H., Gu, M., Qu, H., Xu, G. (2015). Phosphate transporter OsPht1;8 in rice plays in important role in phosphorus redistribution from source to

sink organs and allocation between embryo and endosperm of seeds. *Plant Sci.* **230**, 23–32.
Li, M., Liu, J., Xu, Y., Qian, G. (2016). Phosphate adsorption on metal oxides and metal hydroxides: A comparative review. *Environ. Rev.* **24**, 319–332.
Lin, S.I., Chiang, S.F., Lin, W.Y., Chen, J.W., Tseng, C.Y., Wu, P.C., Chiou, T.J. (2008). Regulatory network of microRNA399 and *PHO2* by systemic signaling. *Plant Physiol.* **147**, 732–746.
Lipton, D.S., Blanchar, R.W., Blevins, D.G. (1987). Citrate, malate, and succinate concentration in exudates from P-sufficient and P-stressed *Medicago sativa* L. seedlings. *Plant Physiol*. **85**, 315–317.
Liu, C., Muchhal, U.S., Uthappa, M., Kononowicz, A.K., Ragothama, K.G. (1998). Tomato phosphate transporter genes are differently regulated in plant tissues by phosphorus. *Plant Physiol.* **116**, 91–99.
Loeppert, R.H., Inskeep, W.P. (1996). In: Sparks, *et al.* (Eds.), Methods of soil analysis. Part 3, Chemical Methods. Book series No 5 SSSA and ASA, Madison, pp. 639–664.
López-Bucio, J., Cruz-Ramırez, A., Herrera-Estrella, L. (2003). The role of nutrient availability in regulating root architecture. *Curr. Opin. Plant Biol.* **6**, 280–287.
Lopez-Obando, M., Ligerot, Y., Bonhomme, S., Boyer, F.D., Rameau, C. (2015). Strigolactone biosynthesis and signaling in plant development. *Development* **142**, 3615–3619.
López-Ráez, J.A., Charnikhova, T., Gómez-Roldán, V., Matusova, R., Kohlen, W., De Vos, R., Verstappen, F., Puech-Pages, V., Bécard, G., Mulder, P., Bouwmeester, H.J. (2008). Tomato strigolactones are derived from carotenoids and their biosynthesis is promoted by phosphate starvation. *New Phytol.* **178**, 863–874.
López-Ráez, J.A., Pozo, M.J., García-Garrido, J.M. (2011). Strigolactones: a cry for help in the rhizosphere. *Botany* **89**, 513–522.
López-Ráez, J.A., Shirasu, K., Foo, E. (2018). Strigolactones in plant interactions with beneficial and detrimental organisms: the yin and yang. *Trends Plant Sci*. **22** (6), 527–537.
Lynch, J.P. (2007). Roots of the second green revolution. *Aust. J. Bot*. **55**, 493–512.
Lynch, J.P. (2011). Root phenes for enhanced soil exploration and phosphorus acquisition: Tools for future crops. *Plant Physiol*. **156**, 1041–1049.
Ma, Z., Baskin, T.I., Brown, K.M., Lynch, J.P. (2003). Regulation of root elongation under phosphorus stress involves changes in ethylene responsiveness. *Plant Physiol*. **131**, 1381–1390.
Machin, D.C., Hamon-Josse, M., Bennett, T. (2020). Fellowship of the rings: a saga of strigolactones and other small signals. *New Phytol*. **225** (2), 621–636.
Magid, J., Tiessen, H., Condron, L.M. (1996). Dynamics of organic phosphorus in soils under natural and agricultural ecosystems. In: Piccolo, A. (Ed.), Humic Substances in Terrestrial Ecosystems. Elsevier Science, Amsterdam, pp. 429–466.
Mairhofer, S., Pridmore, T., Johnson, J., Wells, D.M., Bennett, M.J., Mooney, S.J., Sturrock, C.J. (2017). X-ray computed tomography of crop plant Root systems grown in soil. *Curr. Protoc. Plant Biol.* **2**, 270–286.
Mallet, M., Barthelemy, K., Ruby, C., Renard, A., Naille, S. (2013). Investigation of phosphate adsorption onto ferrihydrite by X-ray photoelectron spectroscopy. *J. Colloid Interface Sci.* **407**, 95–101.
Marschner, H. (1995). Rhizosphere pH effects on phosphorus nutrition. In: Johansen, C., Lee, K.K., Sharma, K.K., Subbarao, G.V., Kueneman, E.A. (Eds.), Genetic manipulation of crop plants to enhance integrated nutrient management in cropping systems-1. Phosphorus: proceedings of an FAO-ICRISA expert consultancy workshop, 15-18 Mar 1994, ICRISAT Asia Center. India. Patancheru 502 324,

Andhra Pradesh, India: International Crops Research Institute for the Semi-Arid Tropics.
Marschner, H. (2012). Marschner's Mineral Nutrition of Higher Plants, 3rd ed.; Academic Press: San Diego, CA, USA.
Martin, C.J., Evans, W.J. (1987). Phytic acid: divalent cation interactions. V. Titrimetric, calorimetric, and binding studies with cobalt(II) and nickel(II) and their comparison with other metal ions. *J. Inorg. Biochem.* **30** (2), 101–119.
Martin, M., Celi, L., Barberis, E. (1999). Determination of low concentrations of organic phosphorus in soil solution. *Commun. Soil Sci. Plant Anal.* **30** (13–14), 1909–1917.
Martin, M., Celi, L., Barberis, E. (2004). Desorption and plant availability of myo-inositol hexaphosphate adsorbed on goethite. *Soil Sci.* **169** (2), 115–124.
Marzec, M., Muszynska, A., Gruszka, D. (2013). The role of strigolactones in nutrient-stress responses in plants. *Int. J Mol. Sci.* **14**, 9286–9304.
Matusova, R., Rani, K., Verstappen, F.W.A., Franssen, M.C.R., Beale, M.H., Bouwmeester, H.J. (2005). The strigolactone germination stimulants of the plant-parasitic *Striga* and *Orobanche* spp. are derived from the carotenoid pathway. *Plant Physiol.* **139**, 920–934.
Mayzlish-Gati, E., De-Cuyper, C., Goormachtig, S., Beeckman, T., Vuylsteke, M., Brewer, P.B., Beveridge, C.A., Yermiyahu, U., Kaplan, Y., Enzer, Y., Wininger, S., Resnick, N., Cohen, M., Kapulnik, Y., Koltai, H. (2012). Strigolactones are involved in root response to low phosphate conditions in Arabidopsis. *Plant Physiol.* **160**, 1329–1341.
Mikutta, R., Lorenz, D., Guggenberger, G., Haumaier, L., Freund, A. (2014). Properties and reactivity of Fe-organic matter associations formed by coprecipitation versus adsorption: clues from arsenate batch adsorption. *Geochim. Cosmochim. Acta* **144**, 258–276.
Moulder, J.F., Stickle, W.F., Sobol, P.E., Bomben, K.D. (1995). In: Chastain, J. (Ed.), Handbook of X-ray Photoelectron Spectroscopy. Perkin-Elmer Corporation, Physical Electronics Division, Minneapolis.
Müller, J., Toev, T., Heisters, M., Teller, J., Moore, K.L., Hause, G., Dinesh, D.C., Bürstenbinder, K., Abel, S. (2015). Iron-dependent callose deposition adjusts root meristem maintenance to phosphate availability. *Dev. Cell* **33**, 216–230.
Murashige, T., Skoog, F. (1962). A revised medium for rapid growth and bio assays with tobacco tissue cultures. *Physiol. Plant.* **15**, 473–497.
Murthy, P.P.N. (2006). Identification of inositol phosphates by nuclear magnetic resonance spectroscopy: unravelling structural diversity. In: Turner, B.L., Richardson, A.E., Mullaney, E.J. (Eds.), Inositol phosphates: linking agriculture and the environment. CABI Publishing, Wallingford, UK, pp. 7–22.
Nagahashi, G., Douds Jr., D.D. (2004). Isolated root caps, border cells, and mucilage from host roots stimulate hyphal branching of the arbuscular mycorrhizal fungus, *Gigaspora gigantea**. *Mycol. Res*. **108** (9), 1079–1088.
Nasto, M.K., Alvarez-Clare, S., Lekberg, Y., Sullivan, B.W., Townsend, A.R., Cleveland, C.C. (2014). Interactions among nitrogen fixation and soil phosphorus acquisition strategies in lowland tropical rain forests. *Ecol. Lett*. **17** (10), 1282–1289.
Neto, A.P., Favarin, J.L., Hammond, J.P., Tezotto, T., Couto, H.T.Z. (2016) Analysis of phosphorus use efficiency traits in coffea genotypes reveals coffea arabica and coffea canephora have contrasting phosphorus uptake and utilization efficiencies. *Front. Plant Sci.* **7**, 408.
Neumann, G., Römheld, V. (1999). Root excretion of carboxylic acids and protons in phosphorus-deficient plants. *Plant Soil* **211**, 121–130.
Neumann, G., Massonneau, A., Langlade, N., Dinkelaker, B., Hengeler, C., Romheld, V., Martinoia, E. (2000). Physiological aspects of cluster root function and

development in phosphorus-deficient white lupin (*Lupinus albus* L.). *Ann. Bot.* **85**, 909–919.
Neumann, G., Römheld, V. (2002). Root-induced changes in the availability of nutrients in the rhizosphere. In: Waisel, Y., Eshe,l A., Kafkafi, U. (Eds.), Plant roots: The hidden half. Marcel Dekker, New York, pp 617–649.
Niu, Y.F., Chai, R.S., Jin, G.L., Wang, H., Tang, C.X., Zhang, Y.S. (2013). Responses of root architecture development to low phosphorus availability: A review. *Ann. Bot.* **112**, 391–408.
Ognalaga, M., Frossard, E., Thomas, F. (1994). Glucose-1-phosphate and *myo*-inositol hexaphosphate adsorption mechanisms on goethite. *Soil Sci. Soc. Am. J.* **58** (2), 332–337.
Ohno, T., Zibilske, L.M. (1991). Determination of low concentration of phosphorus in soil extracts using malachite green. *Soil Sci. Soc. Am. J.* **55** (3), 892–895.
Omoarelojie, L.O., Kulkarni, M.G., Finnie, J.F., Van Staden, J. (2019). Strigolactones and their crosstalk with other phytohormones. *Ann. Bot.* **124**, 749–767.
Pagliarani, C., Vitali, M., Ferrero, M., Vitulo, N., Incarbone, M., Lovisolo, C., Valle, G., Schubert, A. (2017). The accumulation of miRNAs differentially modulated by drought stress is affected by grafting in grapevine. *Plant Physiol*. **173**, 2180–2195.
Pant, B.D., Buhtz, A., Kehr, J., Scheible, W.R. (2008). MicroRNA399 is a long-distance signal for the regulation of plant phosphate homeostasis. *Plant J.* **53**, 731–738.
Parfitt, R.L. (1989). Phosphate reactions with natural allophane, ferrihydrite and goethite. *J. Soil Sci.* **40**, 359–369.
Pearse, S.J., Veneklaas, E.J., Cawthray, G., Bolland, M.D.A., Lambers, H. (2007). Carboxylate composition of root exudates does not relate consistently to a crop species' ability to use phosphorus from aluminium, iron or calcium phosphate sources. *New Phytol.* **173**, 181–190.
Pedrot, M., Le Boudec, A., Davranche, M., Dia, A., Henin, O. (2011). How does organic matter constrain the nature, size and availability of Fe nanoparticles for biological reduction? *J. Colloid Interface Sci*. **359** (1), 75–85.
Péret, B., Clément, M., Nussaume, L., Desnos, T. (2011). Root developmental adaptation to phosphate starvation: Better safe than sorry. *Trends Plant Sci.* **16**, 442–450.
Péret, B., Desnos, T., Jost, R., Kanno, S., Berkowitz, O., Nussaume, L. (2014). Root architecture responses: In search of phosphate. *Plant Physiol.* **166**, 1713–1723.
Pérez-Torres, C.A., López-Bucio, J., Cruz-Ramírez, A., Ibarra-Laclette, E., Dharmasiri, S., Estelle, M., Herrera-Estrella, L. (2008). Phosphate availability alters lateral root development in Arabidopsis by modulating auxin sensitivity via a mechanism involving the TIR1 auxin receptor. *Plant Cell* **20**, 3258–3272.
Persson, P., Nilsson, N., Sjoberg, S. (1996). Structure and bonding of orthophosphate ions at the iron oxide-aqueous interface. *J. Colloid Interface Sci.* **177** (1), 263–275.
Pham, A.N., Waite, T.D. (2008). Oxygenation of Fe(II) in the presence of citrate in aqueous solution at pH 6.0-8.0 and 25°C: interpretation from an Fe(II)/citrate speciation perspective. *J. Phys. Chem. A* **112** (4), 643–651.
Plaxton, W.C., Tran, H.T. (2011). Metabolic adaptations of phosphate-starved plants. *Plant Physiol*. **156**, 1006–1015.
Purnell, H. (1960). Studies of the family proteaceae. I. Anatomy and morphology of the roots of some victorian species. *Aust. J. Bot.* **8**, 38–50.
R Core Team (2020). R: A language and environment for statistical computing. R Foundation for Statistical Computing, Vienna, Austria. URL https://www.R-project.org/.
Raghothama, K.G. (1999). Phosphorus and plant nutrition: An overview. In: Sims, J.T., Sharpley, A.N. (Eds.), Phosphorus: Agriculture and the environment. ASA, CSSA, and SSSA, Madison, WI, pp. 355–378.

Ramaekers, L., Remans, R., Rao, I.M., Blair, M.W., Vanderleyden, J. (2010). Strategies for improving phosphorus acquisition efficiency of crop plants. *Field Crops Res.* **117** (2–3), 169–176.

Rameau, C., Bertheloot, J., Leduc, N., Andrieu, B., Foucher, F., Sakr, S. (2015). Multiple pathways regulate shoot branching. *Front. Plant Sci.* **5**, 741.

Rao, I.M., Miles, J.W., Beebe, S.E., Horst, W.J. (2016). Root adaptations to soils with low fertility and aluminium toxicity. *Ann. Bot.* **118** (4), 593−605.

Rasmussen, A., Depuydt, S., Goormachtig, S., Geelen, D. (2013). Strigolactones fine-tune the root system. *Planta* **238**, 615–626.

Rausch, C., Bucher, M. (2002). Molecular mechanisms of phosphate transport in plants. *Planta* **216**, 23–37.

Redecker, D., Raab, P. (2006). Phylogeny of the Glomeromycota (arbuscular mycorrhizal fungi): recent developments and new gene markers. *Mycologia* **98** (6), 885–895.

Ren, C.G., Kong, C.C., Xie, Z.H. (2018). Role of abscisic acid in strigolactone-induced salt stress tolerance in arbuscular mycorrhizal Sesbania cannabina seedlings. *BMC Plant Biol.* **18** (74).

Ren, C., Guo, Y., Kong, J., Lecourieux, F., Dai, Z., Li, S., Liang, Z. (2020). Knockout of *VvCCD8* gene in grapevine affects shoot branching. *BMC Plant Biol*. **20** (47).

Rial, C., Varela, R.M., Molinillo, J.M.G., López-Ráez, J.A., Macías, F.A. (2019). A new UHPLC-MS/MS method for the direct determination of strigolactones in root exudates and extracts. *Phytochem. Anal*. **30**, 110–116.

Richardson, A.E., Barea, J.M., McNeill, A.M., Prigent-Combaret, C. (2009). Acquisition of phosphorus and nitrogen in the rhizosphere and plant growth promotion by microorganisms. *Plant Soil* **321**, 305–339.

Rodriguez, J.A.M., Morcillo, R.L., Vierheilig, H., Ocampo, J.A., Ludwig-Muller, J., Garrido, J.M.G. (2010). Mycorrhization of the notabilis and sitiens tomato mutants in relation to abscisic acid and ethylene contents. *J. Plant Physiol.* **167**, 606–613.

Römheld, V., Marschner, H. (1990). Genotypical differences among graminaceous species in release of phytosideriphores and uptake of iron phytosiderophores. *Plant Soil* **123**, 147–153.

Rouached, H., Arpat, A.B., Poirier, Y. (2010). Regulation of phosphate starvation responses in plants: Signaling players and cross-talks. *Mol. Plant* **3**, 288–299.

Ruyter-Spira, C., Kohlen, W., Charnikhova, T., van Zeijl, A., van Bezouwen, L., de Ruijter, N., Cardoso, C., López-Ráez, J.A., Matusova, R., Bours, R., Verstappen, F., Bouwmeester, H.J. (2011). Physiological effects of the synthetic strigolactone analog GR24 on root system architecture in Arabidopsis: Another belowground role for strigolactones? *Plant Physiol.* **155**, 721–734.

Ryan, P.R., Delhaize, E., Jones, D.L. (2001). Function and mechanism of organic anion exudation from plant roots. *Annu. Rev. Plant Biol*. **52** (1), 527–560.

Sánchez-Calderón, L., López-Bucio, J., Chacón-López, A., Cruz-Ramírez, A., Nieto-Jacobo, F., Dubrovsky, J.G., Herrera-Estrella, L. (2005). Phosphate starvation induces a determinate developmental program in the roots of *Arabidopsis thaliana*. *Plant Cell Physiol.* **46**, 174–184.

Santoro, V., Martin, M., Persson, P., Lerda, C., Said-Pullicino, D., Magnacca, G., Celi, L. (2019). Inorganic and organic P retention by coprecipitation during ferrous iron oxidation. *Geoderma* **348**, 168–180.

Santoro, V., Schiavon, M., Gresta, F., Ertani, A., Cardinale, F., Sturrock, C.J., Celi, L., Schubert, A. (2020). Strigolactones control root system architecture and tip anatomy in *Solanum lycopersicum* L. plants under P starvation. *Plants* **9**, 612.

Sato, D., Awad, A.A., Chae, S.H., Yokota, T., Sugimoto, Y., Takeuchi, Y., Yoneyama, K. (2003). Analysis of strigolactones, germination stimulants for *Striga* and

Orobanche, by high-performance liquid chromatography/tandem mass spectrometry. *J. Agric. Food Chem.* **51** (5), 1162–1168.
Sato, D., Awad, A.A., Takeuchi, Y., Yoneyama, K. (2005). Confirmation and quantification of strigolactones, germination stimulants for root parasitic plants *Striga* and *Orobanche*, produced by cotton. *Biosci. Biotechnol. Biochem*. **69** (1), 98–102.
Scaffidi, A., Waters, M.T., Bond, C.S., Dixon, K.W., Smith, S.M., Ghisalberti, E.L., Flematti, G.R. (2012). Exploring the molecular mechanism of karrikins and strigolactones. *Bioorg. Med. Chem. Lett.* **22** (11), 3743–3746.
Scaffidi, A., Waters, M.T., Sun, Y.K., Skelton, B.W., Dixon, K.W., Ghisalberti, E.L., Flematti, G.R., Smith, S.M. (2014). Strigolactone hormones and their stereoisomers signal through two related receptor proteins to induce different physiological responses in *Arabidopsis*. *Plant Physiol*. **165**, 1221–1232.
Schachtman, D.P., Reid, R.J., Ayling, S.M. (1998). Phosphorus uptake by plants: From soil to cell. *Plant Physiol.* **116**, 447–453.
Schlesinger, W.H., Bernhard, E.S. (2013). Biogeochemistry: An analysis of Global Change, 3rd ed.; Academic Press: Waltham, MA, USA.
Schleuss, P.M., Widdig, M., Heintz-Buschart, A., Kirkman, K., Spohn, M. (2020). Interactions of nitrogen and phosphorus cycling promote P acquisition and explain synergistic plant-growth responses. *Ecology* **101** (5), e03003.
Schmitz, A.M., Harrison, M.J. (2014). Signaling events during initiation of arbuscular mycorrhizal symbiosis. *J. Integr. Plant Biol.* **56**, 250–61.
Schroeder, M.S., Janos, D.P. (2005). Plant growth, phosphorus nutrition, and root morphological responses to arbuscular mycorrhizas, phosphorus fertilization, and intraspecific density. *Mycorrhiza* **15**, 203–216.
Senn, A.C., Kaegi, R., Hug, S.J., Hering, J.G., Mangold, S., Voegelin, A. (2015). Composition and structure of Fe(III)-precipitates formed by Fe(II) oxidation in water at near-neutral pH: interdependent effects of phosphates, silicate and Ca. *Geochim. Cosmochim. Acta* **162**, 220–246.
Seto, Y., Yamaguchi, S. (2014). Strigolactone biosynthesis and perception. *Plant J.* **105** (2), 335–350.
Shane, M.W., Cawthray, G.R., Cramer, M.D., Kuo, J., Lambers, H. (2006). Specialized 'dauciform' roots of Cyperaceae are structurally distinct, but functionally analogous with 'cluster' roots. *Plant Cell Env.* **29**, 1989–1999.
Shen, J., Yuan, L., Zhang, J., Li, H., Bai, Z., Chen, X., Zhang, W., Zhang, F. (2011). Phosphorus dynamics: From soil to plant. *Plant Physiol.* **156**, 997–1005.
Shen, Q., Wen, Z., Dong, Y., Li, H., Miao, Y., Shen, J. (2018). The responses of root morphology and phosphorus mobilizing exudations in wheat to increasing shoot phosphorus concentration. *AoB Plants* **10**, ply054.
Shimizu, M., Zhou, J., Schroder, C., Obst, M., Kappler, A., Borch, T. (2013). Dissimilatory reduction and transformation of ferrihydrite-humic acid coprecipitates. *Environ. Sci. Technol.* **47** (23), 13375–13384.
Siao, W., Coskun, D., Baluška, F., Kronzucker, H.J., Xu, W. (2020). Root-apex proton fluxes at the centre of soil-stress acclimation. *Trends Plant Sci.* **25** (8), 794–804.
Smith, S.E., Read, D.J. (2008). Mycorrhizal symbiosis. Cambridge, UK: Academic Press.
Sodano, M., Said-Pullicino, D., Fiori, A.F., Catoni, M., Martin, M., Celi, L. (2016). Sorption of paddy soil-derived dissolved organic matter on hydrous iron oxide-vermiculite mineral phases. *Geoderma* **261**, 169–177.
Spohn, M. (2016). Element cycling as driven by stoichiometric homeostasis of soil microorganisms. *Basic Appl. Ecol.* **17**, 471–478.
Steiner, A.A. (1984). The universal nutrient solution. In Proceedings of the Sixth International Congress on Soilless Culture. pp. 633–649. International Society for Soilless Culture, Wageningen.

Sun, H., Tao, J., Liu, S., Huang, S., Chen, S., Xie, X., Yoneyama, K., Zhang, Y., Xu, G. (2014). Strigolactones are involved in phosphate- and nitrate-deficiency-induced root development and auxin transport in rice. *J. Exp. Bot.* **65**, 6735–6746.

Sun, H., Xu, F., Guo, X., Wu, D., Zhang, X., Lou, M., Luo, F., Zhao, Q., Xu, G., Zhang, Y. (2019). A Strigolactone signal inhibits secondary lateral root development in rice. *Front. Plant Sci.* **10**, 1527.

Svistoonoff, S., Creff, A., Reymond, M., Sigoillot-Claude, C., Ricaud, L., Blanchet, A., Nussaume, L., Desnos, T. (2007). Root tip contact with low-phosphate media reprograms plant root architecture. *Nat. Gen*. **39**, 792–796.

Tarafdar, J.C., Claassen, N. (2001). Comparative efficiency of acid phosphatase originated from plant and fungal sources. *J. Plant Nutr. Soil Sci.* **164**, 279–282.

Ticconi, C.A., Abel, S. (2004). Short on phosphate: plant surveillance and countermeasures. *Trends Plant Sci.* **9** (11), 548–555.

Tiziani, R., Pii, Y., Celletti, S., Cesco, S., Mimmo, T. (2020). Phosphorus deficiency changes carbon isotope fractionation and triggers exudate reacquisition in tomato plants. *Sci. Rep.* **10**, 15970.

Turner, B.L., McKelvie, I.D., Haygarth, P.M. (2002). Characterisation of water extractable soil organic phosphorus by phosphatase hydrolysis. *Soil Biol. Biochem.* **34**, 27–35.

Turner, B.L. (2006). Organic phosphorus in Madagascan rice soils. *Geoderma* **136** (1–2), 279–288.

Ueda, H., Kusaba, M. (2015). Strigolactone regulates leaf senescence in concert with ethylene in Arabidopsis. *Plant Physiol.* **169**, 138–147.

Ueno, K., Furumoto, T., Umeda, S., Mizutani, M., Takikawa, H., Batchvarova, R., Sugimoto, Y. (2014). Heliolactone, a non-sesquiterpene lactone germination stimulant for root parasitic weeds from sunflower. *Phytochemistry* **108**, 122–128.

Ugliengo, P., Viterbo, D., Chiari, G. (1993). MOLDRAW: Molecular graphics on a personal computer. *Z. Kristallogr*. **207**, 9–23.

Umehara, M., Hanada, A., Yoshida, S., Akiyama, K., Arite, T., Takeda-Kamiya, N., Magome, H., Kamiya, Y., Shirasu, K., Yoneyama, K., Kyozuka, J., Yamaguchi, S. (2008). Inhibition of shoot branching by new terpenoid plant hormones. *Nature* **455**, 195–200.

Umehara, M., Hanada, A., Magome, H., Takeda-Kamiya, N., Yamaguchi, S. (2010). Contribution of strigolactones to the inhibition of tiller bud outgrowth under phosphate deficiency in rice. *Plant Cell Physiol*. **51**, 1118–1126.

Umehara, M. (2011). Strigolactone, a key regulator of nutrient allocation in plants. *Plant Biotechnol.* **28**, 429–437.

van der Grift, B., Behrends, T., Oste, L.A., Schot, P.P., Wassen, M.J., Griffioen, J. (2016). Fe hydroxyphosphate precipitation and Fe(II) oxidation kinetics upon aeration of Fe(II) and phosphate-containing synthetic and natural solution. *Geochim. Cosmochim. Acta* **186**, 71–90.

Vance, C.P., Uhde-Stone, C., Allan, D.L. (2003). Phosphorus acquisition and use: Critical adaptations by plants for securing a nonrenewable resource. *New Phytol.* **157**, 423–447.

Villaécija-Aguilar, J.A., Hamon-Josse, M., Carbonnel, S., Kretschmar, A., Schmid, C., Dawid, C., Bennett, T., Gutjahr, C. (2019). SMAX1/SMXL2 regulate root and root hair development downstream of KAI2-mediated signaling in *Arabidopsis*. *PLoS Genet*. **15**, e1008327.

Voegelin, A., Kaegi, R., Frommer, J., Vantelon, D., Hug, S.J. (2010). Effect of phosphate, silicate, and Ca on Fe(III)-precipitates formed in aerated Fe(II)- and As(III)-containing water studied by X-ray absorption spectroscopy. *Geochim. Cosmochim. Acta* **74** (1), 164–186.

Voegelin, A., Senn, A.C., Kaegi, R., Hug, S.J., Mangold, S. (2013). Dynamic Fe-precipitate formation induced by Fe(II) oxidation in aerated phosphate-containing water. *Geochim. Cosmochim. Acta* **117**, 216–231.

Vogel, J.T., Walter, M.H., Giavalisco, P., Lytovchenko, A., Kohlen,W., Charnikhova, T., Simkin, A.J., Goulet, C., Strack, D., Bouwmeester, H.J., Fernie, A.R., Klee, H.J. (2010). SlCCD7 controls strigolactone biosynthesis, shoot branching and mycorrhiza-induced apocarotenoid formation in tomato. *Plant J.* **61**, 300–311.

Wan, B., Yan, Y., Liu, F., Tan, W., He, J., Feng, X., (2016). Surface speciation of *myo*-inositol hexakisphosphate adsorbed on TiO_2 nanoparticles and its impact on their colloidal stability in aqueous suspension: a comparative study with orthophosphate. *Sci. Total Sci. Total Environ.* **544** (0), 134–142.

Wang, L., Smith, S.M. (2016). Strigolactones redefine plant hormones. *Sci. China Life Sci*. **59**, 1083–1085.

Wang, N.Q., Kong, C.H., Wang, P., Meiners, S.J. (2020). Root exudate signals in plant–plant interactions. *Plant Cell Environ.* 1–15.

Ward, J.T., Lahner, B., Yakubova, E., Salt, D.E., Raghothama, K.G. (2008). The effect of iron on the primary root elongation of Arabidopsis during phosphate deficiency. *Plant Physiol*. **147**, 1181–1191.

Waters, M.T., Gutjahr, C., Bennett, T., Nelson, D.C. (2017). Strigolactone signaling and evolution. *Annu. Rev. Plant Biol.* **68**, 291–322.

Weishaar, J.L., Aiken, G.R., Bergamaschi, B.A., Fram, M.S., Fujii, R., Mopper, K. (2003). Evaluation of specific ultraviolet absorbance as an indicator of the chemical composition and reactivity of dissolved organic carbon. *Environ. Sci. Technol*. **37** (20), 4702–4708.

Widdig, M., Schleuss, P.M., Weig, A.R., Guhr, A., Biederman, L.A., Borer, E.T., Crawley, M.J., Kirkman, K.P., Seabloom, E., Wragg, P. (2019). Nitrogen and phosphorus additions alter the abundance of phosphorus-solubilizing bacteria and phosphatase activity in grassland soils. *Front. Environ. Sci.* **7**, 185.

Williamson, L.C., Ribrioux, S.P.C.P., Fitter, A.H., Leyser, H.M.O. (2001). Phosphate availability regulates root system architecture in Arabidopsis. *Plant Physiol.* **126**, 875–882.

Wissuwa, M., Gamat, G., Ismail, A.M. (2005). Is root growth under phosphorus deficiency affected by source or sink limitations? *J. Exp. Bot*. **56**, 1943–1950.

Xie, X., Yoneyama, K., Yoneyama, K. (2010). The Strigolactone Story. *Annu. Rev. Phytopathol*. **48**, 93–117.

Xu, X., Fang, P., Zhang, H., Chi, C., Song, L., Xia, X., Shi, K., Zhou, Y., Zhou, J., Yu, J. (2019). Strigolactones positively regulate defense against root-knot nematodes in tomato. *J. Exp. Bot*. **70** (4), 1325–1337.

Yamada, Y., Furusawa, S., Nagasaka, S., Shimomura, K., Yamaguchi, S., Umehara, M. (2014). Strigolactone signaling regulates rice leaf senescence in response to a phosphate deficiency. *Planta* **240**, 399–408.

Yan, Y., Li, W., Yang, J., Zheng, A., Liu, F., Feng, X., Sparks, D.L. (2014). Mechanism of *myo*-inositol hexakisphosphate sorption on amorphous aluminum hydroxide: spectroscopic evidence for rapid surface precipitation. *Environ. Sci. Technol.* **48** (12), 6735–6742.

Yang, T., Lian, Y., Wang, C. (2019). Comparing and contrasting the multiple roles of butenolide plant growth regulators: strigolactones and karrikins in plant development and adaptation to abiotic stresses. *Int. J. Mol. Sci.* **20** (24), 6270.

Yoneyama, K., Xie, X., Kusumoto, D., Sekimoto, H., Sugimoto, Y., Takeuchi, Y., Yoneyama, K. (2007). Nitrogen deficiency as well as phosphorus deficiency in sorghum promotes the production and exudation of 5-deoxystrigol, the host

recognition signal for arbuscular mycorrhizal fungi and root parasites. *Planta* **227**, 125–132.
Yoneyama, K., Yoneyama, K., Takeuchi, Y., Sekimoto, H. (2007a). Phosphorus deficiency in red clover promotes exudation of orobanchol, the signal for mycorrhizal symbionts and germination stimulant for root parasites. *Planta* **225**, 1031–1038.
Yoneyama, K., Xie, X., Sekimoto, H., Takeuchi, Y., Ogasawara, S., Akiyama, K., Hayashi, H., Yoneyama, K. (2008). Strigolactones, host recognition signals for root parasitic plants and arbuscular mycorrhizal fungi, from Fabaceae plants. *New Phytol.* **179** (2), 484–494.
Yoneyama, K., Xie, X., Yoneyama, K., Takeuchi, Y. (2009). Strigolactones: structures and biological activities. *Pest. Manag. Sci.* **65**, 467–470.
Yoneyama, K., Awad, A.A., Xie, X., Yoneyama, K., Takeuchi, Y. (2010). Strigolactones as germination stimulants for root parasitic plants. *Plant Cell Physiol.* **51** (7), 1095–1103.
Yoneyama, K., Xie, X., Kim, H.I., Kisugi, T., Nomura, T., Sekimoto, H., Yokota, T., Yoneyama, K. (2012). How do nitrogen and phosphorus deficiencies affect strigolactone production and exudation? *Planta* **235**, 1197–1207.
Yoneyama, K., Xie, X. (2013). Strigolactones and biological activity. In: Ramawat, K.G., Mérillon, J.M. (Eds.), Natural products. Berlin, Heidelberg, Germany: Springer, 3583–3604.
Yoneyama, K., Xie, X., Yoneyama, K., Kisugi, T., Nomura, T., Nakatani, Y., Akiyama, K., McErlean, C.S.P. (2018). Which are the major players, canonical or non-canonical strigolactones? *J. Exp. Bot.* **69** (9), 2231–2239.
Yu, W., Kan, Q., Zhang, J., Zeng, B., Chen, Q. (2016). Role of the plasma membrane H^+-ATPase in the regulation of organic acid exudation under aluminum toxicity and phosphorus deficiency. *Plant Signal. Behav.* **11** (1), e1106660–1.
Zhang, Y.S., Werner, W., Scherer, H.W., Sun, X. (1994). Effect of organic manure on organic phosphorus fractions in two paddy soils. *Biol. Fertil. Soils* **17** (1), 64–68.
Zhang, L., Li, G., Li, Y., Min, J., Kronzucker, H.J., Shi, W. (2018). Tomato plants ectopically expressing *Arabidopsis GRF9* show enhanced resistance to phosphate deficiency and improved fruit production in the field. *J. Plant Physiol*. **226**, 31–39.
Zhao, K., Wu, Y. (2014). Rhizosphere calcareous soil P-extraction at the expense of organic carbon from root-exuded organic acids induced by phosphorus deficiency in several plant species. *Soil Sci. Plant Nutr.* **60**, 640–650.
Zwanenburg, B., Pospisil, T. (2013). Structure and activity of strigolactones: new plant hormones with a rich future. *Mol. Plant* **6**, 38–62.